Competition between Weak Quantum Measurement and Many-Body Dynamics in Ultracold Bosonic Gases

Wojciech Kozlowski

Supervisor: Dr. Igor B. Mekhov

Department of Physics

University of Oxford

This dissertation is submitted for the degree of

Doctor of Philosophy

St. Catherine's College

Trinity Term 2016

Moim rodzicom, bez których nie byłbym w stanie osiągnąć tego wszystkiego.

To my parents, without whom I would not have been able to achieve any of this.

Acknowledgements

First and foremost, I would like to thank my supervisor Dr. Igor Mekhov who has been an excellent mentor throughout my time at Oxford. It is primarily thanks to his brilliant insights and professionalism that I was able to reach my full potential during my doctoral studies. The work contained in this thesis would also not have been possible without the help of the other members of the group, Gabriel Mazzucchi and Dr. Santiago Caballero-Benitez. Without our frequent casual discussions in the Old Library office I would have still been stuck on the third chapter. I would also like to acknowledge all members of Prof. Dieter Jaksch's and Prof. Christopher Foot's groups for various helpful discussions. I must also offer a special mention for Edward Owen who provided much needed reality checks on some of my wishful theoretical thinking. I would also like to express my gratitude to EPSRC, St. Catherine's College, the ALP sub-department, and the Institute of Physics for providing me with the financial means to live and study in Oxford as well as attend several conferences in the UK and abroad.

On a personal note, I would like to thank my parents who provided me with all the skills necessary to work towards any goals I set myself. Needless to say, without them I would have never been able to be where I am right now. I would like to thank all the new and old friends that have kept me company for the last four years. The time spent together provided a welcome respite from the sweat and toil of my DPhil.

Oxford, September 2016

Competition between Weak Quantum Measurement and Many-Body Dynamics in Ultracold Bosonic Gases

Wojciech Kozlowski, St. Catherine's College

A thesis submitted for the degree of Doctor of Philosophy

Trinity Term 2016

Abstract

Trapping ultracold atoms in optical lattices enabled the study of strongly correlated phenomena in an environment that is far more controllable and tunable than what was possible in condensed matter. Here, we consider coupling these systems to quantised light where the quantum nature of both the optical and matter fields play equally important roles in order to push the boundaries of what is possible in ultracold atomic systems.

We show that light can serve as a nondestructive probe of the quantum state of matter. By considering a global measurement we show that it is possible to distinguish a highly delocalised phase like a superfluid from the Bose glass and Mott insulator. We also demonstrate that light scattering reveals not only density correlations, but also matter-field interference.

By taking into account the effect of measurement backaction we show that the measurement can efficiently compete with the local atomic dynamics of the quantum gas. This can generate long-range correlations and entanglement which in turn leads to macroscopic multimode oscillations across the whole lattice when the measurement is weak and correlated tunnelling, as well as selective suppression and enhancement of dynamical processes beyond the projective limit of the quantum Zeno effect in the strong measurement regime.

We also consider quantum measurement backaction due to the measurement of matter-phase-related variables such as global phase coherence. We show how this unconventional approach opens up new opportunities to affect system evolution and demonstrate how this can lead to a new class of measurement projections thus extending the measurement postulate for the case of strong competition with the system's own evolution.

Table of contents

List of figures

List of tables

Chapter 1

Introduction

The field of ultracold gases has been rapidly growing ever since the first Bose-Einstein condensate (BEC) was obtained in 1995 [1–3]. This new quantum state of matter is characterised by a macroscopic occupancy of the single particle ground state at which point the whole system behaves like a single many-body quantum object [4]. This was revolutionary as it enabled the study of coherent properties of macroscopic systems rather than single atoms or photons. Furthermore, the advanced state of laser cooling and manipulation technologies meant that the degree of control and isolation from the environment was far greater than was possible in condensed matter systems [5, 6]. Initially, the main focus of the research was on the properties of coherent matter waves, such as interference properties [7], long-range phase coherence [8], or quantised vortices [9–11]. Fermi degeneracy in ultracold gases was obtained shortly afterwards opening a similar field for fermions [12–14].

In 1998 it was shown that a degenerate ultracold gas trapped in an optical lattice is a near-perfect realisation of the Bose-Hubbard model [15] and in 2002 it was already demonstrated in a ground-breaking experiment [16]. The Bose-Hubbard Hamiltonian was previously known in the field of condensed matter where it was considered a simple toy model. Despite its simplicity the model exhibits a variety of different interesting phenomena such as the quantum phase transition from a delocalised superfluid state to a Mott insulator as the on-site

interaction is increased above a critical point which was originally studied in the context of liquid helium [17]. In contrast to a thermodynamic phase transition, a quantum phase transition is driven by quantum fluctuations and can occur at zero temperature. The ability to achieve a Bose-Hubbard Hamiltonian where the model parameters can be easily tuned by varying the lattice potential opened up a new regime in the many-body physics of atomic gases. Unlike Bose-Einstein condensates in free space which are described by weakly interacting theories [18], the behaviour of ultracold gases trapped in an optical lattice is dominated by atomic interactions opening the possibility of studying strongly correlated behaviour with unprecedented control.

The modern field of strongly correlated ultracold gases is successful due to its interdisciplinarity [5, 6]. Originally condensed matter effects are now mimicked in controlled atomic systems finding applications in areas such as quantum information processing. A really new challenge is to identify novel phenomena which were unreasonable to consider in condensed matter, but will become feasible in new systems. One such direction is merging quantum optics and many-body physics [19, 20]. Quantum optics has been developing as a branch of quantum physics independently of the progress in the many-body community. It describes delicate effects such as quantum measurement, state engineering, and systems that can generally be easily isolated from their environment due to the non-interacting nature of photons [21]. However, they are also the perfect candidate for studying open systems due the advanced state of cavity technologies [22, 23]. On the other hand ultracold gases are now used to study strongly correlated behaviour of complex macroscopic ensembles where decoherence is not so easy to avoid or control. Recent experimental progress in combining the two fields offered a very promising candidate for taking many-body physics in a direction that would not be possible for condensed matter [24–26]. Furthermore, two very recent breakthrough experiments have even managed to couple an ultracold gas trapped in an optical lattice to an optical cavity enabling the study of strongly correlated systems coupled

to quantised light fields where the quantum properties of the atoms become imprinted in the scattered light [27, 28].

There are three prominent directions in which the field of quantum optics of quantum gases has progressed in. First, the use of quantised light enables direct coupling to the quantum properties of the atoms [19, 29–32]. This allows us to probe the many-body system in a nondestructive manner and under certain conditions even perform quantum non-demolition (QND) measurements. QND measurements were originally developed in the context of quantum optics as a tool to measure a quantum system without significantly disturbing it [33–36]. This has naturally been extended into the realm of ultracold gases where such non-demolition schemes have been applied to both fermionic [37, 38] and bosonic systems [39, 40]. In this thesis, we consider light scattering in free space from a bosonic ultracold gas and show that there are many prominent features that go beyond classical optics. Even the scattering angular distribution is nontrivial with Bragg conditions that are significantly different from the classical case. Furthermore, we show that the direct coupling of quantised light to the atomic systems enables the nondestructive probing beyond a standard mean-field description. We demonstrate this by showing that the whole phase diagram of a disordered one-dimensional Bose-Hubbard Hamiltonian, which consists of the superfluid, Mott insulating, and Bose glass phases, can be mapped from the properties of the scattered light. Additionally, we go beyond standard QND approaches, which only consider coupling to density observables, by also considering the direct coupling of the quantised light to the interference between neighbouring lattice sites. We show that not only is this possible to achieve in a nondestructive manner, it is also achieved without the need for single-site resolution. This is in contrast to the standard destructive time-of-flight measurements currently used to perform these measurements [41]. Within a mean-field treatment this enables probing of the order parameter as well as matter-field quadratures and their squeezing. This can have an impact on atom-wave metrology and information

processing in areas where quantum optics has already made progress, e.g., quantum imaging with pixellised sources of non-classical light [42, 43], as an optical lattice is a natural source of multimode nonclassical matter waves.

Second, coupling a quantum gas to a cavity also enables us to study open system many-body dynamics either via dissipation where we have no control over the coupling to the environment or via controlled state reduction using the measurement backaction due to photodetections. Initially, a lot of effort was expanded in an attempt to minimise the influence of the environment in order to extend decoherence times. However, theoretical progress in the field has shown that instead being an obstacle, dissipation can actually be used as a tool in engineering quantum states [44]. Furthermore, as the environment coupling is varied the system may exhibit sudden changes in the properties of its steady state giving rise to dissipative phase transitions [45–52]. An alternative approach to open systems is to look at quantum measurement where we consider a quantum state conditioned on the outcome of a single experimental run [22, 23]. In this approach we consider the solutions to a stochastic Schrödinger equation which will be a pure state, which in contrast to dissipative systems where this is generally not the case. The question of measurement and its effect on the quantum state has been around since the inception of quantum theory and still remains a largely open question [53]. It was not long after the first condensate was obtained that theoretical work on the effects of measurement on BECs appeared [54–56]. Recently, work has also begun on combining weak measurement with the strongly correlated dynamics of ultracold gases in optical lattices [19, 57–64].

In this thesis we focus on the latter by considering a quantum gas in an optical lattice coupled to a cavity [19]. This provides us with a flexible setup where the global light scattering can be engineered. We show that this introduces a new competing energy scale into the system and by considering continuous measurement, as opposed to discrete projective measurements, we demonstrate the quantum backaction can effectively compete with the

standard short-range processes of the Bose-Hubbard model. The global nature of the optical fields leads to new phenomena driven by long-range correlations that arise from the measurement. The flexibility of the optical setup lets us not only consider coupling to different observables, but by carefully choosing the optical geometry we can suppress or enhance specific dynamical processes, realising spatially nonlocal quantum Zeno dynamics.

The quantum Zeno effect happens when frequent measurements slow the evolution of a quantum system [65, 66]. This effect was already considered by von Neumann and it has been successfully observed in a variety of systems [67–73]. The generalisation of this effect to measurements with multidimensional projections leads to quantum Zeno dynamics where unitary evolution is uninhibited within this degenerate subspace, i.e. the Zeno subspace [66, 74–76]. Here, by combining quantum optical measurements with the complex Hilbert space of a many-body quantum gas we go beyond conventional quantum Zeno dynamics. By considering the case of measurement near, but not in, the projective limit the system is still confined to a Zeno subspace, but intermediate transitions are allowed via virtual Raman-like processes. In a lattice system, like the Bose-Hubbard model we can use global measurement to engineer these dynamics to be highly nonlocal leading to the generation of long-range correlations and entanglement. Furthermore, we show that this behaviour can be approximated by a non-Hermitian Hamiltonian thus extending the notion of quantum Zeno dynamics into the realm of non-Hermitian quantum mechanics joining the two paradigms. Non-Hermitian systems themselves exhibit a range of interesting phenomena ranging from localisation [77, 78] and $\mathcal{PT}$ symmetry [79–81] to spatial order [82] and novel phase transitions [83, 84].

Just like for the nondestructive measurements we also consider measurement backaction due to coupling to the interference terms between the lattice sites. This effectively amounts to coupling to the phase observables of the system. As this is the conjugate variable of density, this allows to enter a new regime of quantum control using measurement backaction. Whilst

such interference measurements have been previously proposed for BECs in double-wells [54–56], the extension to a lattice system is not straightforward. However, we will show it is possible to achieve with our proposed setup by a careful optical arrangement. Within this context we demonstrate a novel type of projection which occurs even when there is significant competition with the Hamiltonian dynamics. This projection is fundamentally different to the standard formulation of the Copenhagen postulate projection or the quantum Zeno effect [65, 66] thus providing an extension of the measurement postulate to dynamical systems subject to weak measurement.

Finally, the cavity field that builds up from the scattered photons can also create a quantum optical potential which will modify the Hamiltonian in a way that depends on the state of the atoms that scattered the light. This can lead to new quantum phases due to new types of long-range interactions being mediated by the global quantum optical fields [85–89]. However, this aspect of quantum optics of quantum gases is beyond the scope of this thesis.

List of Publications

The work contained in this thesis is based on seven publications [90–96]:

[90] W. Kozlowski, S. F. Caballero-Benitez, and I. B. Mekhov. "Probing matter-field and atom-number correlations in optical lattices by global nondestructive addressing". *Physical Review A*, 92(1):013613, 2015.

[91] T. J. Elliott, W. Kozlowski, S. F. Caballero-Benitez, and I. B. Mekhov. "Multipartite Entangled Spatial Modes of Ultracold Atoms Generated and Controlled by Quantum Measurement". *Physical Review Letters*, 114:113604, 2015.

[92] T. J. Elliott, G. Mazzucchi, W. Kozlowski, S. F. Caballero- Benitez, and I. B. Mekhov. "Probing and Manipulating Fermionic and Bosonic Quantum Gases with Quantum Light". *Atoms*, 3(3):392–406, 2015.

[93] G. Mazzucchi*, W. Kozlowski*, S. F. Caballero-Benitez, T. J. Elliott, and I. B. Mekhov. "Quantum measurement-induced dynamics of many-body ultracold bosonic and fermionic systems in optical lattices". *Physical Review A*, 93:023632, 2016. **Equally contributing authors*.

[94] W. Kozlowski, S. F. Caballero-Benitez, and I. B. Mekhov. "Non-Hermitian dynamics in the quantum Zeno limit". *Physical Review A*, 94:012123, 2016.

[95] G. Mazzucchi, W. Kozlowski, S. F. Caballero-Benitez, and I. B Mekhov. "Collective dynamics of multimode bosonic systems induced by weak quantum measurement". *New Journal of Physics*, 18(7):073017, 2016.

[96] W. Kozlowski, S. F. Caballero-Benitez, and I. B. Mekhov. "Quantum State Reduction by Matter-Phase-Related Measurements in Optical Lattices". *arXiv preprint arXiv:1605.06000*, 2016.

Chapter 2

Quantum Optics of Quantum Gases

2.1 Introduction

In this chapter, we present the derivation of a general Hamiltonian that describes the coupling of atoms with far-detuned optical beams originally presented in Ref. [19]. This will serve as the basis from which we explore the system in different parameter regimes, such as nondestructive measurement in free space or quantum measurement backaction in a cavity. As this model extends the Bose-Hubbard Hamiltonian to include the effects of interactions with quantised light we also present a brief overview of the properties of the Bose-Hubbard model itself and its quantum phase transition. This is followed by a description of the behaviour of the scattered light with a particular focus on how to couple the optical fields to phase observables as opposed to density observables as is typically the case. Finally, we conclude with an overview of possible experimental realisability.

We consider N two-level atoms in an optical lattice with M sites. For simplicity we will restrict our attention to spinless bosons, although it is straightforward to generalise to fermions, which yields its own set of interesting quantum phenomena [92, 93, 97], and other spin particles. The theory can be also be generalised to continuous systems, but the restriction to optical lattices is convenient for a variety of reasons. Firstly, it allows us to precisely

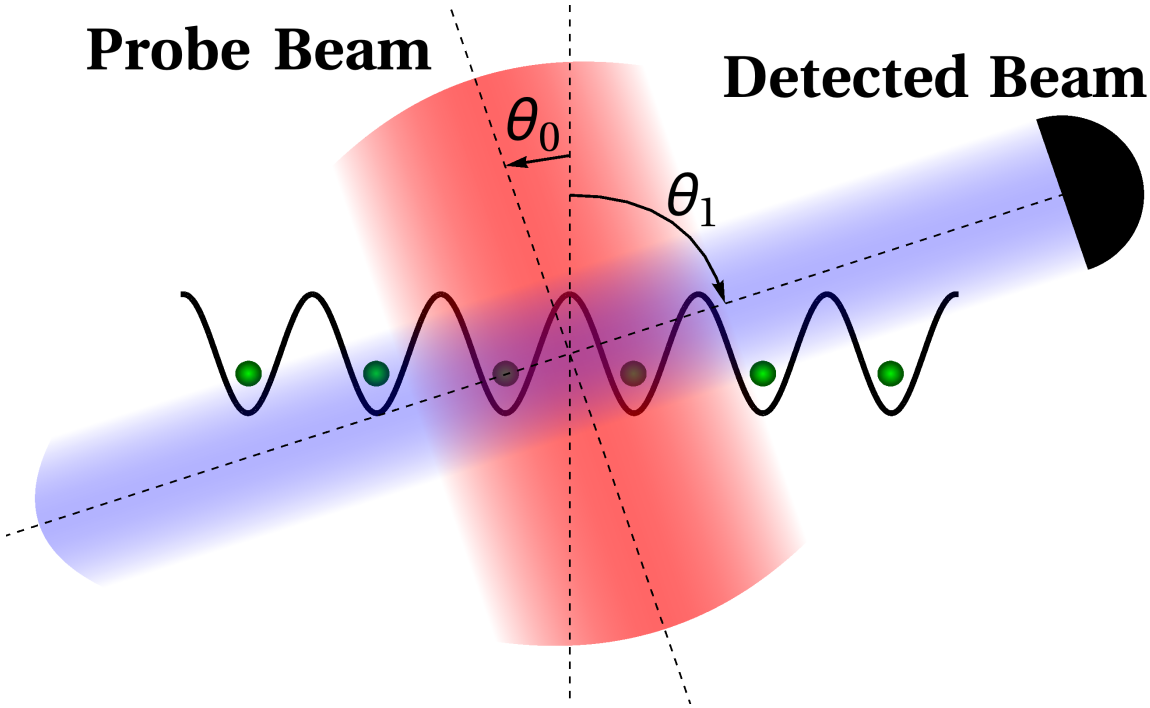

Fig. 2.1 Atoms (green) trapped in an optical lattice are illuminated by a coherent probe beam (red), a_0, with a mode function $u_0(\mathbf{r})$ which is at an angle θ_0 to the normal to the lattice. The light scatters (blue) into the mode a_1 in free space or into a cavity and is measured by a detector. Its mode function is given by $u_1(\mathbf{r})$ and it is at an angle θ_1 relative to the normal to the lattice. If the experiment is in free space light can scatter in any direction. A cavity on the other hand enhances scattering in one particular direction.

describe a many-body atomic state over a broad range of parameter values, from free particles to strongly correlated systems, due to the inherent tunability of such lattices. Furthermore, this model is capable of describing a range of different experimental setups ranging from a small number of sites with a large filling factor (e.g. BECs trapped in a double-well potential) to an extended multi-site lattice with a low filling factor (e.g. a system with one atom per site which will exhibit the Mott insulator to superfluid quantum phase transition).

An optical lattice can be formed with classical light beams that form standing waves. Depending on the detuning with respect to the atomic resonance, the nodes or antinodes form the lattice sites in which atoms accumulate. As shown in Fig. 2.1 the trapped bosons (green) are illuminated with a coherent probe beam (red) and scatter light into a different mode (blue) which is then measured with a detector. The most straightforward measurement is to

simply count the number of photons with a photodetector, but it is also possible to perform a quadrature measurement by using a homodyne detection scheme [22, 92]. The experiment can be performed in free space where light can scatter in any direction. The atoms can also be placed inside a cavity which has the advantage of being able to enhance light scattering in a particular direction [98–100]. Furthermore, cavities allow for the formation of a fully quantum potential in contrast to the classical lattice trap.

For simplicity we will be considering one-dimensional lattices most of the time. However, the model itself is derived for any number of dimensions and since none of our arguments will ever rely on dimensionality our results straightforwardly generalise to two- and three-dimensional systems. This simplification allows us to present a much more intuitive picture of the physical setup where we only need to concern ourselves with a single angle for each optical mode. As shown in Fig. 2.1 the angle between the normal to the lattice and the probe and detected beam are denoted by θ_0 and θ_1 respectively. We will consider these angles to be tunable although the same effect can be achieved by varying the wavelength of the light modes. However, it is much more intuitive to consider variable angles in our model as this lends itself to a simpler geometrical representation.

2.2 Derivation of the Hamiltonian

A general many-body Hamiltonian coupled to a quantised light field in second quantised can be separated into three parts,

$$\hat{H} = \hat{H}_f + \hat{H}_a + \hat{H}_{fa}. \tag{2.1}$$

The term $\hat{H}_f$ represents the optical part of the Hamiltonian,

$$\hat{H}_f = \sum_l \hbar\omega_l a_l^\dagger a_l - i\hbar \sum_l \left(\eta_l^* a_l - \eta_l a^\dagger\right). \tag{2.2}$$

The operators a_l ($a_l^\dagger$) are the annihilation (creation) operators of light modes with frequencies ω_l, wave vectors $\mathbf{k}_l$, and mode functions $u_l(\mathbf{r})$, which can be pumped by coherent fields with amplitudes η_l. The second part of the Hamiltonian, $\hat{H}_a$, is the matter-field component given by

$$\hat{H}_a = \int \mathrm{d}^3\mathbf{r}\Psi^\dagger(\mathbf{r})\hat{H}_{1,a}\Psi(\mathbf{r}) + \frac{2\pi a_s\hbar^2}{m}\int \mathrm{d}^3\mathbf{r}\Psi^\dagger(\mathbf{r})\Psi^\dagger(\mathbf{r})\Psi(\mathbf{r})\Psi(\mathbf{r}). \tag{2.3}$$

Here, $\Psi(\mathbf{r})$ ($\Psi^\dagger(\mathbf{r})$) are the matter-field operators that annihilate (create) an atom at position $\mathbf{r}$, a_s is the s-wave scattering length characterising the interatomic interaction, and $\hat{H}_{1,a}$ is the atomic part of the single-particle Hamiltonian $\hat{H}_1$. The final component of the total Hamiltonian is the interaction given by

$$\hat{H}_{fa} = \int \mathrm{d}^3\mathbf{r}\Psi^\dagger(\mathbf{r})\hat{H}_{1,fa}\Psi(\mathbf{r}), \tag{2.4}$$

where $\hat{H}_{1,fa}$ is the interaction part of the single-particle Hamiltonian, $\hat{H}_1$.

The single-particle Hamiltonian in the rotating-wave and dipole approximation is given by

$$\hat{H}_1 = \hat{H}_f + \hat{H}_{1,a} + \hat{H}_{1,fa}, \tag{2.5}$$

$$\hat{H}_{1,a} = \frac{\mathbf{p}^2}{2m_a} + \frac{\hbar\omega_a}{2}\sigma_z, \tag{2.6}$$

$$\hat{H}_{1,fa} = -i\hbar\sum_l \left[\sigma^+ g_l a_l u_l(\mathbf{r}) - \sigma^- g_l^* a_l^\dagger u_l^*(\mathbf{r})\right]. \tag{2.7}$$

In the equations above, $\mathbf{p}$ and $\mathbf{r}$ are the momentum and position operators of an atom of mass m_a and resonance frequency ω_a. The operators $\sigma^+ = |g\rangle\langle e|$, $\sigma^- = |e\rangle\langle g|$, and $\sigma_z = |e\rangle\langle e| - |g\rangle\langle g|$ are the atomic raising, lowering and population difference operators, where $|g\rangle$ and $|e\rangle$ denote the ground and excited states of the two-level atom respectively. g_l are the atom-light coupling constants for each mode. It is the inclusion of the interaction of the boson with quantised light that distinguishes our work from the typical approach to

ultracold atoms where all the optical fields, including the trapping potentials, are treated classically.

We will now simplify the single-particle Hamiltonian by adiabatically eliminating the upper excited level of the atom. The equations of motion for the time evolution of operator $\hat{A}$ in the Heisenberg picture are given by

$$\dot{\hat{A}} = \frac{i}{\hbar}\left[\hat{H},\hat{A}\right]. \tag{2.8}$$

Therefore, the Heisenberg equation for the lowering operator of a single particle is

$$\dot{\sigma}^- = \frac{i}{\hbar}\left[\hat{H}_1,\hat{\sigma}^-\right] = \hbar\omega_a\sigma^- + i\hbar\sum_l \sigma_z g_l a_l u_l(\mathbf{r}). \tag{2.9}$$

We will consider nonresonant interactions between light and atoms where the detunings between the light fields and the atomic resonance, $\Delta_{la} = \omega_l - \omega_a$, are much larger than the spontaneous emission rate and Rabi frequencies $g_l a_l$. Therefore, the atom will be predominantly found in the ground state and we can set $\sigma_z = -1$ which is also known as the linear dipole approximation as the dipoles respond linearly to the light amplitude when the excited state has negligible population. Moreover, we can adiabatically eliminate the polarization σ^-. Firstly we will re-write its equation of motion in a frame rotating at ω_p, the external probe frequency, such that $\sigma^- = \tilde{\sigma}^-\exp(i\omega_p t)$, and similarly for $\tilde{a}_l$. The resulting equation is given by

$$\dot{\tilde{\sigma}}^- = -\hbar\Delta_a\tilde{\sigma}^- - i\hbar\sum_l g_l\tilde{a}_l u_l(\mathbf{r}), \tag{2.10}$$

where $\Delta_a = \omega_p - \omega_a$ is the atom-probe detuning. Within this rotating frame we will take $\dot{\tilde{\sigma}}^- \approx 0$ and thus obtain the following equation for the lowering operator

$$\sigma^- = -\frac{i}{\Delta_a}\sum_l g_l a_l u_l(\mathbf{r}). \tag{2.11}$$

Therefore, by inserting this expression into the Heisenberg equation for the light mode m given by

$$\dot{a}_m = -\sigma^- g_m u_m^*(\mathbf{r}) \tag{2.12}$$

we get the following equation of motion

$$\dot{a}_m = \frac{i}{\Delta_a} \sum_l g_l g_m u_l(\mathbf{r}) u_m^*(\mathbf{r}) a_l. \tag{2.13}$$

An effective Hamiltonian which results in the same optical equations of motion can be written as $\hat{H}_1^{\text{eff}} = \hat{H}_f + \hat{H}_{1,a}^{\text{eff}} + \hat{H}_{1,fa}^{\text{eff}}$. The effective atomic and interaction Hamiltonians are

$$\hat{H}_{1,a}^{\text{eff}} = \frac{\mathbf{p}^2}{2m_a} + V_{\text{cl}}(\mathbf{r}), \tag{2.14}$$

$$\hat{H}_{1,fa}^{\text{eff}} = \frac{\hbar}{\Delta_a} \sum_{l,m} u_l^*(\mathbf{r}) u_m(\mathbf{r}) g_l g_m a_l^\dagger a_m, \tag{2.15}$$

where we have explicitly extracted $V_{\text{cl}}(\mathbf{r}) = \hbar g_{\text{cl}}^2 |a_{\text{cl}} u_{\text{cl}}(\mathbf{r})|^2 / \Delta_{\text{cl},a}$, the classical trapping potential, from the interaction terms. However, we consider the trapping beam to be sufficiently detuned from the other light modes that we can neglect any scattering between them. A later inclusion of this scattered light would not be difficult due to the linearity of the dipoles we assumed.

Normally we will consider scattering of modes a_l much weaker than the field forming the lattice potential $V_{\text{cl}}(\mathbf{r})$. Therefore, we assume that the trapping is entirely due to the classical potential and the field operators $\Psi(\mathbf{r})$ can be expanded using localised Wannier functions of $V_{\text{cl}}(\mathbf{r})$. By keeping only the lowest vibrational state we get

$$\Psi(\mathbf{r}) = \sum_i^M b_i w(\mathbf{r} - \mathbf{r}_i), \tag{2.16}$$

where b_i ($b_i^\dagger$) is the annihilation (creation) operator of an atom at site i with coordinate $\mathbf{r}_i$, $w(\mathbf{r})$ is the lowest band Wannier function, and M is the number of lattice sites. Substituting this expression in Eq. (2.1) with $\hat{H}_{1,a} = \hat{H}_{1,a}^{\text{eff}}$ and $\hat{H}_{1,fa} = \hat{H}_{1,fa}^{\text{eff}}$ given by Eq. (2.14) and (2.15) respectively yields the following generalised Bose-Hubbard Hamiltonian, $\hat{H} = \hat{H}_f + \hat{H}_a + \hat{H}_{fa}$,

$$\hat{H} = \hat{H}_f + \sum_{m,n}^{M} J_{m,n}^{\text{cl}} b_m^\dagger b_n + \sum_{i,j,k,l}^{M} \frac{U_{ijkl}}{2} b_i^\dagger b_j^\dagger b_k b_l + \frac{\hbar}{\Delta_a} \sum_{l,m} g_l g_m a_l^\dagger a_m \left(\sum_{i,j}^{K} J_{i,j}^{l,m} b_i^\dagger b_j \right). \quad (2.17)$$

The optical field part of the Hamiltonian, $\hat{H}_f$, has remained unaffected by all our approximations and is given by Eq. (2.2). The matter-field Hamiltonian is now given by the well known Bose-Hubbard Hamiltonian

$$\hat{H}_a = \sum_{i,j}^{M} J_{i,j}^{\text{cl}} b_i^\dagger b_j + \sum_{i,j,k,l}^{M} \frac{U_{ijkl}}{2} b_i^\dagger b_j^\dagger b_k b_l, \quad (2.18)$$

where the first term represents atoms tunnelling between sites with a hopping rate given by

$$J_{i,j}^{\text{cl}} = \int \mathrm{d}^3\mathbf{r} w(\mathbf{r} - \mathbf{r}_i) \left(-\frac{\mathbf{p}^2}{2m_a} + V_{\text{cl}}(\mathbf{r}) \right) w(\mathbf{r} - \mathbf{r}_j), \quad (2.19)$$

and U_{ijkl} is the atomic interaction term given by

$$U_{ijkl} = \frac{4\pi a_s \hbar^2}{m_a} \int \mathrm{d}^3\mathbf{r} w(\mathbf{r} - \mathbf{r}_i) w(\mathbf{r} - \mathbf{r}_j) w(\mathbf{r} - \mathbf{r}_k) w(\mathbf{r} - \mathbf{r}_l). \quad (2.20)$$

Both integrals above depend on the overlap between Wannier functions corresponding to different lattice sites. This overlap decreases rapidly as the distance between sites increases. Therefore, in both cases we can simply neglect all terms but the one that corresponds to the most significant overlap. Thus, for $J_{i,j}^{\text{cl}}$ we will only consider i and j that correspond to nearest neighbours. Furthermore, since we will only be looking at lattices that have the same separation between all its nearest neighbours (e.g. cubic or square lattice) we can

define $J^{\mathrm{cl}}_{i,j} = -J$ (negative sign, because this way $J > 0$). For the inter-atomic interactions this simplifies to simply considering on-site collisions where $i = j = k = l$ and we define $U_{iiii} = U$. Finally, we end up with the canonical form for the Bose-Hubbard Hamiltonian

$$\hat{H}_a = -J \sum_{\langle i,j \rangle}^{M} b_i^\dagger b_j + \frac{U}{2} \sum_{i}^{M} \hat{n}_i(\hat{n}_i - 1), \tag{2.21}$$

where $\langle i, j \rangle$ denotes a summation over nearest neighbours and $\hat{n}_i = b_i^\dagger b_i$ is the atom number operator at site i.

Finally, we have the light-matter interaction part of the Hamiltonian given by

$$\hat{H}_{fa} = \frac{\hbar}{\Delta_a} \sum_{l,m} g_l g_m a_l^\dagger a_m \left(\sum_{i,j}^{K} J_{i,j}^{l,m} b_i^\dagger b_j \right), \tag{2.22}$$

where the coupling between the matter and optical fields is determined by the coefficients

$$J_{i,j}^{l,m} = \int \mathrm{d}^3\mathbf{r} w(\mathbf{r} - \mathbf{r}_i) u_l^*(\mathbf{r}) u_m(\mathbf{r}) w(\mathbf{r} - \mathbf{r}_j). \tag{2.23}$$

This contribution can be separated into two parts, one which couples directly to the on-site atomic density and one that couples to the tunnelling operators. We will define the operator

$$\hat{F}_{l,m} = \hat{D}_{l,m} + \hat{B}_{l,m}, \tag{2.24}$$

where $\hat{D}_{l,m}$ is the direct coupling to atomic density

$$\hat{D}_{l,m} = \sum_{i}^{K} J_{i,i}^{l,m} \hat{n}_i, \tag{2.25}$$

and $\hat{B}_{l,m}$ couples to the matter-field via the nearest-neighbour tunnelling operators

$$\hat{B}_{l,m} = \sum_{\langle i,j \rangle}^{K} J_{i,j}^{l,m} b_i^\dagger b_j, \tag{2.26}$$

where K denotes a sum over the illuminated sites and we neglect couplings beyond nearest neighbours for the same reason as before when deriving the matter Hamiltonian. Thus the interaction part of the Hamiltonian is given by

$$\hat{H}_{fa} = \frac{\hbar}{\Delta_a} \sum_{l,m} g_l g_m a_l^\dagger a_m \hat{F}_{l,m} \tag{2.27}$$

These equations encapsulate the simplicity and flexibility of the measurement scheme that we are proposing. The operators given above are entirely determined by the values of the $J_{i,j}^{l,m}$ coefficients and despite its simplicity, this is sufficient to give rise to a host of interesting phenomena via measurement backaction such as the generation of multipartite entangled spatial modes in an optical lattice [58, 91, 92], the appearance of long-range correlated tunnelling capable of entangling distant lattice sites, and in the case of fermions, the break-up and protection of strongly interacting pairs [93, 94]. Additionally, these coefficients are easy to manipulate experimentally by adjusting the optical geometry via the light mode functions $u_l(\mathbf{r})$.

It is important to note that we are considering a situation where the contribution of quantised light is much weaker than that of the classical trapping potential. If that was not the case, it would be necessary to determine the Wannier functions in a self-consistent way which takes into account the depth of the quantum potential generated by the quantised light modes. This significantly complicates the treatment, but can lead to interesting physics. Amongst other things, the atomic tunnelling and interaction coefficients will now depend on the quantum state of light [101].

Therefore, combining these final simplifications we finally arrive at our quantum light-matter Hamiltonian

$$\hat{H} = \hat{H}_f - J \sum_{\langle i,j \rangle}^{M} b_i^\dagger b_j + \frac{U}{2} \sum_{i}^{M} \hat{n}_i(\hat{n}_i - 1) + \frac{\hbar}{\Delta_a} \sum_{l,m} g_l g_m a_l^\dagger a_m \hat{F}_{l,m} - i \sum_{l} \kappa_l a_l^\dagger a_l, \tag{2.28}$$

where we have phenomenologically included the cavity decay rates κ_l of the modes a_l. A crucial observation about the structure of this Hamiltonian is that in the interaction term, the light modes a_l couple to the matter in a global way. Instead of considering individual coupling to each site, the optical field couples to the global state of the atoms within the illuminated region via the operator $\hat{F}_{l,m}$. This will have important implications for the system and is one of the leading factors responsible for many-body behaviour beyond the Bose-Hubbard Hamiltonian paradigm.

Furthermore, it is also vital to note that light couples to the matter via an operator, namely $\hat{F}_{l,m}$, which makes it sensitive to the quantum state of matter. This is a key element of our treatment of the ultimate quantum regime of light-matter interaction that goes beyond previous treatments.

2.3 The Bose-Hubbard Hamiltonian

2.3.1 The Model

The original Hubbard model was developed as a model for the motion of electrons within transition metals [102]. The key elements were the confinement of the motion to a lattice and the approximation of the Coulomb screening interaction as a simple on-site interaction. Despite these enormous simplifications the model was very successful [103]. The Bose-Hubbard model is an even simpler variation where instead of fermions we consider spinless bosons. It was originally devised as a toy model and applied to liquid helium [17], but in 1998 it was shown by Jaksch *et. al.* that it can be realised with ultracold atoms in an optical lattice [15]. Shortly afterwards it was obtained in a ground-breaking experiment [16]. The model has been the subject of intense research since then, because despite its simplicity it possesses highly nontrivial properties such as the superfluid to Mott insulator quantum phase

transition. Furthermore, it is one of the most controllable quantum many-body systems thus providing a solid basis for new experiments and technologies.

The model we have derived is essentially an extension of the well-known Bose-Hubbard model that also includes interactions with quantised light. Therefore, it should come as no surprise that if we eliminate all the quantised fields from the Hamiltonian we obtain exactly the Bose-Hubbard model

$$\hat{H}_a = -J \sum_{\langle i,j \rangle}^{M} b_i^\dagger b_j + \frac{U}{2} \sum_{i}^{M} \hat{n}_i(\hat{n}_i - 1). \tag{2.29}$$

The first term is the kinetic energy term and denotes the hopping of atoms between neighbouring sites at a hopping rate given by J. The second term describes the on-site repulsion which acts mainly to suppress multiple occupancies of any site, but at the same time it lies at the heart of strongly correlated phenomena in the Bose-Hubbard model. Unfortunately, despite its simplicity, this system is not solvable for any finite value U/J using known techniques in finite dimensions [104–106]. However, exact solutions exist for the ground state in the two limits of $U = 0$ and $J = 0$ which already provide some insight as they correspond to the two different phases of the quantum phase transition that is present in the model. In higher dimensions (e.g. two or three) the system is reasonably well described by a mean-field approximation which provides us with a good understanding of the full quantum phase diagram.

2.3.2 The Superfluid and Mott Insulator Ground States

Before trying to understand the quantum phase transition itself we will look at the ground states of the two extremal cases first and for simplicity we will consider only homogeneous systems with periodic boundary conditions here. We will begin with the $U = 0$ limit where the Hamiltonian's kinetic term can be diagonalised by transforming to momentum space

defined by the annihilation operator

$$b_{\mathbf{k}} = \frac{1}{\sqrt{M}} \sum_m b_m e^{i\mathbf{k}\cdot\mathbf{r}_m}, \tag{2.30}$$

where $\mathbf{k}$ denotes the wave vector running over the first Brillouin zone. The Hamiltonian then is given by

$$\hat{H}_a = \sum_{\mathbf{k}} \varepsilon_{\mathbf{k}} b_{\mathbf{k}}^\dagger b_{\mathbf{k}}, \tag{2.31}$$

where the free particle dispersion is

$$\varepsilon_{\mathbf{k}} = -2J \sum_{d=1}^{D} \cos(k_d a), \tag{2.32}$$

and d denotes the dimension out of a total of D dimensions. It should now be obvious that the ground state is simply the state with all the atoms in the $\mathbf{k} = 0$ state and thus it is given by

$$|\Psi_{\mathrm{SF}}\rangle = \frac{(b_{\mathbf{k}=0}^\dagger)^N}{\sqrt{N!}}|0\rangle = \frac{1}{\sqrt{N!}} \left(\frac{1}{\sqrt{M}} \sum_m^M b_m^\dagger \right)^N |0\rangle, \tag{2.33}$$

where $|0\rangle$ denotes the vacuum state. This state is called a superfluid (SF) due to its viscous-free flow properties [107]. The macroscopic occupancy of the single-particle ground state is the signature and defining property of a Bose-Einstein condensate. Note that the zero momentum states consist of a superposition of an atom at all the sites of the optical lattice highlighting the fact that kinetic energy is minimised by delocalising the particles. This in turn implies that a superfluid state will have infinite range correlations. It is also important to note that in the thermodynamic limit the superfluid state is gapless, i.e. it takes zero energy to excite the system.

At the other end of the spectrum, i.e. $J = 0$, the kinetic term vanishes and the system is dominated by the on-site interactions. This has the effect of decoupling the Hamiltonian into a sum of identical single-site Hamiltonians which are already diagonal in the atom number

basis. Therefore, the ground state for $N = gM$, where g is an integer, is given by

$$|\Psi_{\mathrm{MI}}\rangle = \prod_{m}^{M} \frac{1}{\sqrt{g!}} (b_m^\dagger)^g |0\rangle. \tag{2.34}$$

This state has precisely the same number of bosons, g, at each site and is commonly known as the Mott insulator (MI). Unlike in the superfluid state, the atoms are all localised to a specific lattice site and thus not only are there no long-range correlations, there are actually no two-site correlations in this state at all. Additionally, this state is gapped, i.e. it costs a finite amount of energy to excite the system into its lowest excited state even in the thermodynamic limit. In fact, the existence of the gap is the defining property that distinguishes the Mott insulator from the superfluid in the Bose-Hubbard model. Note that we have only considered a commensurate case (number of atoms an integer multiple of the number of sites). If we were to insert another atom on top of the Mott insulator, the energy of the system would not depend on the lattice site in which it is inserted. This implies that as soon as J becomes finite, the ground state would prefer this atom be delocalised and effectively becomes gapless which means the system is a superfluid and it will not exhibit a quantum phase transition.

2.3.3 Mean-Field Theory

Now that we have a basic understanding of the two limiting cases we can now consider the model in between these two extremes. We have already mentioned that an exact solution is not known, but fortunately a very good mean-field approximation exists [17]. In this approach the interaction term is treated exactly, but the kinetic energy term is decoupled as

$$b_m^\dagger b_n = \langle b_m^\dagger \rangle b_n + b_m^\dagger \langle b_n \rangle - \langle b_m^\dagger \rangle \langle b_n \rangle = \Phi^* b_n + \Phi b_m^\dagger - |\Phi|^2, \tag{2.35}$$

where the expectation values are for the $T = 0$ ground state. Note that we have assumed that $\Phi = \langle b_m \rangle$ is non-zero and homogeneous. Φ describes the influence of hopping between

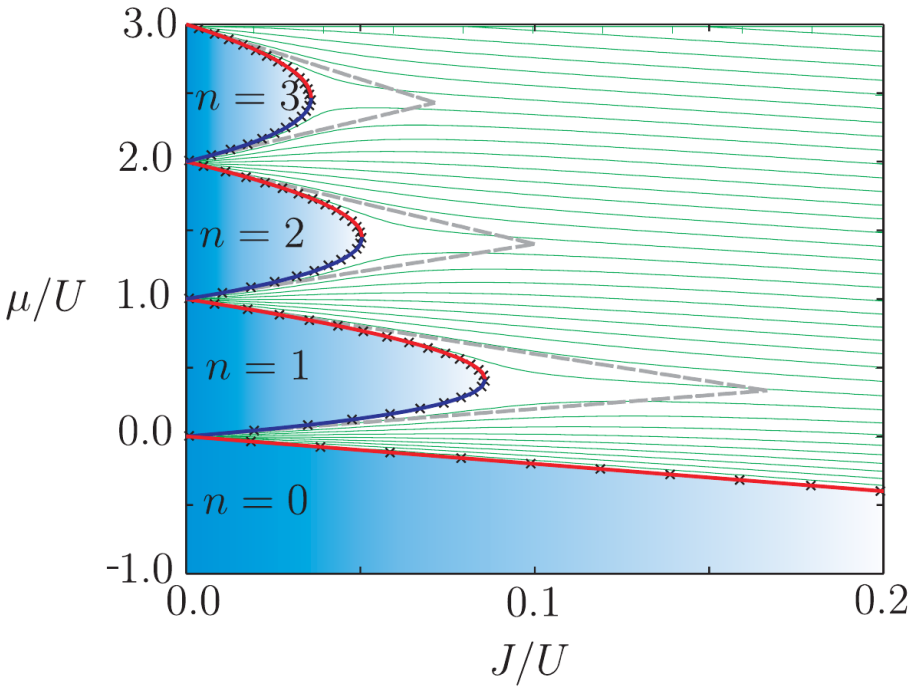

Fig. 2.2 Mean-field phase diagram of the Bose-Hubbard model in 1D, i.e. $z = 2$, from Ref. [108]. The shaded regions are the Mott insulator lobes and each lobe corresponds to a different on-site filling labelled by n. The rest of the space corresponds to the superfluid phase. The dashed lines are the phase boundaries obtained from first-order perturbation theory. The solid lines are lines of constant density in the superfluid phase.

neighbouring sites and is the mean -field order parameter. This decoupling effect means that we can write the Hamiltonian as $\hat{H}_a = \sum_m^M \hat{h}_a$, where

$$\hat{h}_a = -zJ(\Phi b^\dagger + \Phi^* b) + zJ|\Phi|^2 + \frac{U}{2}\hat{n}(\hat{n}-1) - \mu\hat{n}, \tag{2.36}$$

and z is the coordination number, i.e. the number of nearest neighbours of a single site. We have also introduced the chemical potential μ since we now consider the grand canonical ensemble as the Hamiltonian no longer conserves the total atom number. The ground state of the $|\Psi_0\rangle$ of the overall system will be a site-wise product of the individual ground states of $\hat{h}_a$. These can be found very easily using standard diagonalisation techniques where Φ is self-consistently determined by minimising the energy of the ground state with respect to Φ.

The main advantage of the mean-field treatment is that it lets us study the quantum phase transition between the superfluid and Mott insulator phases discussed in the previous sections. The phase boundaries can be obtained from second-order perturbation theory as

$$\left(\frac{\mu}{U}\right)_{\pm} = \frac{1}{2}\left[2g - 1 - \left(\frac{zJ}{U}\right) \pm \sqrt{1 - 2(2g+1)\left(\frac{zJ}{U}\right) + \left(\frac{zJ}{U}\right)^2}\right]. \tag{2.37}$$

This yields a phase diagram with multiple Mott insulating lobes as seen in Fig. 2.2 where each lobe represents a Mott insulator with a different number of atoms per site. The tip of the lobe which corresponds to the quantum phase transition along a line of fixed density is obtained by equating the two branches of the above equation to get

$$\left(\frac{J}{U}\right) = \frac{1}{z(2g+1+\sqrt{4g^2+4g})}. \tag{2.38}$$

It is important to note that the fact that this formalism predicts a phase transition is in contrast to other mean-field theories such as the Bogoliubov approximation [4]. This highlights the fact that the interactions, which are treated exactly here, are the dominant driver leading to this phase transition and other strongly correlated effects in the Bose-Hubbard model.

2.3.4 The Bose-Hubbard Model in One Dimension

The mean-field theory in the previous section is very useful tool for studying the quantum phase transition in the Bose-Hubbard model. However, it is effectively an infinite-dimensional theory and in practice it only works in two dimensions or more. The phase transition in 1D is poorly described, because it actually belongs to a different universality class [109–113]. This is clearly seen from the one dimensional phase diagram shown in Fig. 2.3.

Some general conclusions can be obtained by looking at Haldane's prescription for Luttinger liquids [114, 115]. Without a periodic potential the low-energy physics of the

system is described by the Hamiltonian

$$\hat{H}_a = \frac{1}{2\pi}\int \mathrm{d}x \left\{ vK[\hat{\Pi}(x)]^2 + \frac{v}{K}[\partial_x \hat{\Phi}(x)]^2 \right\}, \tag{2.39}$$

where we have expressed the bosonic field operators in terms of a density operator $\hat{\rho}(x)$ and a phase operator $\hat{\Phi}(x)$ as $\hat{\Psi}(x) = \sqrt{\hat{\rho}(x)}e^{i\hat{\Phi}(x)}$ and $\hat{\Pi}(x)$ is the density fluctuation operator. Provided the parameters v and K can be correctly determined this Hamiltonian gives the correct description of the gapless superfluid phase of the Bose-Hubbard model. Most importantly it gives an expression for the spatial correlation functions such as

$$\langle b_i^\dagger b_j \rangle = A\left(\frac{\alpha}{|i-j|}\right)^{K/2}, \tag{2.40}$$

where A is some amplitude and α is a necessary cutoff to regularise the theory at short distances. Unlike the superfluid ground state in Eq. (2.33) this state does not have infinite range correlations. They decay according to a power-law. However, for non-interacting systems $K = 0$ and long-range order is re-established as before though it is important to note that in higher dimensions this long-range order persists in the whole superfluid phase even with interactions present.

In order to describe the phase transition and the Mott insulating phase it is necessary to introduce a periodic lattice potential. It can be shown that this system exhibits at $T = 0$ a Berezinskii-Kosterlitz-Thouless phase transition as the parameter K is varied with a critical point at $K_c = \frac{1}{2}$ where $K < \frac{1}{2}$ is a superfluid. Above $K = \frac{1}{2}$ the value of K jumps discontinuously to $K \to \infty$ producing the Mott insulator phase. Unlike the gapless superfluid phase the spatial correlations decay exponentially as

$$\langle b_i^\dagger b_j \rangle = Be^{-|i-j|/\xi}, \tag{2.41}$$

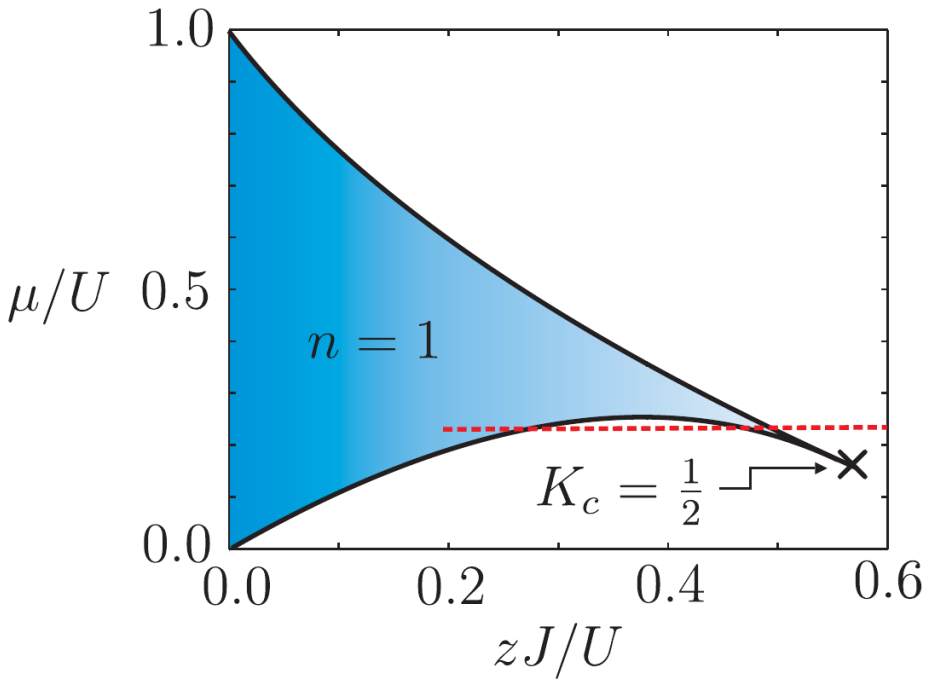

Fig. 2.3 Exact phase diagram of the Bose-Hubbard model in 1D, i.e. $z = 2$, from Ref. [108]. The shaded region corresponds to the $n = 1$ Mott insulator lobe. The sharp tip distinguishes it from the mean-field phase diagram. The red dotted line denotes the reentrant phase transition which occurs for a fixed μ.The critical point for the fixed density $n = 1$ transition is denoted by an 'x'.

where B is some constant and the correlation length is given by $\xi = v/\Delta$ where Δ is the energy gap.

Using advanced numerical methods such as density matrix renormalisation group (DMRG) calculations it is possible to identify the critical point by fitting the power-law decay correlations in order to obtain K. The resulting phase transition is shown in Fig. 2.3 and the critical point was shown to be $(U/zJ) = 1.68$. Note that unusually the phase diagram exhibits a reentrant phase transition for a fixed μ.

2.4 Scattered light behaviour

Having derived the full quantum light-matter Hamiltonian we will now look at the behaviour of the scattered light. We begin by looking at the equations of motion in the Heisenberg

picture

$$\dot{a}_l = \frac{i}{\hbar}[\hat{H}, a_l] = -i\left(\omega_l + U_{l,l}\hat{F}_{1,1}\right)a_l - i\sum_{m\neq l} U_{l,m}\hat{F}_{l,m}a_m - \kappa_l a_l + \eta_l, \tag{2.42}$$

where we have defined $U_{l,m} = g_l g_m/\Delta_a$. By considering the steady state solution in the frame rotating with the probe frequency ω_p we can show that the stationary solution is given by

$$a_l = \frac{\sum_{m\neq l} U_{l,m}a_m\hat{F}_{l,m} + i\eta_l}{(\Delta_{lp} - U_{l,l}\hat{F}_{l,l}) + i\kappa_l}, \tag{2.43}$$

where $\Delta_{lp} = \omega_p - \omega_l$ is the detuning between the probe beam and the light mode a_l. This equation gives us a direct relationship between the light operators and the atomic operators. In the stationary limit, the quantum state of the light field adiabatically follows the quantum state of matter.

The above equation is quite general as it includes an arbitrary number of light modes which can be pumped directly into the cavity or produced via scattering from other modes. To simplify the equation slightly we will neglect the cavity resonance shift, $U_{l,l}\hat{F}_{l,l}$ which is possible provided the cavity decay rate and/or probe detuning are large enough. We will also only consider probing with an external coherent beam, a_0 with mode function $u_0(\mathbf{r})$, and thus we neglect any cavity pumping η_l. We also limit ourselves to only a single scattered mode, a_1 with a mode function $u_1(\mathbf{r})$. This leads to a simple linear relationship between the light mode and the atomic operator $\hat{F}_{1,0}$

$$a_1 = \frac{U_{1,0}a_0}{\Delta_p + i\kappa}\hat{F} = C\hat{F}, \tag{2.44}$$

where we have defined $C = U_{1,0}a_0/(\Delta_p + i\kappa)$ which is essentially the Rayleigh scattering coefficient into the cavity. Furthermore, since there is no longer any ambiguity in the indices l and m, we have dropped indices on $\Delta_{1p} \equiv \Delta_p$, $\kappa_1 \equiv \kappa$, and $\hat{F}_{1,0} \equiv \hat{F}$. We also do the same for the operators $\hat{D}_{1,0} \equiv \hat{D}$, $\hat{B}_{1,0} \equiv \hat{B}$, and the coefficients $J^{1,0}_{i,j} \equiv J_{i,j}$. We will adhere to this convention from now on.

The operator a_1 itself is not an observable. However, it is possible to combine the outgoing light field with a stronger local oscillator beam in order to measure the light quadrature

$$\hat{X}_\phi = \frac{1}{2}\left(a_1 e^{-i\phi} + a_1^\dagger e^{i\phi}\right), \tag{2.45}$$

which in turn can expressed via the quadrature of $\hat{F}$, $\hat{X}_\beta^F$, as

$$\hat{X}_\phi = |C|\hat{X}_\beta^F = \frac{|C|}{2}\left(\hat{F}e^{-i\beta} + \hat{F}^\dagger e^{i\beta}\right), \tag{2.46}$$

where $\beta = \phi - \phi_C$, $C = |C|\exp(i\phi_C)$, and ϕ is the local oscillator phase.

Whilst the light amplitude and the quadratures are only linear in atomic operators, we can easily have access to higher moments via related quantities such as the photon number $a_1^\dagger a_1 = |C|^2\hat{F}^\dagger\hat{F}$ or the quadrature variance

$$(\Delta X_\phi)^2 = \langle\hat{X}_\phi^2\rangle - \langle\hat{X}_\phi\rangle^2 = \frac{1}{4} + |C|^2(\Delta X_\beta^F)^2, \tag{2.47}$$

which reflect atomic correlations and fluctuations.

Finally, even though we only consider a single scattered mode, this model can be applied to free space by simply varying the direction of the scattered light mode if multiple scattering events can be neglected. This is likely to be the case since the interactions will be dominated by photons scattering from the much larger coherent probe.

2.5 Density and Phase Observables[1]

Light scatters due to its interactions with the dipole moment of the atoms which for off-resonant light, like the type that we consider, results in an effective coupling with atomic density, not the matter-wave amplitude. Therefore, it is challenging to couple light to the

[1]The results of this section were first published in Ref. [90]

phase of the matter-field as is typical in quantum optics for optical fields. Most of the existing work on measurement couples directly to atomic density operators [19, 32, 40, 63, 64]. However, it has been shown that one can couple to the interference term between two condensates (e.g. a BEC in a double-well) by using interference measurements [54–56, 116, 117]. Such measurements establish a relative phase between the condensates even though the two components have initially well-defined atom numbers which is phase's conjugate variable. In a lattice geometry, one would ideally measure between two sites similarly to single-site addressing [118, 119], which would measure a single term $\langle b_i^\dagger b_{i+1} + b_i b_{i+1}^\dagger \rangle$. This could be achieved, for example, by superposing a deeper optical lattice shifted by $d/2$ with respect to the original one, catching and measuring the atoms in the new lattice sites. However, a single-shot success rate of atom detection will be small and as single-site addressing is challenging, we proceed with our global scattering scheme.

In our model light couples to the operator $\hat{F}$ which consists of a density component, $\hat{D} = \sum_i J_{i,i}\hat{n}_i$, and a phase component, $\hat{B} = \sum_{\langle i,j \rangle} J_{i,j} b_i^\dagger b_j$. In general, the density component dominates, $\hat{D} \gg \hat{B}$, and thus $\hat{F} \approx \hat{D}$ [19]. Physically, this is a consequence of the fact that there are more atoms to scatter light at the lattice sites than in between them. However, it is possible to engineer an optical geometry in which $\hat{D} = 0$ leaving $\hat{B}$ as the dominant term in $\hat{F}$. This approach is fundamentally different from the aforementioned double-well proposals as it directly couples to the interference terms caused by atoms tunnelling rather than combining light scattered from different sources. Furthermore, it is not limited to a double-well setup and naturally extends to a lattice structure which is a key advantage. Such a counter-intuitive configuration may affect works on quantum gases trapped in quantum potentials [19, 85, 101, 120–123] and quantum measurement-induced preparation of many-body atomic states [57, 91, 93, 124].

For clarity we will consider a 1D lattice as shown in Fig. 2.1 with lattice spacing d along the x-axis direction, but the results can be applied and generalised to higher dimensions.

Central to engineering the $\hat{F}$ operator are the coefficients $J_{i,j}$ given by

$$J_{i,j} = \int \mathrm{d}x \; w(x-x_i)u_1^*(x)u_0(x)w(x-x_j). \tag{2.48}$$

The operators $\hat{B}$ and $\hat{D}$ depend on the values of $J_{i,i+1}$ and $J_{i,i}$ respectively. These coefficients are determined by the convolution of the coupling strength between the probe and scattered light modes, $u_1^*(x)u_0(x)$, with the relevant Wannier function overlap shown in Fig. 2.5a. For the $\hat{B}$ operator we calculate the convolution with the nearest neighbour overlap, $W_1(x) \equiv w(x-d/2)w(x+d/2)$, and for the $\hat{D}$ operator we calculate the convolution with the square of the Wannier function at a single site, $W_0(x) \equiv w^2(x)$. Therefore, in order to enhance the $\hat{B}$ term we need to maximise the overlap between the light modes and the nearest neighbour Wannier overlap, $W_1(x)$. This can be achieved by concentrating the light between the sites rather than at the positions of the atoms.

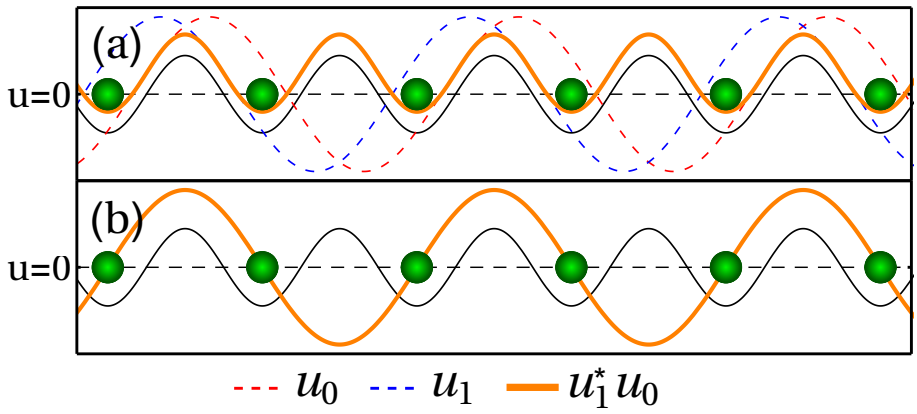

Fig. 2.4 Light field arrangements which maximise coupling, $u_1^*u_0$, between lattice sites. The thin black line indicates the trapping potential (not to scale). (a) Arrangement for the uniform pattern $J_{i,i+1} = J_1$. (b) Arrangement for spatially varying pattern $J_{i,i+1} = (-1)^i J_2$; here $u_0 = 1$ so it is not shown and u_1 is real thus $u_1^*u_0 = u_1$.

In order to calculate the $J_{i,j}$ coefficients we perform numerical calculations using realistic Wannier functions [125]. However, it is possible to gain some analytic insight into the behaviour of these values by looking at the Fourier transforms of the Wannier function

overlaps, $\mathcal{F}[W_{0,1}](k)$, shown in Fig. 2.5b. This is because for plane and standing wave light modes the product $u_1^*(x)u_0(x)$ can be in general decomposed into a sum of oscillating exponentials of the form e^{ikx} making the integral in Eq. (2.48) a sum of Fourier transforms of $W_{0,1}(x)$. We consider both the detected and probe beam to be standing waves which gives the following expressions for the $\hat{D}$ and $\hat{B}$ operators

$$\begin{aligned}\hat{D} =& \frac{1}{2}[\mathcal{F}[W_0](k_-)\sum_i \hat{n}_i \cos(k_- x_i + \varphi_-) \\ &+ \mathcal{F}[W_0](k_+)\sum_i \hat{n}_i \cos(k_+ x_i + \varphi_+)], \\ \hat{B} =& \frac{1}{2}[\mathcal{F}[W_1](k_-)\sum_i \hat{B}_i \cos(k_- x_i + \frac{k_- d}{2} + \varphi_-) \\ &+ \mathcal{F}[W_1](k_+)\sum_i \hat{B}_i \cos(k_+ x_i + \frac{k_+ d}{2} + \varphi_+)],\end{aligned} \tag{2.49}$$

where $k_\pm = k_{0x} \pm k_{1x}$, $k_{(0,1)x} = k_{0,1}\sin(\theta_{0,1})$, $\hat{B}_i = b_i^\dagger b_{i+1} + b_i b_{i+1}^\dagger$, and $\varphi_\pm = \varphi_0 \pm \varphi_1$. The key result is that the $\hat{B}$ operator is phase shifted by $k_\pm d/2$ with respect to the $\hat{D}$ operator since it depends on the amplitude of light in between the lattice sites and not at the positions of the atoms allowing to decouple them at specific angles.

The simplest case is to find a diffraction maximum where $J_{i,i+1} = J^B_{\max}$, where $J^B_{\max}$ is a constant. This results in a diffraction maximum where each bond (inter-site term) scatters light in phase and the operator is given by

$$\hat{B}_{\max} = J^B_{\max}\sum_i^K \hat{B}_i. \tag{2.50}$$

This can be achieved by crossing the light modes such that $\theta_0 = -\theta_1$ and $k_{0x} = k_{1x} = \pi/d$ and choosing the light mode phases such that $\varphi_+ = 0$. Fig. 2.4a shows the resulting light mode functions and their product along the lattice and Fig. 2.5c shows the value of the $J_{i,j}$ coefficients under these circumstances. In order to make the $\hat{B}$ contribution to light scattering

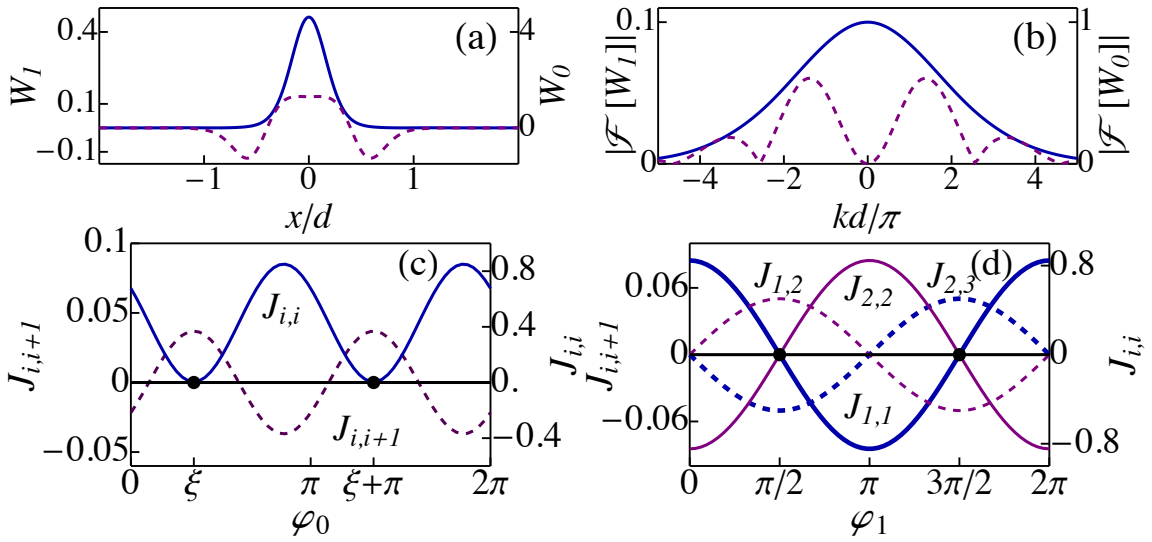

Fig. 2.5 The Wannier function products: (a) $W_0(x)$ (solid line, right axis), $W_1(x)$ (dashed line, left axis) and their (b) Fourier transforms $\mathcal{F}[W_{0,1}]$. The Density $J_{i,i}$ and matter-interference $J_{i,i+1}$ coefficients in diffraction maximum (c) and minimum (d) as are shown as functions of standing wave shifts φ or, if one were to measure the quadrature variance $(\Delta X^F_\beta)^2$, the local oscillator phase β. The black points indicate the positions, where light measures matter interference $\hat{B} \neq 0$, and the density-term is suppressed, $\hat{D} = 0$. The trapping potential depth is approximately 5 recoil energies.

dominant we need to set $\hat{D} = 0$ which from Eq. (2.49) we see is possible if

$$\xi \equiv \varphi_0 = -\varphi_1 = \frac{1}{2}\arccos\left[\frac{-\mathcal{F}[W_0](2\pi/d)}{\mathcal{F}[W_0](0)}\right]. \tag{2.51}$$

Under these conditions, the coefficient $J^B_{\max}$ is simply given by $J^B_{\max} = \mathcal{F}[W_1](2\pi/d)$. This arrangement of light modes maximizes the interference signal, $\hat{B}$, by suppressing the density signal, $\hat{D}$, via interference compensating for the spreading of the Wannier functions.

Another possibility is to obtain an alternating pattern similar corresponding to a diffraction minimum where each bond scatters light in anti-phase with its neighbours giving

$$\hat{B}_{\min} = J^B_{\min}\sum_i^K (-1)^i \hat{B}_i, \tag{2.52}$$

where $J^B_{\min}$ is a constant. We consider an arrangement where the beams are arranged such that $k_{0x} = 0$ and $k_{1x} = \pi/d$ which gives the following expressions for the density and interference terms

$$\begin{aligned}\hat{D} =& \mathcal{F}[W_0]\left(\frac{\pi}{d}\right)\sum_i (-1)^i \hat{n}_i \cos(\varphi_0)\cos(\varphi_1)\\ \hat{B} =& -\mathcal{F}[W_1]\left(\frac{\pi}{d}\right)\sum_i (-1)^i \hat{B}_i \cos(\varphi_0)\sin(\varphi_1).\end{aligned} \tag{2.53}$$

For $\varphi_0 = 0$ the corresponding $J_{i,j}$ coefficients are given by $J_{i,i+1} = (-1)^i J^B_{\min}$, where $J^B_{\min} = -\mathcal{F}[W_1](\pi/d)$, and are shown in Fig. 2.5d. The light mode coupling along the lattice is shown in Fig. 2.4b. It is clear that for $\varphi_1 = \pm\pi/2$, $\hat{D} = 0$, which is intuitive as this places the lattice sites at the nodes of the mode $u_1(x)$. This is a diffraction minimum as the light amplitude is also zero, $\langle\hat{B}\rangle = 0$, because contributions from alternating inter-site regions interfere destructively. However, the intensity $\langle a_1^\dagger a\rangle = |C|^2\langle\hat{B}^2\rangle$ is proportional to the variance of $\hat{B}$ and is non-zero.

Alternatively, one can use the arrangement for a diffraction minimum described above, but use travelling instead of standing waves for the probe and detected beams and measure the light quadrature variance. In this case $\hat{X}^F_\beta = \hat{D}\cos(\beta) + \hat{B}\sin(\beta)$ and by varying the local oscillator phase, one can choose which conjugate operator to measure.

2.6 Electric Field Strength[2]

The electric field operator at position $\mathbf{r}$ and at time t is usually written in terms of its positive and negative components:

$$\hat{\mathbf{E}}(\mathbf{r},t) = \hat{\mathbf{E}}^{(+)}(\mathbf{r},t) + \hat{\mathbf{E}}^{(-)}(\mathbf{r},t), \tag{2.54}$$

[2]The derivation has not been published before, but the final numerical results were included in Ref. [90]

where

$$\hat{\mathbf{E}}^{(+)}(\mathbf{r},t) = \sum_{\mathbf{k}} \hat{\boldsymbol{\varepsilon}}_{\mathbf{k}} \mathcal{E}_{\mathbf{k}} a_{\mathbf{k}} e^{-i\omega_{\mathbf{k}} t + i\mathbf{k}\cdot\mathbf{r}}, \tag{2.55a}$$

$$\hat{\mathbf{E}}^{(-)}(\mathbf{r},t) = \sum_{\mathbf{k}} \hat{\boldsymbol{\varepsilon}}_{\mathbf{k}} \mathcal{E}_{\mathbf{k}} a_{\mathbf{k}}^{\dagger} e^{i\omega_{\mathbf{k}} t - i\mathbf{k}\cdot\mathbf{r}}, \tag{2.55b}$$

$\hat{\boldsymbol{\varepsilon}}_{\mathbf{k}}$ is a unit polarization vector, $\mathbf{k}$ is the wave vector, $\mathcal{E}_{\mathbf{k}} = \sqrt{\hbar\omega_{\mathbf{k}}/2\varepsilon_0 V}$, ε_0 is the free space permittivity, V is the quantisation volume and $a_{\mathbf{k}}$ and $a_{\mathbf{k}}^{\dagger}$ are the annihilation and creation operators respectively of a photon in mode $\mathbf{k}$, and $\omega_{\mathbf{k}}$ is the angular frequency of mode $\mathbf{k}$.

In Ref. [21] it was shown that the operator $\hat{\mathbf{E}}^{(+)}(\mathbf{r},t)$ due to light scattering from a single atom located at $\mathbf{r}'$ at the observation point $\mathbf{r}$ is given by

$$\hat{\mathbf{E}}^{(+)}(\mathbf{r},\mathbf{r}',t) = \frac{\omega_a^2 d_A \sin\eta}{4\pi\varepsilon_0 c^2 |\mathbf{r}-\mathbf{r}'|} \hat{\varepsilon}\sigma^{-}\left(\mathbf{r}', t - \frac{|\mathbf{r}-\mathbf{r}'|}{c}\right), \tag{2.56}$$

with a similar expression for $\mathbf{E}^{(-)}(\mathbf{r},\mathbf{r}',t)$. Eq. (2.56) is valid only in the far field, η is the angle the dipole makes with $\mathbf{r}-\mathbf{r}'$, $\hat{\varepsilon}$ is the polarization vector which is perpendicular to $\mathbf{r}-\mathbf{r}'$ and lies in the plane defined by $\mathbf{r}-\mathbf{r}'$ and the dipole, ω_a is the atomic transition frequency, and d_A is the dipole matrix element between the two levels, and c is the speed of light in vacuum.

We have already derived an expression for the atomic lowering operator, σ^{-}, in Eq. (2.11) and it is given by

$$\sigma^{-}(\mathbf{r},t) = -\frac{i}{\Delta_a} \sum_{\mathbf{k}} g_{\mathbf{k}} a_{\mathbf{k}}(t) u_{\mathbf{k}}(\mathbf{r}). \tag{2.57}$$

We will want to substitute this expression into Eq. (2.56), but first we note that in the setup we consider the coherent probe will be much stronger than the scattered modes. This in turn implies that the expression for σ^{-} will be dominated by this external probe. Therefore, we drop the sum and consider only a single wave vector, $\mathbf{k}_0$, of the dominant contribution from the external beam corresponding to the mode a_0.

We now use the definition of the atom-light coupling constant [21] to make the substitution $g_0 a_0 = -i\Omega_0 e^{-i\omega_0 t}/2$, where Ω_0 is the Rabi frequency for the probe-atom system. We now evaluate the polarisation operator at the retarded time

$$\sigma^- \left(\mathbf{r}', t - \frac{|\mathbf{r} - \mathbf{r}'|}{c} \right) = -\frac{\Omega_0}{2\Delta_a} u_0(\mathbf{r}') \exp\left[-i\omega_0 \left(t - \frac{|\mathbf{r} - \mathbf{r}'|}{c} \right) \right]. \tag{2.58}$$

We are considering observation in the far field regime so $|\mathbf{r} - \mathbf{r}'| \approx r - \hat{\mathbf{r}} \cdot \mathbf{r}'$. We also consider the incoming, $\mathbf{k}_0$, and the outgoing, $\mathbf{k}_1$, waves to be of the same wavelength, $|\mathbf{k}_0| = |\mathbf{k}_1| = k = \omega_0/c$, hence $(\omega_0/c)|\mathbf{r} - \mathbf{r}'| \approx k(r - \hat{\mathbf{r}} \cdot \mathbf{r}') = \mathbf{k}_1 \cdot (\mathbf{r} - \mathbf{r}')$ and

$$\sigma^- \left(\mathbf{r}', t - \frac{|\mathbf{r} - \mathbf{r}'|}{c} \right) \approx -\frac{\Omega_0}{2\Delta_a} u_0(\mathbf{r}') \exp\left[i\mathbf{k}_1 \cdot (\mathbf{r} - \mathbf{r}') - i\omega_0 t \right]. \tag{2.59}$$

The many-body version of the electric field operator is given by

$$\hat{\mathbf{E}}_N^{(+)}(\mathbf{r}, t) = \int \mathrm{d}^3\mathbf{r}' \Psi^\dagger(\mathbf{r}') \hat{\mathbf{E}}^{(+)}(\mathbf{r}, \mathbf{r}', t) \Psi(\mathbf{r}'), \tag{2.60}$$

where $\Psi(\mathbf{r})$ is the atomic matter-field operator. As before, we expand this field operator using localized Wannier functions corresponding to the lattice potential and keeping only the lowest vibrational state at each site: $\Psi(\mathbf{r}) = \sum_i b_i w(\mathbf{r} - \mathbf{r}_i)$, where b_i is the annihilation operator of an atom at site i with the coordinate $\mathbf{r}_i$. Thus, the relevant many-body operator is

$$\hat{\mathbf{E}}_N^{(+)}(\mathbf{r}, t) = \hat{\varepsilon} C_E \sum_{i,j}^{K} b_i^\dagger b_j \int \mathrm{d}^3\mathbf{r}' w^*(\mathbf{r}' - \mathbf{r}_i) \frac{u_0(\mathbf{r}')}{|\mathbf{r} - \mathbf{r}'|} e^{i\mathbf{k}_1 \cdot (\mathbf{r} - \mathbf{r}') - i\omega_0 t} w(\mathbf{r}' - \mathbf{r}_j), \tag{2.61a}$$

$$C_E = -\frac{\omega_a^2 \Omega_0 d \sin\eta}{8\pi\varepsilon_0 c^2 \Delta_a} \tag{2.61b}$$

where K is the number of illuminated sites. We now assume that the lattice is deep and that the light scattering occurs on time scales much shorter than atom tunnelling. Therefore, we ignore all terms for which $i \neq j$ and the remaining integrals become $\int \mathrm{d}^3\mathbf{r}_0 w^*(\mathbf{r}_0 -$

$\mathbf{r}_i) f(\mathbf{r}) w(\mathbf{r}_0 - \mathbf{r}_i) = f(\mathbf{r}_i)$. The final form of the many body operator is then

$$\hat{\mathbf{E}}_N^{(+)}(\mathbf{r},t) = \hat{\varepsilon} C_E \sum_{j=1}^{K} \hat{n}_j \frac{u_0(\mathbf{r}_j)}{|\mathbf{r}-\mathbf{r}_j|} e^{i\mathbf{k}_1\cdot(\mathbf{r}-\mathbf{r}_j)-i\omega_0 t}, \tag{2.62}$$

where $\hat{n}_i = b_i^\dagger b_i$ is the atom number operator at site i. We will now consider the incoming probe to be a plane wave, $u_0(\mathbf{r}) = e^{i\mathbf{k}_0\cdot\mathbf{r}}$, and we approximate $|\mathbf{r}-\mathbf{r}_j| \approx r$ in the denominator. Thus,

$$\mathbf{E}_N^{(+)}(\mathbf{r},t) = \hat{\varepsilon} C_E \frac{e^{ikr-i\omega_0 t}}{r} \sum_{j=1}^{K} \hat{n}_j e^{i(\mathbf{k}_0-\mathbf{k}_1)\cdot\mathbf{r}_j}. \tag{2.63}$$

We note that this is exactly the same form of the optical field as derived from a generalised Bose-Hubbard model which considers a fully quantum light-matter interaction Hamiltonian [29, 30, 19]. We can even express the result in terms of the $\hat{D} = \sum_j^K u_1^*(\mathbf{r}_j) u_0(\mathbf{r}_j) \hat{n}_j$ formalism used in those works

$$\mathbf{E}_N^{(+)}(\mathbf{r},t) = \hat{\varepsilon} C_E \frac{e^{ikr-i\omega_0 t}}{r} \hat{D}. \tag{2.64}$$

The average light intensity at point $\mathbf{r}$ at time t is given by the formula $I = c\varepsilon_0 |E|^2/2$ and yields

$$\langle I(\mathbf{r},t)\rangle = c\varepsilon_0 \langle E^{(-)}(\mathbf{r},t) E^{(+)}(\mathbf{r},t)\rangle = \frac{c\varepsilon_0}{r^2} C_E^2 \langle \hat{D}^* \hat{D}\rangle. \tag{2.65}$$

The scattering is dominated by a uniform background for which $\langle \hat{D}^* \hat{D}\rangle \approx N_K$ for a superfluid [19], where N_K is the mean number of atoms in the illuminated volume. Thus, the approximate number of photons scattered per second can be obtained by integrating over a sphere

$$n_\Phi = \frac{4\pi c \varepsilon_0}{3\hbar\omega_a} \left(\frac{\omega_a^2 \Omega_0 d}{8\pi\varepsilon_0 c^2 \Delta_a} \right)^2 N_K. \tag{2.66}$$

In the Weisskopf-Wigner approximation it can be shown [21] that for a two level system the decay constant, Γ, is

$$\Gamma = \frac{\omega_a^3 d^2}{3\pi\varepsilon_0 \hbar c^3}. \tag{2.67}$$

Value	Miyake *et al.*	Weitenberg *et al.*
ω_a	$2\pi \cdot 384$ THz	
Γ	$2\pi \cdot 6.07$ MHz	
Δ_a	$2\pi \cdot 30$ MHz	$2\pi \cdot 85$ MHz
I	4250 Wm^{-2}	N/A
Ω_0	293×10^6 s^{-1}	42.5×10^6 s^{-1}
N_K	10^5	147
n_Φ	6×10^{11} s^{-1}	2×10^6 s^{-1}

Table 2.1 Experimental parameters used in estimating the photon scattering rates.

Therefore, we can now express the quantity n_Φ as

$$n_\Phi = \frac{1}{8}\left(\frac{\Omega_0}{\Delta_a}\right)^2 \frac{\Gamma}{2} N_K. \tag{2.68}$$

Estimates of the scattering rate using real experimental parameters are given in Table 2.1. Rubidium atom data has been taken from Ref. [126]. The two experiments were chosen as state of the art setups that collected light scattered from ultracold atoms in free space. Miyake *et al.* experimental parameters are from Ref. [41]. The $5^2S_{1/2}$, $F = 2 \rightarrow 5^2P_{3/2}$, $F' = 3$ transition of ^{87}Rb is considered. For this transition the Rabi frequency is actually larger than the detuning and effects of saturation should be taken into account in a more complete analysis. However, it is included for discussion. The detuning was specified as "a few linewidths" and note that it is much smaller than Ω_0. The Rabi frequency is $\Omega_0 = (d_{\mathrm{eff}}/\hbar)\sqrt{2I/c\varepsilon_0}$ which is obtained from definition of Rabi frequency, $\Omega = \mathbf{d}\cdot\mathbf{E}/\hbar$, assuming the electric field is parallel to the dipole, and the relation $I = c\varepsilon_0|E|^2/2$. We used $d_{\mathrm{eff}} = 1.73\times10^{-29}$ Cm [126]. Weitenberg *et al.* experimental parameters are based on Ref. [127, 128]. The $5^2S_{1/2} \rightarrow 5^2P_{3/2}$ transition of ^{87}Rb is used. Ref. [127] gives the free space detuning to be $\Delta_{\mathrm{free}} = -2\pi \cdot 45$ MHz, but Ref. [128] clarifies that the relevant detuning is $\Delta = \Delta_{\mathrm{free}} + \Delta_{\mathrm{lat}}$, where $\Delta_{\mathrm{lat}} = -2\pi \cdot 40$ MHz. Ref. [128] uses a saturation parameter s_{tot} to quantify the intensity of the beams which is related to the Rabi frequency,

$s_{\text{tot}} = 2\Omega^2/\Gamma^2$ [126, 129]. We can extract s_{tot} for the experiment from the total scattering rate by $\Gamma_{\text{sc}} = (\Gamma/2)(s_{\text{tot}})/(1 + s_{\text{tot}} + (2\Delta/\Gamma)^2)$. A scattering rate of 60 kHz per atom [127] gives $s_{\text{tot}} = 2.5$.

2.7 Possible Experimental Issues

There are many possible experimental issues that we have neglected so far in our theoretical treatment which need to be answered in order to consider the experimental feasibility of our proposal. The two main concerns are photodetector efficiency and heating losses.

In our theoretical models we treat the detectors as if they were capable of detecting every scattered photon, but real photodetectors can have efficiencies as low as 5%. For the case of nondestructive measurement as covered in Chapter 3 this is not an issue provided a sufficient number of photons can be collected to calculate reliable expectation values. The case of scattering into a cavity and the effect of efficiency on the conditioned state was addressed in Ref. [95] where it was shown that detector efficiencies are not a problem provided that the photon scattering pattern is periodic in some way, e.g. oscillatory as was the case in Ref. [95] or constant. This way it is only necessary to detect a sufficient number of photons to deduce the correct phase of the oscillations or the rate for the case of a constant scattering rate. In this thesis we deal predominantly with these two cases so photodetector efficiency is not an issue.

The other issue is the heating of the trapped gas which will limit the lifetime of the experiment. For free space scattering appropriate conditions have been achieved by for example using molasses beams that simultaneously cool and trap the atoms [127, 128]. Similar feats have been achieved with atoms coupled to a leaky cavity in Ref. [130] where self-organisation effects were well observable. Crucially, the cavity in said experiment has a decay rate of the order of MHz which is necessary to observe measurement backaction which we will consider in the subsequent chapters.

Chapter 3

Probing Correlations by Global Nondestructive Addressing[1]

3.1 Introduction

Having developed the basic theoretical framework within which we can treat the fully quantum regime of light-matter interactions we now consider possible applications. We will first look at nondestructive measurement where measurement backaction can be neglected and we focus on what expectation values can be extracted via optical methods.

In this chapter we develop a method to measure properties of ultracold gases in optical lattices by light scattering. In the previous chapter we have shown that the quantum light field couples to the bosons via the operator $\hat{F}$. This is the key element of the scheme we propose as this makes it sensitive to the quantum state of the matter and all of its possible superpositions which will be reflected in the quantum state of the light itself. We have also shown in section 2.2 that this coupling consists of two parts, a density component $\hat{D}$ given by Eq. (2.25), and a phase component $\hat{B}$ given by Eq. (2.26). Therefore, when probing the quantum state of the ultracold gas we can have access to not only density correlations, but

[1] The results of this chapter were first published in Ref. [90]

also matter-field interference at its shortest possible distance in an optical lattice, i.e. the lattice period. Previous work on quantum non-demolition (QND) schemes [29, 40, 131] probe only the density component as it is generally challenging to couple to the matter-field observables directly. Here, we will consider nondestructive probing of both density and interference operators.

Firstly, we will consider the simpler and more typical case of coupling to the atom number operators via $\hat{F} = \hat{D}$. However, we show that light diffraction in this regime has several nontrivial characteristics due to the fully quantum nature of the interaction. Firstly, we show that the angular distribution has multiple interesting features even when classical diffraction is forbidden facilitating their experimental observation. We derive new generalised Bragg diffraction conditions which are different to their classical counterpart. Furthermore, due to the fully quantum nature of the interaction our proposal is capable of probing the quantum state beyond mean-field prediction. We demonstrate this by showing that this scheme is capable of distinguishing all three phases in the Mott insulator - superfluid - Bose glass phase transition in a 1D disordered optical lattice which is not very well described by a mean-field treatment [109–113]. We underline that transitions in 1D are much more visible when changing an atomic density rather than for fixed-density scattering. It was only recently that an experiment distinguished a Mott insulator from a Bose glass via a series of destructive measurements [132]. Our proposal, on the other hand, is nondestructive and is capable of extracting all the relevant information in a single experiment making our proposal timely.

Having shown the possibilities created by this nondestructive measurement scheme we move on to considering light scattering from the phase related observables via the operator $\hat{F} = \hat{B}$. This enables in-situ probing of the matter-field coherence at its shortest possible distance in an optical lattice, i.e. the lattice period, which defines key processes such as tunnelling, currents, phase gradients, etc. This is in contrast to standard destructive time-of-flight measurements which deal with far-field interference although a relatively near-field

scheme was used in Ref. [41]. We show how within the mean-field treatment, this enables measurements of the order parameter, matter-field quadratures and squeezing. This can have an impact on atom-wave metrology and information processing in areas where quantum optics already made progress, e.g., quantum imaging with pixellised sources of non-classical light [42, 43], as an optical lattice is a natural source of multimode nonclassical matter waves.

3.2 Coupling to the Quantum State of Matter

As we have seen in section 2.4 under certain approximations the scattered light mode, a_1, is linked to the quantum state of matter via

$$a_1 = C\hat{F} = C\left(\hat{D} + \hat{B}\right), \tag{3.1}$$

where the atomic operators $\hat{D}$ and $\hat{B}$, given by Eq. (2.25) and Eq. (2.26), are responsible for the coupling to on-site density and inter-site interference respectively. It is crucial to note that light couples to the bosons via an operator as this makes it sensitive to the quantum state of the matter as this will imprint the fluctuations in the quantum state of the scattered light.

Here, we will use this fact that the light is sensitive to the atomic quantum state due to the coupling of the optical and matter fields via operators in order to develop a method to probe the properties of an ultracold gas. Therefore, we neglect the measurement backaction and we will only consider expectation values of light observables. Since the scheme is nondestructive (in some cases, it even satisfies the stricter requirements for a QND measurement [19, 30]) and the measurement only weakly perturbs the system, many consecutive measurements can be carried out with the same atoms without preparing a new sample. We will show how the extreme flexibility of the measurement operator $\hat{F}$ allows us to probe a variety of different atomic properties in-situ ranging from density correlations to matter-field interference.

3.3 On-site Density Measurements

3.3.1 Diffraction Patterns and Bragg Conditions

We have seen in section 2.5 that typically the dominant term in $\hat{F}$ is the density term $\hat{D}$ [30, 32, 133–135]. This is simply due to the fact that atoms are localised with lattice sites leading to an effective coupling with atom number operators instead of inter-site interference terms. Therefore, we will first consider nondestructive probing of the density related observables of the quantum gas. However, we will focus on the novel nontrivial aspects that go beyond the work in Ref. [19, 29, 30] which only considered a few extremal cases.

As we are only interested in the quantum information imprinted in the state of the optical field we will simplify our analysis by considering the light scattering to be much faster than the atomic tunnelling. Therefore, our scheme is actually a QND scheme [29, 30, 40, 131] as normally density-related measurements destroy the matter-phase coherence since it is its conjugate variable, but here we neglect the $b_i^\dagger b_j$ terms. Furthermore, we will consider a deep lattice. Therefore, the Wannier functions will be well localised within their corresponding lattice sites and thus the coefficients $J_{i,i}$ reduce to $u_1^*(\mathbf{r}_i)u_0(\mathbf{r}_i)$ leading to

$$\hat{D} = \sum_i^K u_1^*(\mathbf{r}_i)u_0(\mathbf{r}_i)\hat{n}_i, \tag{3.2}$$

which for travelling $[u_l(\mathbf{r}) = \exp(i\mathbf{k}_l \cdot \mathbf{r} + i\varphi_l)]$ or standing $[u_l(\mathbf{r}) = \cos(\mathbf{k}_l \cdot \mathbf{r} + \varphi_l)]$ waves is just a density Fourier transform at one or several wave vectors $\pm(\mathbf{k}_1 \pm \mathbf{k}_0)$.

We will now define a new auxiliary quantity to aid our analysis,

$$R = \langle a_1^\dagger a_1 \rangle - |\langle a_1 \rangle|^2, \tag{3.3}$$

which we will call the "quantum addition" to light scattering. By construction R is simply the full light intensity minus the classical field diffraction. In order to justify its name we will show that this quantity depends on purely quantum mechanical properties of the ultracold gas. We substitute $a_1 = C\hat{D}$ using Eq. (3.2) into our expression for R in Eq. (3.3) and we make use of the shorthand notation $A_i = u_1^*(\mathbf{r}_i)u_0(\mathbf{r}_i)$. The result is

$$R = |C|^2 \sum_{i,j}^{K} A_i^* A_j \langle \delta\hat{n}_i \delta\hat{n}_j \rangle, \tag{3.4}$$

where $\delta\hat{n}_i = \hat{n}_i - \langle \hat{n}_i \rangle$. Thus, we can clearly see that R is a result of light scattering from fluctuations in the atom number which is a purely quantum mechanical property of a system. Therefore, R, the "quantum addition" faithfully represents the new contribution from the quantum light-matter interaction to the diffraction pattern.

Another interesting quantity to measure are the quadratures of the light fields which we have seen in section 2.4 are related to the quadrature of $\hat{F}$ by $\hat{X}_\phi = |C|\hat{X}_\beta^F$. An interesting feature of quadratures is that the coupling strength at different sites can be tuned using the local oscillator phase β. To see this we consider the case when both the scattered mode and probe are travelling waves the quadrature

$$\hat{X}_\beta^F = \frac{1}{2}\left(\hat{F}e^{-i\beta} + \hat{F}^\dagger e^{i\beta}\right) = \sum_i^K \hat{n}_i \cos[(\mathbf{k}_0 - \mathbf{k}_1)\cdot\mathbf{r}_i + (\phi_0 - \phi_1) - \beta]. \tag{3.5}$$

Different light quadratures are differently coupled to the atom distribution, hence by varying the local oscillator phase, β, and/or the detection angle one can scan the whole range of couplings. This is similar to the case for $\hat{D}$ for a standing wave probe, where instead of varying β scanning is achieved by varying the position of the wave with respect to atoms. Additionally, the quadrature variance, $(\Delta X_\beta^F)^2$, will have a similar form to R given in Eq. (3.4),

$$(\Delta X_\beta^F)^2 = |C|^2 \sum_{i.j}^{K} A_i^\beta A_j^\beta \langle \delta\hat{n}_i \delta\hat{n}_j \rangle, \tag{3.6}$$

where $A_i^\beta = (A_i e^{-i\beta} + A_i^* e^{i\beta})/2$. However, this has the advantage that unlike in the case of R there is no need to subtract a spatially varying classical signal to obtain this quantity.

The "quantum addition", R, and the quadrature variance, $(\Delta X_\beta^F)^2$, are both quadratic in a_1 and both rely heavily on the quantum state of the matter. Therefore, they will have a nontrivial angular dependence showing more peaks than classical diffraction. Furthermore, these peaks can be tuned very easily with β or φ_l. Fig. 3.1 shows the angular dependence of R for the case when the probe is a travelling wave scattering from an ideal superfluid in a 3D optical lattice into a standing wave mode. The first noticeable feature is the isotropic background which does not exist in classical diffraction. This background yields information about density fluctuations which, according to mean-field estimates (i.e. inter-site correlations are ignored), are related by $R = |C|^2 K(\langle \hat{n}^2 \rangle - \langle \hat{n} \rangle^2)/2$. In Fig. 3.1 we can see a significant signal of $R = |C|^2 N_K/2$, because it shows scattering from an ideal superfluid which has significant density fluctuations with correlations of infinite range. However, as the parameters of the lattice are tuned across the phase transition into a Mott insulator the signal goes to zero. This is because the Mott insulating phase has well localised atoms at each site which suppresses density fluctuations entirely leading to absolutely no "quantum addition".

We can also observe maxima at several different angles in Fig. 3.1. Interestingly, they occur at different angles than predicted by the classical Bragg condition. Moreover, the classical Bragg condition is actually not satisfied which means there actually is no classical diffraction on top of the "quantum addition" shown here. Therefore, these features would be easy to see in an experiment as they would not be masked by a stronger classical signal. This difference in behaviour is due to the fact that classical diffraction is ignorant of any quantum correlations as it is given by the square of the light field amplitude squared

$$|\langle a_1 \rangle|^2 = |C|^2 \sum_{i,j} A_i^* A_j \langle \hat{n}_i \rangle \langle \hat{n}_j \rangle, \tag{3.7}$$

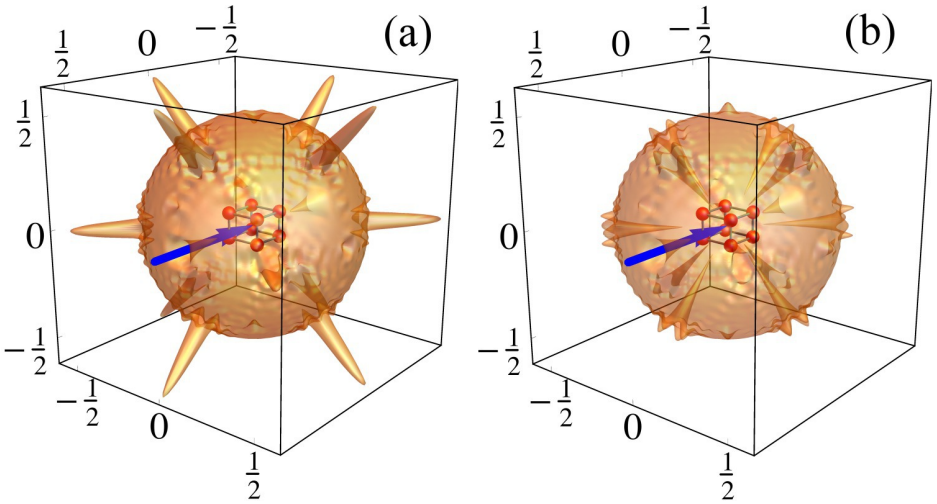

Fig. 3.1 Light intensity scattered into a standing wave mode from a superfluid in a 3D lattice (units of $R/(|C|^2 N_K)$). Arrows denote incoming travelling wave probes. The classical Bragg condition, $\Delta\mathbf{k} = \mathbf{G}$, is not fulfilled, so there is no classical diffraction, but intensity still shows multiple peaks, whose heights are tunable by simple phase shifts of the optical beams: (a) $\varphi_1 = 0$; (b) $\varphi_1 = \pi/2$. Interestingly, there is also a significant uniform background level of scattering which does not occur in its classical counterpart.

which is independent of any two-point correlations unlike R. On the other hand the full light intensity (classical signal plus "quantum addition") of the quantum light does include higher-order correlations

$$\langle a_1^\dagger a_1 \rangle = |C|^2 \sum_{i,j} A_i^* A_j \langle \hat{n}_i \hat{n}_j \rangle. \tag{3.8}$$

Therefore, we see that in the fully quantum picture light scattering not only depends on the diffraction structure due to the distribution of atoms in the lattice, but also on the quantum correlations between different lattice sites which will in turn be dependent on the quantum state of the matter. These correlations are imprinted in R as shown in Eq. (3.4) and it highlights the key feature of our model, i.e. the light couples to the quantum state directly via operators.

We can even derive the generalised Bragg conditions for the peaks that we can see in Fig. 3.1. The exact conditions under which diffraction peaks emerge for the "quantum addition" will depend on the optical setup as well as on the quantum state of the matter as it is the

density fluctuation correlations, $\langle \delta\hat{n}_i \delta\hat{n}_j \rangle$, that provide the structure for R and not the lattice itself as seen in Eq. (3.4). For classical light it is straightforward to develop an intuitive physical picture to find the Bragg condition by considering angles at which the distance travelled by light scattered from different points in the lattice is equal to an integer multiple of the wavelength. The "quantum addition" is more complicated and less intuitive as we now have to consider quantum correlations which are not only nonlocal, but can also be negative.

We will consider scattering from a superfluid, because the Mott insulator has no "quantum addition" due to a lack of density fluctuations. The wave function of a superfluid on a lattice is given by Eq. (2.33). This state has infinite range correlations and thus has the convenient property that all two-point density fluctuation correlations are equal regardless of their separation, i.e. $\langle \delta\hat{n}_i \delta\hat{n}_j \rangle \equiv \langle \delta\hat{n}_a \delta\hat{n}_b \rangle$ for all $(i \neq j)$, where the right hand side is a constant value. This allows us to extract all correlations from the sum in Eq. (3.4) to obtain

$$\frac{R}{|C|^2} = (\langle \delta\hat{n}^2 \rangle - \langle \delta\hat{n}_a \delta\hat{n}_b \rangle) \sum_i^K |A_i|^2 + \langle \delta\hat{n}_a \delta\hat{n}_b \rangle |A|^2 = \frac{N}{M} \sum_i^K |A_i|^2 - \frac{N}{M^2} |A|^2, \tag{3.9}$$

where $A = \sum_i^K A_i$, and we have dropped the index from $\langle \delta\hat{n}^2 \rangle$ as it is equal at every site. The second equality follows from the fact that for a superfluid state $\langle \delta\hat{n}^2 \rangle = N/M - N/M^2$ and $\langle \delta\hat{n}_a \delta\hat{n}_b \rangle = -N/M^2$. Naturally, we get an identical expression for the quadrature variance $(\Delta X_\beta^F)^2$ with the coefficients A_i replaced by the real A_i^β.

The "quantum addition" for the case when both the scattered and probe modes are travelling waves is actually trivial. It has no peaks and thus it has no generalised Bragg condition and it only consists of a uniform background. This is a consequence of the fact that travelling waves couple equally strongly with every atom as only the phase is different between lattice sites. Therefore, since superfluid correlations lack structure as they're uniform we do no get a strong coherent peak. The contribution from the lattice structure is included in the classical Bragg peaks which we have subtracted in order to obtain the quantity R. However, if we consider the case where the scattered mode is collected as a standing wave

using a pair of mirrors we get the diffraction pattern that we saw in Fig. 3.1. This time we get strong visible peaks, because at certain angles the standing wave couples to the atoms maximally at all lattice sites and thus it uses the structure of the lattice to amplify the signal from the quantum fluctuations. This becomes clear when we look at Eq. (3.9). We can neglect the second term as it is always negative and it has the same angular distribution as the classical diffraction pattern and thus it is mostly zero except when the classical Bragg condition is satisfied. Since in Fig. 3.1 we have chosen an angle such that the Bragg condition is not satisfied this term is essentially zero. Therefore, we are left with the first term $\sum_i^K |A_i|^2$ which for a travelling wave probe and a standing wave scattered mode is

$$\sum_i^K |A_i|^2 = \sum_i^K \cos^2(\mathbf{k}_0 \cdot \mathbf{r}_i + \phi_0) = \frac{1}{2}\sum_i^K [1 + \cos(2\mathbf{k}_0 \cdot \mathbf{r}_i + 2\phi_0)]\,. \tag{3.10}$$

Therefore, it is straightforward to see that unless $2\mathbf{k}_0 = \mathbf{G}$, where $\mathbf{G}$ is a reciprocal lattice vector, there will be no coherent signal and we end up with the mean uniform signal of strength $|C|^2 N_k/2$. When this condition is satisfied all the cosine terms will be equal and they will add up constructively instead of cancelling each other out. Note that this new Bragg condition is different from the classical one $\mathbf{k}_0 - \mathbf{k}_1 = \mathbf{G}$. This result makes it clear that the uniform background signal is not due to any coherent scattering, but rather due to the lack of structure in the quantum correlations. Furthermore, we see that the peak height is actually tunable via the phase, ϕ_0, which is illustrated in Fig. 3.1b.

For light field quadratures the situation is different, because as we have seen in Eq. (3.5) even for travelling waves we can tune the contributions to the signal from different sites by changing the angle of measurement or tuning the local oscillator signal β. The rest is similar to the case we discussed for R with a standing wave mode and we can show that the new Bragg condition in this case is $2(\mathbf{k}_0 - \mathbf{k}_1) = \mathbf{G}$ which is different from the condition we had for R and is still different from the classical condition $\mathbf{k}_0 - \mathbf{k}_1 = \mathbf{G}$. Furthermore, just like in Fig. 3.1b the peak height can be tuned using β.

A quantum signal that is not masked by classical diffraction is very useful for future experimental realisability. However, it is still unclear whether this signal would be strong enough to be visible. After all, a classical signal scales as N_K^2 whereas here we have only seen a scaling of N_K. In section 2.6 we have estimated the mean photon scattering rates integrated over the solid angle for the only two experiments so far on light diffraction from truly ultracold bosons where the measurement object was light

$$n_\Phi = \left(\frac{\Omega_0}{\Delta_a}\right)^2 \frac{\Gamma K}{8}(\langle \hat{n}^2 \rangle - \langle \hat{n} \rangle^2). \tag{3.11}$$

These results can be applied directly to the scattering patters in Fig. 3.1. Therefore, the background signal should reach $n_\Phi \approx 10^6$ s^{-1} in Ref. [127] (150 atoms in 2D), and $n_\Phi \approx 10^{11}$ s^{-1} in Ref. [41] (10^5 atoms in 3D). These numbers show that the diffraction patterns we have seen due to the "quantum addition" should be visible using currently available technology, especially since the most prominent features, such as Bragg diffraction peaks, do not coincide at all with the classical diffraction pattern.

3.3.2 Mapping the Quantum Phase Diagram

We have shown that scattering from atom number operators leads to a purely quantum diffraction pattern which depends on the density fluctuations and their correlations. We have also seen that this signal should be strong enough to be visible using currently available technology. However, so far we have not looked at what this can tell us about the quantum state of matter. We have briefly mentioned that a deep superfluid will scatter a lot of light due to its infinite range correlations and a Mott insulator will not contribute any "quantum addition" at all, but we have not looked at the quantum phase transition between these two phases. In two or higher dimensions this has a rather simple answer as the Bose-Hubbard phase transition is described well by mean-field theories and it has a sharp transition at the

critical point. This means that the "quantum addition" signal would drop rapidly at the critical point and go to zero as soon as it was crossed. However, R given by Eq. (3.3) clearly contains much more information.

There are many situations where the mean-field approximation is not a valid description of the physics. A prominent example is the Bose-Hubbard model in 1D [109–113] as we have seen in section 2.3.4. Observing the transition in 1D by light at fixed density was considered to be difficult [40] or even impossible [136]. This is because the one-dimensional quantum phase transition is in a different universality class than its higher dimensional counterparts. The energy gap, which is the order parameter, decays exponentially slowly across the phase transition making it difficult to identify the phase transition even in numerical simulations. Here, we will show the available tools provided by the "quantum addition" that allows one to nondestructively map this phase transition and distinguish the superfluid and Mott insulator phases.

The 1D phase transition is best understood in terms of two-point correlations as a function of their separation [115]. In the Mott insulating phase, the two-point correlations $\langle b_i^\dagger b_j \rangle$ and $\langle \delta\hat{n}_i \delta\hat{n}_j \rangle$ ($\delta\hat{n}_i = \hat{n}_i - \langle \hat{n}_i \rangle$) decay exponentially with $|i-j|$. This is a characteristic of insulators. On the other hand the superfluid will exhibit long-range order which in dimensions higher than one, manifests itself with an infinite correlation length. However, in 1D only pseudo long-range order happens and both the matter-field and density fluctuation correlations decay algebraically [115].

The method we propose gives us direct access to the structure factor, which is a function of the two-point correlation $\langle \delta\hat{n}_i \delta\hat{n}_j \rangle$. This quantity can be extracted from the measured light intensity by considering the "quantum addition". We will consider the case when both the probe and scattered modes are plane waves which can be easily achieved in free space. We will again consider the case of light being maximally coupled to the density ($\hat{F} = \hat{D}$).

Therefore, the quantum addition is given by

$$R = \sum_{i,j} \exp[i(\mathbf{k}_1 - \mathbf{k}_0)(\mathbf{r}_i - \mathbf{r}_j)] \langle \delta\hat{n}_i \delta\hat{n}_j \rangle. \tag{3.12}$$

This alone allows us to analyse the phase transition quantitatively using our method. Unlike in higher dimensions where an order parameter can be easily defined within the mean-field approximation as a simple expectation value, the situation in 1D is more complex as it is difficult to directly access the excitation energy gap which defines this phase transition. However, a valid description of the relevant 1D low energy physics is provided by Luttinger liquid theory [115] as seen in section 2.3.4. In this model correlations in the superfluid phase as well as the superfluid density itself are characterised by the Tomonaga-Luttinger parameter, K. This parameter also identifies the critical point in the thermodynamic limit at $K_c = 1/2$. This quantity can be extracted from various correlation functions and in our case it can be extracted directly from R [110]. This quantity was used in numerical calculations that used highly efficient density matrix renormalisation group (DMRG) methods to calculate the ground state to subsequently fit the Luttinger theory to extract this parameter K. These calculations yield a theoretical estimate of the critical point in the thermodynamic limit for commensurate filling in 1D to be at $U/2J \approx 1.64$ [110]. Our proposal provides a method to directly measure R nondestructively in a lab which can then be used to experimentally determine the location of the critical point in 1D.

However, whilst such an approach will yield valuable quantitative results we will instead focus on its qualitative features which give a more intuitive understanding of what information can be extracted from R. This is because the superfluid to Mott insulator phase transition is well understood, so there is no reason to dwell on its quantitative aspects. However, our method is much more general than the Bose-Hubbard model as it can be easily applied to many other systems such as fermions, photonic circuits, optical lattices with quantum potentials, etc. Therefore, by providing a better physical picture of what information is

carried by the "quantum addition" it should be easier to see its usefulness in a broader context.

We calculate the phase diagram of the Bose-Hubbard Hamiltonian given by

$$\hat{H}_{\rm dis} = -J \sum_{\langle i,j \rangle} b_i^\dagger b_j + \frac{U}{2} \sum_i \hat{n}_i(\hat{n}_i - 1) - \mu \sum_i \hat{n}_i, \tag{3.13}$$

where the μ is the chemical potential. We have introduced the last term as we are interested in grand canonical ensemble calculations as we want to see how the system's behaviour changes as density is varied. We perform numerical calculations of the ground state using DMRG methods [137] from which we can compute all the necessary atomic observables. Experiments typically use an additional harmonic confining potential on top of the optical lattice to keep the atoms in place which means that the chemical potential will vary in space. However, with careful consideration of the full $(\mu/2J, U/2J)$ phase diagrams in Fig. 3.2(d,e) our analysis can still be applied to the system [138].

We then consider probing these ground states using our optical scheme and we calculate the "quantum addition", R, based on these ground states. The angular dependence of R for a Mott insulator and a superfluid is shown in Fig. 3.2(a), and we note that there are two variables distinguishing the states. Firstly, maximal R, $R_{\rm max} \propto \sum_i \langle \delta \hat{n}_i^2 \rangle$, probes the fluctuations and compressibility κ' ($\langle \delta \hat{n}_i^2 \rangle \propto \kappa' \langle \hat{n}_i \rangle$). The Mott insulator is incompressible and thus will have very small on-site fluctuations and it will scatter little light leading to a small $R_{\rm max}$. The deeper the system is in the insulating phase (i.e. the larger the $U/2J$ ratio is), the smaller these values will be until ultimately it will scatter no light at all in the $U \to \infty$ limit. In Fig. 3.2(a) this can be seen in the value of the peak in R. The value $R_{\rm max}$ in the superfluid phase ($U/2J = 0$) is larger than its value in the Mott insulating phase ($U/2J = 10$) by a factor of $\sim$25. Figs. 3.2(b,d) show how the value of $R_{\rm max}$ changes across the phase transition. There are a few things to note at this point. Firstly, if we follow the transition along the line corresponding to commensurate filling (i.e. any line that is in between the

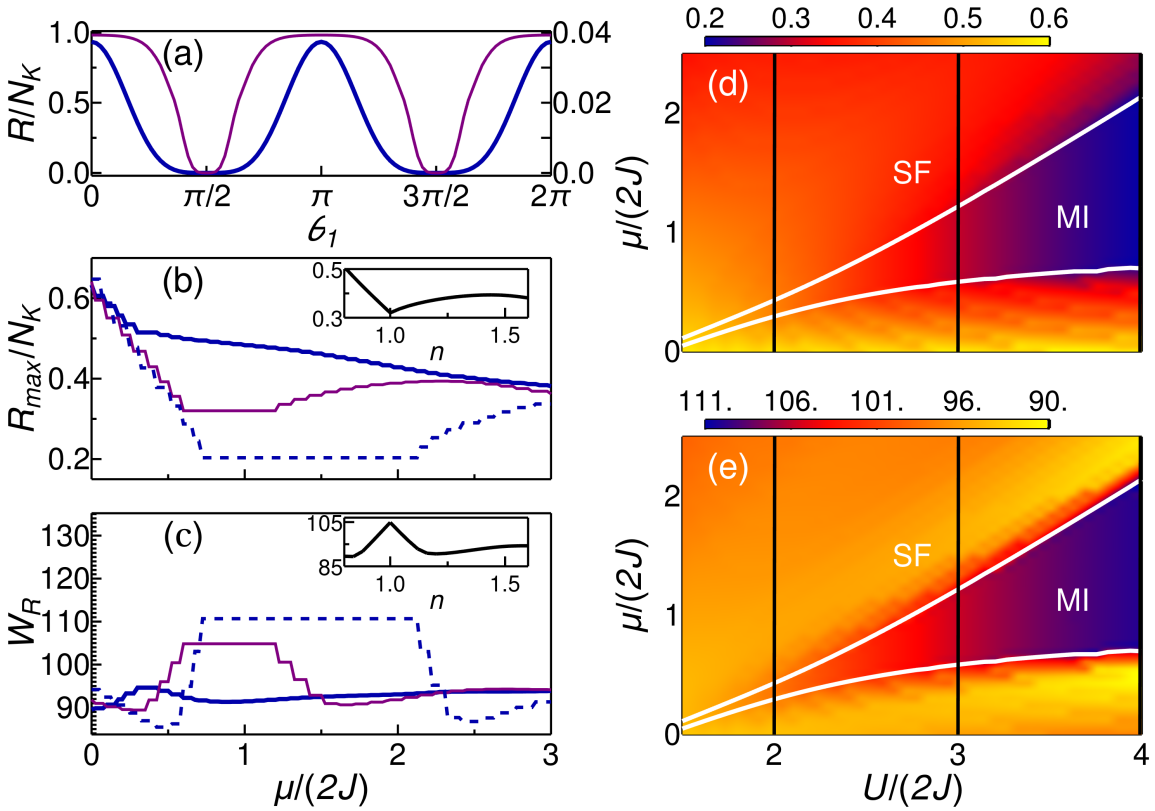

Fig. 3.2 (a) The angular dependence of scattered light R for a superfluid (thin purple, left scale, $U/2J = 0$) and Mott insulator (thick blue, right scale, $U/2J = 10$). The two phases differ in both their value of $R_{\max}$ as well as W_R showing that density correlations in the two phases differ in magnitude as well as extent. Light scattering maximum $R_{\max}$ is shown in (b, d) and the width W_R in (c, e). It is very clear that varying chemical potential μ or density $\langle n \rangle$ sharply identifies the superfluid-Mott insulator transition in both quantities. (b) and (c) are cross-sections of the phase diagrams (d) and (e) at $U/2J = 2$ (thick blue), 3 (thin purple), and 4 (dashed blue). Insets show density dependencies for the $U/(2J) = 3$ line. $K = M = N = 25$.

two white lines in Fig. 3.2(d)) we see that the transition is very smooth and it is hard to see a definite critical point. This is due to the energy gap closing exponentially slowly which makes precise identification of the critical point extremely difficult. The best option at this point would be to fit Tomonaga-Luttinger theory to the results in order to find this critical point. However, we note that there is a drastic change in signal as the chemical potential (and thus the density) is varied. This is highlighted in Fig. 3.2(b) which shows how the Mott insulator can be easily identified by a dip in the quantity $R_{\max}$.

Secondly, being a Fourier transform, the width W_R of the dip in R is a direct measure of the correlation length l, $W_R \propto 1/l$. The Mott insulator being an insulating phase is characterised by exponentially decaying correlations and as such it will have a very large W_R. On the other hand, the superfluid in 1D exhibits pseudo long-range order which manifests itself in algebraically decaying two-point correlations [115] which significantly reduces the dip in the R. This can be seen in Fig. 3.2(a). Furthermore, just like for $R_{\max}$ we see that the transition is much sharper as μ is varied. This is shown in Figs. 3.2(c,e). Notably, the difference in angle between a superfluid and an insulating state is fairly significant $\sim 20^\circ$ which should make the two phases easy to identify using this measure. In this particular case, measuring W_R in the Mott phase is not very practical as the insulating phase does not scatter light (small $R_{\max}$). The phase transition information is easier extracted from $R_{\max}$. However, this is not always the case and we will shortly see how certain phases of matter scatter a lot of light and can be distinguished using measurements of W_R where $R_{\max}$ is not sufficient. Another possible concern with experimentally measuring W_R is that it might be obstructed by the classical diffraction maxima which appear at angles corresponding to the minima in R. However, the width of such a peak is much smaller as its width is proportional to $1/M$.

So far both variables we considered, $R_{\max}$ and W_R, provide similar information. They both take on values at one of its extremes in the Mott insulating phase and they change drastically across the phase transition into the superfluid phase. Next, we present a case

where it is very different. We will again consider ultracold bosons in an optical lattice, but this time we introduce some disorder. We do this by adding an additional periodic potential on top of the existing setup that is incommensurate with the original lattice. The resulting Hamiltonian can be shown to be

$$\hat{H}_{\text{dis}} = -J \sum_{\langle i,j \rangle} b_i^\dagger b_j + \frac{U}{2} \sum_i \hat{n}_i(\hat{n}_i - 1) + \frac{V}{2} \sum_i \left[1 + \cos(2r\pi m + 2\phi)\right] \hat{n}_i, \tag{3.14}$$

where V is the strength of the superlattice potential, r is the ratio of the superlattice and trapping wave vectors and ϕ is some phase shift between the two lattice potentials [139]. The first two terms are the standard Bose-Hubbard Hamiltonian and the only modification is an additional spatially varying potential shift. We will only consider the phase diagram at fixed density as the introduction of disorder makes the usual interpretation of the phase diagram in the $(\mu/2J, U/2J)$ plane for a fixed ratio V/U complicated due to the presence of multiple compressible and incompressible phases between successive Mott insulator lobes [139]. Therefore, the chemical potential no longer appears in the Hamiltonian as we are no longer considering the grand canonical ensemble.

The reason for considering such a system is that it introduces a third, competing phase, the Bose glass into our phase diagram. It is an insulating phase like the Mott insulator, but it has local superfluid susceptibility making it compressible. Therefore this localized insulating phase has exponentially decaying correlations just like the Mott phase, but it has large on-site fluctuations just like the compressible superfluid phase. As these are the two physical variables encoded in R measuring both $R_{\max}$ and W_R will provide us with enough information to distinguish all three phases. In a Bose glass we have finite compressibility, but exponentially decaying correlations. This gives a large $R_{\max}$ and a large W_R. A Mott insulator also has exponentially decaying correlations since it is an insulator, but it is incompressible. Thus, it will scatter light with a small $R_{\max}$ and large W_R. Finally, a superfluid has long-range correlations and large compressibility which results in a large $R_{\max}$ and a small W_R.

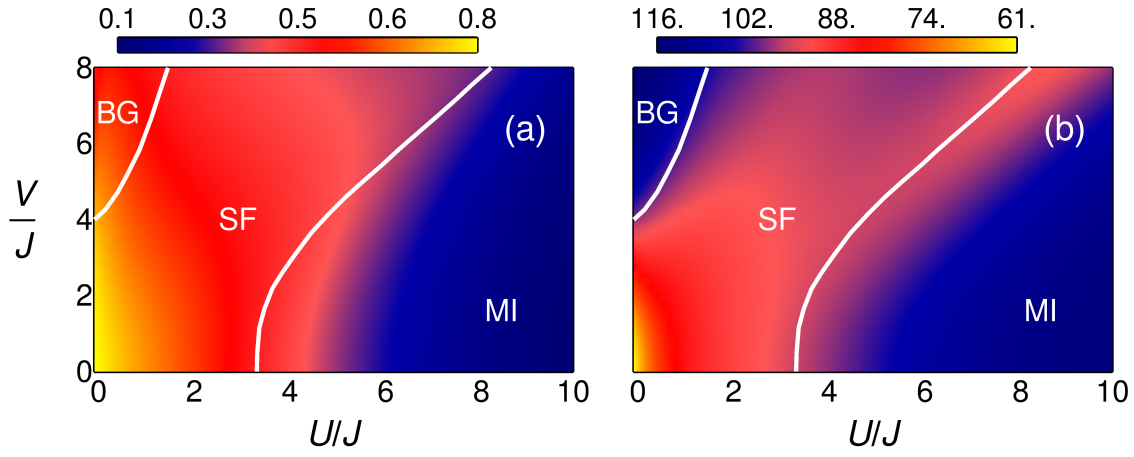

Fig. 3.3 The Mott-superfluid-glass phase diagrams for light scattering maximum $R_{\max}/N_K$ (a) and width W_R (b). Measurement of both quantities distinguish all three phases. Transition lines are shifted due to finite size effects [139], but it is possible to apply well known numerical methods to extract these transition lines from such experimental data extracted from R [110]. $K = M = N = 35$.

We confirm this in Fig. 3.3 for simulations with the ratio of superlattice- to trapping lattice-period $r \approx 0.77$ for various disorder strengths V [139]. From Fig. 3.3 we see that all three phases can indeed be distinguished. From the $R_{\max}$ plot we can distinguish the two compressible phases, the superfluid and Bose glass, from the incompressible phase, the Mott insulator. We can now also distinguish the Bose glass phase from the superfluid, because only one of them is an insulator and thus the angular width of their scattering patterns will reveal this information. However, unlike the Mott insulator, the Bose glass scatters a lot of light (large $R_{\max}$) enabling such measurements. Since we performed these calculations at a fixed density the Mott to superfluid phase transition is not particularly sharp [109–113] just like we have seen in Figs. 3.2(d,e) if we follow the transition through the tip of the lobe which corresponds to a line of unit density. However, despite the lack of an easily distinguishable critical point, as we have already discussed, it is possible to quantitatively extract the location of the transition lines by extracting the Tomonaga-Luttinger parameter from the scattered light, R, in the same way it was done for an unperturbed Bose-Hubbard model [110].

3.4 Matter-field interference measurements

We have shown in section 2.5 that certain optical arrangements lead to a different type of light-matter interaction where coupling is maximised in between lattice sites rather than at the sites themselves yielding $a_1 = C\hat{B}$. This leads to the optical fields interacting directly with the interference terms $b_i^\dagger b_{i+1}$ via the operator $\hat{B}$ given by Eq. (2.26). This opens up a whole new way of probing and interacting with a quantum gas trapped in an optical lattice as this gives an in-situ method for probing the inter-site interference terms at its shortest possible distance, i.e. the lattice period.

Unlike in the previous sections, here we will use the mean-field description of the Bose-Hubbard model in order to obtain a simple physical picture of what information is contained in the quantum light. In the mean-field approximation the inter-site interference terms become

$$b_i^\dagger b_j = \Phi b_i^\dagger + \Phi^* b_j - |\Phi|^2, \tag{3.15}$$

where $\langle b_i \rangle = \Phi$ which we assume is uniform across the whole lattice. This approach has the advantage that the quantity Φ is the mean-field order parameter of the superfluid to Mott insulator phase transition and is effectively a good measure of the superfluid character of the quantum ground state. This greatly simplifies the physical interpretation of our results.

Firstly, we will show that our nondestructive measurement scheme allows one to probe the mean-field order parameter, Φ, directly. Normally, this is achieved by releasing the trapped gas and performing a time-of-flight measurement. Here, this can be achieved in-situ. In section 2.5 we showed that one of the possible optical arrangements leads to a diffraction maximum with the matter operator

$$\hat{B}_{\max} = J^B_{\max} \sum_i \left(b_i^\dagger b_{i+1} + b_i b_{i+1}^\dagger \right), \tag{3.16}$$

where $J^B_{\max} = \mathcal{F}[W_1](2\pi/d)$. Therefore, by measuring the expectation value of the quadrature we obtain the following quantity

$$\langle \hat{X}^F_{\beta=0} \rangle = J^B_{\max}(K-1)|\Phi|^2. \tag{3.17}$$

This quantity is directly proportional to square of the order parameter Φ and thus lets us very easily follow this quantity across the phase transition with a very simple quadrature measurement setup.

In the mean-field treatment, the order parameter also lets us deduce a different quantity, namely matter-field quadratures $\hat{X}^b_\alpha = (be^{-i\alpha} + b^\dagger e^{i\alpha})/2$. Quadrature measurements of optical fields are a standard and common tool in quantum optics. However, this is not the case for matter-fields as normally most interactions lead to an effective coupling with the density as we have seen in the previous sections. Therefore, such measurements provide us with new opportunities to study the quantum matter state which was previously unavailable. We will take Φ to be real which in the standard Bose-Hubbard Hamiltonian can be selected via an inherent gauge degree of freedom in the order parameter. Thus, the quadratures themselves straightforwardly become

$$\hat{X}^b_\alpha = \frac{\Phi}{2}(e^{-i\alpha} + e^{i\alpha}) = \Phi\cos(\alpha). \tag{3.18}$$

From our measurement of the light field quadrature we have already obtained the value of Φ and thus we immediately also know the values of the matter-field quadratures. Unfortunately, the variance of the quadrature is a more complicated quantity given by

$$(\Delta X^b_{0,\pi/2})^2 = \frac{1}{4} + [(n - \Phi^2) \pm \frac{1}{2}(\langle b^2 \rangle - \Phi^2)], \tag{3.19}$$

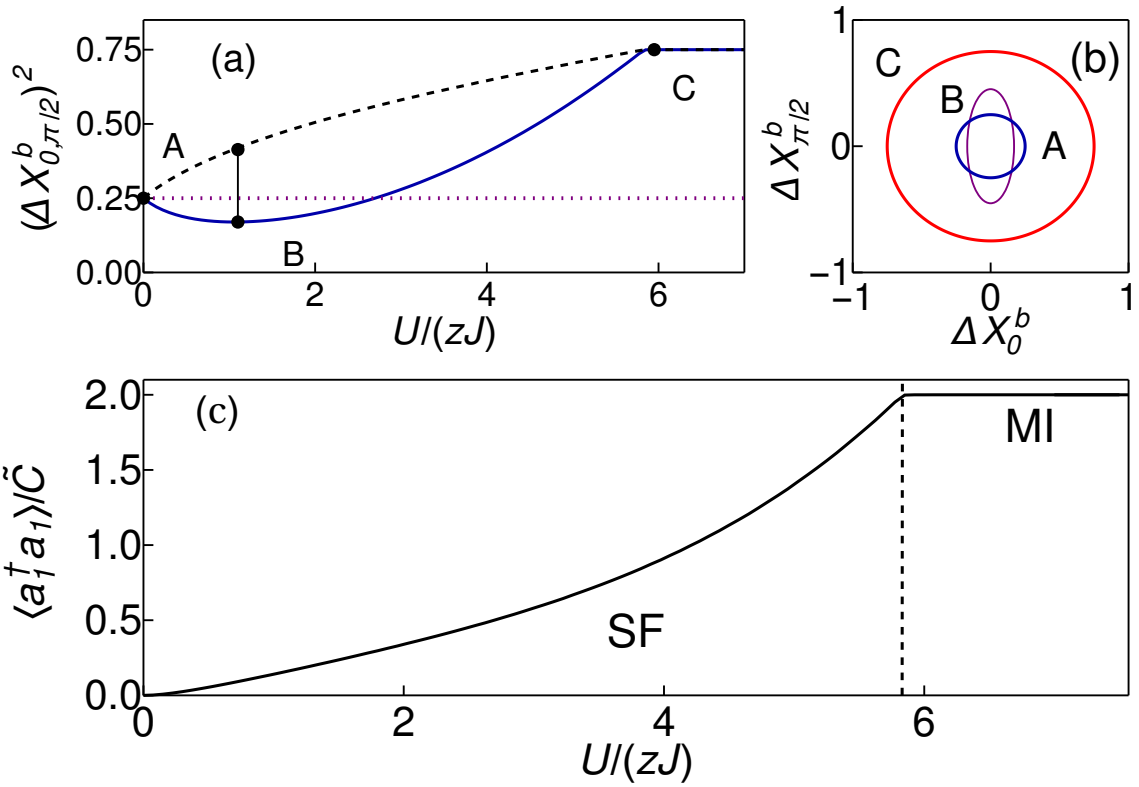

Fig. 3.4 Mean-field quadratures and resulting photon scattering rates. (a) The variances of quadratures ΔX^b_0 (solid) and $\Delta X^b_{\pi/2}$ (dashed) of the matter field across the phase transition. Level 1/4 is the minimal (Heisenberg) uncertainty. There are three important points along the phase transition: the coherent state (SF) at A, the amplitude-squeezed state at B, and the Fock state (MI) at C. (b) The uncertainties plotted in phase space. (c) Photon number scattered in a diffraction minimum, given by Eq. (3.21), where $\tilde{C} = 2|C|^2(K-1)\mathcal{F}^2[W_1](\pi/d)$. More light is scattered from a MI than a SF due to the large uncertainty in phase in the insulator.

where we have arbitrarily selected two orthogonal quadratures $\alpha = 0$ and $\alpha = \pi/2$. This quantity cannot be estimated from light quadrature measurements alone as we do not know the value of $\langle b^2\rangle$. To obtain the value of this quantity we need to consider a second-order light observable such as light intensity. However, in the diffraction maximum this signal will be dominated by a contribution proportional to $K^2\Phi^4$ whereas the terms containing information on $\langle b^2\rangle$ will only scale as K. Therefore, it would be difficult to extract the quantity that we need by measuring in the diffraction maximum.

We now consider the alternative arrangement in which we probe the diffraction minimum and the matter operator is given by

$$\hat{B} = J^B_{\min} \sum_i (-1)^i \left(b_i^\dagger b_{i+1} b_i b_{i+1}^\dagger \right), \tag{3.20}$$

where $J^B_{\min} = -\mathcal{F}[W_1](\pi/d)$ and which unlike the previous case is no longer proportional to the Bose-Hubbard kinetic energy term. Unlike in the diffraction maximum the light intensity in the diffraction minimum does not have the term proportional to K^2 and thus we obtain the following quantity

$$\langle a_1^\dagger a_1 \rangle = 2|C|^2(K-1)\mathcal{F}^2[W_1](\frac{\pi}{d})[(\langle b^2 \rangle - \Phi^2)^2 + (n - \Phi^2)(1 + n - \Phi^2)], \tag{3.21}$$

This is plotted in Fig. 3.4 as a function of $U/(zJ)$. Now, we can easily deduce the value of $\langle b^2 \rangle$ since we will already know the mean density, n, from our experimental setup and we have seen that we can obtain Φ^2 from the diffraction maximum. Thus, we now have access to the quadrature variance of the matter-field as well giving us a more complete picture of the matter-field amplitude than previously possible.

A surprising feature seen in Fig. 3.4 is that the inter-site terms scatter more light from a Mott insulator than a superfluid Eq. (3.21), although the mean inter-site density $\langle \hat{n}(\mathbf{r}) \rangle$ is tiny in the Mott insulating phase. This reflects a fundamental effect of the boson interference in Fock states. It indeed happens between two sites, but as the phase is uncertain, it results in the large variance of $\hat{n}(\mathbf{r})$ captured by light as shown in Eq. (3.21). The interference between two macroscopic BECs has been observed and studied theoretically [140]. When two BECs in Fock states interfere a phase difference is established between them and an interference pattern is observed which disappears when the results are averaged over a large number of experimental realizations. This reflects the large shot-to-shot phase fluctuations corresponding to a large inter-site variance of $\hat{n}(\mathbf{r})$. By contrast, our method enables the

observation of such phase uncertainty in a Fock state directly between lattice sites on the microscopic scale in-situ.

More generally, beyond mean-field, probing $\hat{B}^\dagger\hat{B}$ via light intensity measurements gives us access with 4-point correlations ($b_i^\dagger b_j$ combined in pairs). Measuring the photon number variance, which is standard in quantum optics, will lead up to 8-point correlations similar to 4-point density correlations [30]. These are of significant interest, because it has been shown that there are quantum entangled states that manifest themselves only in high-order correlations [141].

3.5 Conclusions

In this chapter we explored the possibility of nondestructively probing a quantum gas trapped in an optical lattice using quantised light. Firstly, we showed that the density term in scattering has an angular distribution richer than classical diffraction, derived generalized Bragg conditions, and estimated parameters for two relevant experiments [41, 127]. Secondly, we demonstrated how the method accesses effects beyond mean-field and distinguishes all the phases in the Mott-superfluid-glass transition, which is currently a challenge [132]. Finally, we looked at measuring the matter-field interference via the operator $\hat{B}$ by concentrating light between the sites. This corresponds to probing interference at the shortest possible distance in an optical lattice. This is in contrast to standard destructive time-of-flight measurements which deal with far-field interference. This quantity defines most processes in optical lattices. E.g. matter-field phase changes may happen not only due to external gradients, but also due to intriguing effects such quantum jumps leading to phase flips at neighbouring sites and sudden cancellation of tunnelling [142], which should be accessible by our method. We showed how in mean-field, one can measure the matter-field amplitude (order parameter), quadratures and squeezing. This can link atom optics to areas where quantum optics has already made progress, e.g., quantum imaging [42, 43], using an optical lattice as an array of

multimode nonclassical matter-field sources with a high degree of entanglement for quantum information processing. Since our scheme is based on off-resonant scattering, and thus being insensitive to a detailed atomic level structure, the method can be extended to molecules [143], spins, and fermions [135].

Chapter 4

Quantum Measurement Backaction

4.1 Introduction

This thesis is entirely concerned with the question of measuring a quantum many-body system using quantised light. However, so far we have only looked at expectation values in a nondestructive context where we neglect the effect of the quantum wave function collapse. We have shown that light provides information about various statistical quantities of the quantum states of the atoms such as their correlation functions. In general, any quantum measurement affects the system even if it does not physically destroy it. In our model both optical and matter fields are quantised and their interaction leads to entanglement between the two subsystems. When a photon is detected and the electromagnetic wave function of the optical field collapses, the matter state is also affected due to this entanglement resulting in quantum measurement backaction. Therefore, in order to determine these quantities multiple measurements have to be performed to establish a precise measurement of the expectation value which will require repeated preparations of the initial state.

In the following chapters, we consider a different approach to quantum measurement in open systems and instead of considering expectation values we look at a single experimental run and the resulting dynamics due to measurement backaction. Previously, we were mostly

interested in extracting information about the quantum state of the atoms from the scattered light. The flexibility in the measurement model was used to enable probing of as many different quantum properties of the ultracold gas as possible. By focusing on measurement backaction we instead investigate the effect of photodetections on the dynamics of the many-body gas as well as the possible quantum states that we can prepare instead of what information can be extracted.

In this chapter, we introduce the necessary theory of quantum measurement and backaction in open systems in order to lay a foundation for the material that follows in which we apply these concepts to a bosonic quantum gas. We first introduce the concept of quantum trajectories which represent a single continuous series of photon detections. We also present an alternative approach to open systems in which the measurement outcomes are discarded. This will be useful when trying to learn about dynamical features common to every trajectory. In this case we use the density matrix formalism which obeys the master equation. This approach is more common in dissipative systems and we will highlight the differences between these two different types of open systems. We conclude this chapter with a new concept that will be central to all subsequent discussions. In our model measurement is global, it couples to operators that correspond to global properties of the quantum gas rather than single-site quantities. This enables the possibility of performing measurements that cannot distinguish certain sites from each other. Due to a lack of "which-way" information this leads to the creation of spatially nontrivial virtual lattices on top of the physical lattice. This turns out to have significant consequences on the dynamics of the system.

4.2 Quantum Trajectories

A simple intuitive concept of a quantum trajectory is that it is the path taken by a quantum state over time during a single experimental realisation. In particular, we consider states conditioned upon measurement results such as the photodetection times. Such a trajectory is

generally stochastic in nature as light scattering is not a deterministic process. Furthermore, they are in general discontinuous as each detection event brings about a drastic change in the quantum state due to the wave function collapse of the light field.

Before we discuss specifics relevant to our model of quantised light interacting with a quantum gas we present a more general overview which will be useful as some of the results in the following chapters are more general. Measurement always consists of at least two competing processes, two possible outcomes. If there is no competition and only one outcome is possible then our probe is meaningless as it does not reveal any information about the system. In its simplest form measurement consists of a series of detection events, such as the detections of photons. Even though, on an intuitive level it seems that we have defined only a single outcome, the detection event, this arrangement actually consists of two mutually exclusive outcomes. At any point in time an event either happens or it does not, a photon is either detected or the detector remains silent, also known as a null result. Both outcomes reveal some information about the system we are investigating. For example, let us consider measuring the number of atoms by measuring the number of photons they scatter. Each atom will on average scatter a certain number of photons contributing to the detection rate we observe. Therefore, if we record multiple photons at a high rate of arrival we learn that the illuminated region must contain many atoms. On the other hand, if there are few atoms to scatter the light we will observe few detection events which we interpret as a continuous series of non-detection events interspersed with the occasional detector click. This trajectory informs us that there are much fewer atoms being illuminated than previously.

Basic quantum mechanics tells us that such measurements will in general affect the quantum state in some way. Each event will cause a discontinuous quantum jump in the wave function of the system and it will have a jump operator, $\hat{c}$, associated with it. The effect of a detection event on the quantum state is simply the result of applying this jump operator to

the wave function, $|\psi(t)\rangle$,

$$|\psi(t+\mathrm{d}t)\rangle = \frac{\hat{c}|\psi(t)\rangle}{\sqrt{\langle\hat{c}^\dagger\hat{c}\rangle(t)}}, \tag{4.1}$$

where the denominator is simply a normalising factor [23]. The exact form of the jump operator $\hat{c}$ will depend on the nature of the measurement we are considering. For example, if we consider measuring the photons escaping from a leaky cavity then $\hat{c} = \sqrt{2\kappa}a$, where κ is the cavity decay rate and a is the annihilation operator of a photon in the cavity field. It is interesting to note that due to renormalisation the effect of a single quantum jump is independent of the magnitude of the operator $\hat{c}$ itself. However, larger operators lead to more frequent events and thus more frequent applications of the jump operator.

The null measurement outcome will have an opposing effect to the quantum jump, but it has to be treated differently as it does not occur at discrete time points like the detection events themselves [23]. Its effect is accounted for by a modification to the isolated Hamiltonian, $\hat{H}_0$, time evolution in the form

$$|\psi(t+\mathrm{d}t)\rangle = \left\{\hat{1} - \mathrm{d}t\left[i\hat{H}_0 + \frac{\hat{c}^\dagger\hat{c}}{2} - \frac{\langle\hat{c}^\dagger\hat{c}\rangle(t)}{2}\right]\right\}|\psi(t)\rangle. \tag{4.2}$$

The effect of both outcomes can be included in a single stochastic Schrödinger equation given by

$$\mathrm{d}|\psi(t)\rangle = \left[\mathrm{d}N(t)\left(\frac{\hat{c}}{\sqrt{\langle\hat{c}^\dagger\hat{c}\rangle(t)}} - \hat{1}\right) + \mathrm{d}t\left(\frac{\langle\hat{c}^\dagger\hat{c}\rangle(t)}{2} - \frac{\hat{c}^\dagger\hat{c}}{2} - i\hat{H}_0\right)\right]|\psi(t)\rangle, \tag{4.3}$$

where $\mathrm{d}N(t)$ is the stochastic increment to the number of photodetections up to time t which is equal to 1 whenever a quantum jump occurs and 0 otherwise [23]. Note that this equation has a straightforward generalisation to multiple jump operators, but we do not consider this possibility here at all.

All trajectories that we calculate in the following chapters are described by the stochastic Schrödinger equation in Eq. (4.3). The most straightforward way to solve it is to replace

the differentials by small time-steps δt. Then we generate a random number $R(t)$ at every time-step and a jump is applied, i.e. $\mathrm{d}N(t) = 1$, if

$$R(t) < \langle \hat{c}^\dagger \hat{c} \rangle (t) \delta t. \tag{4.4}$$

In practice, this is not the most efficient method for simulation [23]. Instead we will use the following method. At an initial time $t = t_0$ a random number R is generated. We then propagate the unnormalised wave function $|\tilde{\psi}(t)\rangle$ using the non-Hermitian evolution given by

$$\frac{\mathrm{d}}{\mathrm{d}t}|\tilde{\psi}(t)\rangle = -i\left(\hat{H}_0 - i\frac{\hat{c}^\dagger \hat{c}}{2}\right)|\tilde{\psi}(t)\rangle \tag{4.5}$$

up to a time T such that $\langle \tilde{\psi}(T)|\tilde{\psi}(T)\rangle = R$. This problem can be solved efficiently using standard numerical techniques. At time T a quantum jump is applied according to Eq. (4.1) which renormalises the wave function as well and the process is repeated as long as desired. This formulation also has the advantage that it provides a more intuitive picture of what happens during a single trajectory. The quantum jumps are self-explanatory, but now we have a clearer picture of the effect of null outcomes on the quantum state. Its effect is entirely encoded in the non-Hermitian modification to the original Hamiltonian given by $\hat{H} = \hat{H}_0 - i\hat{c}^\dagger \hat{c}/2$. It is now easy to see that for a jump operator, $\hat{c}$, with a large magnitude the no-event outcomes will have a more significant effect on the quantum state. At the same time they will lead to more frequent quantum jumps which have an opposing effect to the non-Hermitian evolution, because the jump condition is satisfied $\langle \tilde{\psi}(T)|\tilde{\psi}(T)\rangle = R$ more frequently. In general, the competition between these two processes is balanced and without any further external influence the distribution of outcomes over many trajectories will be entirely determined by the initial state even though each individual trajectory will be unique and conditioned on the exact detection times that occurred during the given experimental run.

However, individual trajectories can have features that are not present after averaging and this is why we focus our attention on single experimental runs rather than average behaviour.

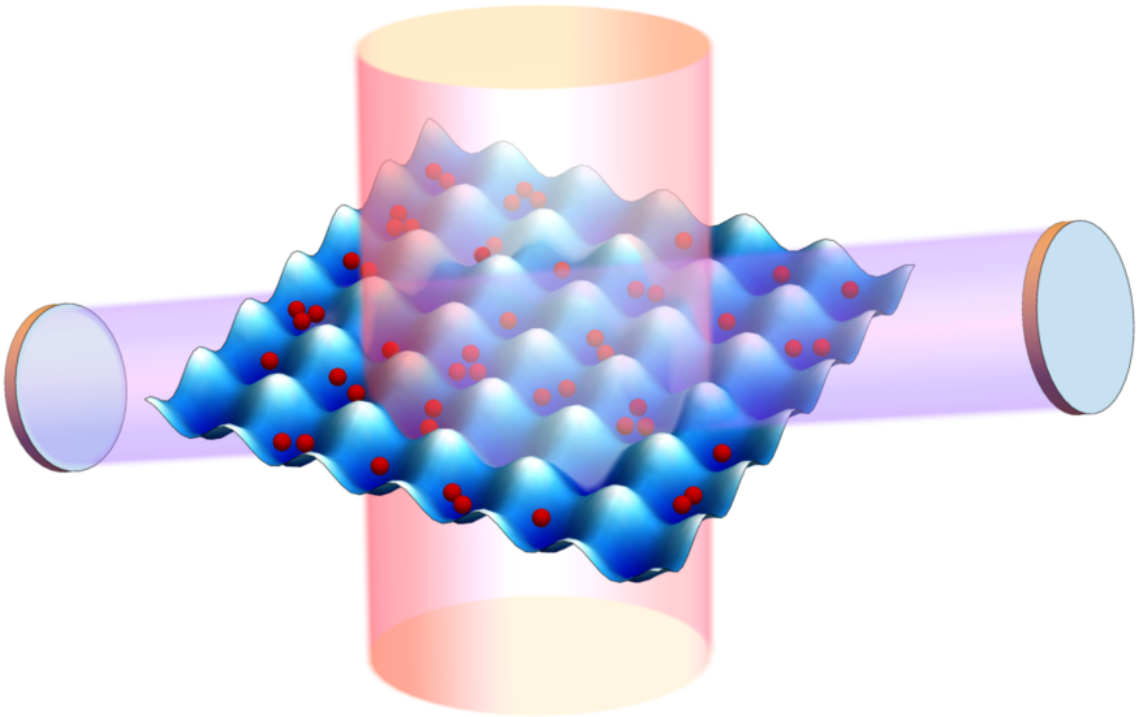

Fig. 4.1 Atoms in an optical lattice are probed by a coherent light beam (red), and the light scattered (blue) at a particular angle is enhanced and collected by a leaky cavity. The photons escaping the cavity are detected, perturbing the atomic evolution via measurement backaction.

The quantum trajectory theory can now be very straightforwardly applied to our model of ultracold bosons in an optical lattice. However, from now on we will only consider the case when the atomic system is coupled to a single mode cavity in order to enhance light scattering in one particular direction as shown in Fig. 4.1. This way we have complete control over the form of the quantum jump operator, because light scattering in different directions corresponds to different measurements as we have seen in Eq. (2.48). On the other hand, in free space we would have to simultaneously consider all the possible directions in which light could scatter and thus include multiple jump operators reducing our ability to control the system.

The model we derived in Eq. (2.28) is in fact already in a form ready for quantum trajectory simulations. The phenomenologically included cavity decay rate $-i\kappa a_1^\dagger a_1$ is in fact the non-Hermitian term $-i\hat{c}^\dagger\hat{c}/2$, where $\hat{c} = \sqrt{2\kappa}a_1$ which is the jump operator we want for measurements of photons leaking from the cavity. However, we will first simplify the system by considering the regime where we can neglect the effect of the quantum potential that builds up in the cavity. Physically, this means that whilst light scatters due to its interaction with matter, the field that builds up due to the scattered photons collecting in the cavity has a negligible effect on the atomic evolution compared to its own dynamics such as inter-site tunnelling or on-site interactions. This can be achieved when the cavity-probe detuning is smaller than the cavity decay rate, $\Delta_p \ll \kappa$ [85]. However, even though the cavity field has a negligible effect on the atoms, measurement backaction will not. This effect is of a different nature. It is due to the wave function collapse due to the destruction of photons rather than an interaction between fields. Therefore, the final form of the Hamiltonian Eq. (2.28) that we will be using in the following chapters is

$$\hat{H} = \hat{H}_0 - i\gamma\hat{F}^\dagger\hat{F} \tag{4.6}$$

$$\hat{H}_0 = -J\sum_{\langle i,j\rangle} b_i^\dagger b_j + \frac{U}{2}\sum_i \hat{n}_i(\hat{n}_i - 1), \tag{4.7}$$

where $\hat{H}_0$ is simply the Bose-Hubbard Hamiltonian, $\gamma = \kappa|C|^2$ is a quantity that measures the strength of the measurement and we have substituted $a_1 = C\hat{F}$. The quantum jumps are applied at times determined by the algorithm described above and the jump operator is given by

$$\hat{c} = \sqrt{2\kappa}C\hat{F}. \tag{4.8}$$

Importantly, we see that measurement introduces a new energy and time scale γ which competes with the two other standard scales responsible for the unitary dynamics of the closed system, tunnelling, J, and on-site interaction, U. If each atom scattered light independently a

different jump operator $\hat{c}_i$ would be required for each site projecting the atomic system into a state where long-range coherence is degraded. This is a typical scenario for spontaneous emission [144, 145], or for local [146–150] and fixed-range addressing [151, 152] which are typically considered in open systems. In contrast to such situations, we consider global coherent scattering with an operator $\hat{c}$ that is nonlocal. Therefore, the effect of measurement backaction is global as well and each jump affects the quantum state in a highly nonlocal way and most importantly not only will it not degrade long-range coherence, it will in fact lead to such long-range correlations itself.

In Chapter 3 we used highly efficient DMRG methods [137] to calculate the ground state of the Bose-Hubbard Hamiltonian. Related techniques such as Time-Evolving Block Decimation (TEBD) or t-DMRG are often used for numerical calculations of time evolution. However, despite the fact that our Hamiltonian in Eq. (4.6) is simply the Bose-Hubbard model with a non-Hermitian term added due to measurement it is actually difficult to apply these methods to our system. The problem lies in the fact that Matrix Product methods we mentioned are only efficient for one-dimensional systems that obey the area law for entanglement entropy, i.e. systems with only short-range quantum correlations. Unfortunately, the global nature of the measurement we consider violates the assumptions made in deriving the area law and, as we shall see in the following chapters, leads to long-range correlations regardless of coupling strength. Therefore, we resort to using alternative methods such as exact diagonalisation which we solve with well-known ordinary differential equation solvers. This means that we can at most simulate a few atoms, but as we shall see it is the geometry of the measurement that matters the most and these effects are already visible in smaller systems.

4.3 The Master Equation

A quantum trajectory is stochastic in nature, it depends on the exact timings of the quantum jumps which are determined randomly. This makes it difficult to obtain conclusive deterministic answers about the behaviour of single trajectories. One possible approach that is very common when dealing with open systems is to look at the unconditioned state which is obtained by averaging over the random measurement results which condition the system [23]. The unconditioned state is no longer a pure state and thus must be described by a density matrix,

$$\hat{\rho} = \sum_i p_i |\psi_i\rangle\langle\psi_i|, \tag{4.9}$$

where p_i is the probability the system is in the pure state $|\psi_i\rangle$. If more than one p_i value is non-zero then the state is mixed, it cannot be represented by a single pure state. The time evolution of the density operator obeys the master equation given by

$$\dot{\hat{\rho}} = -i\left[\hat{H}_0, \hat{\rho}\right] + \hat{c}\hat{\rho}\hat{c}^\dagger - \frac{1}{2}\left(\hat{c}^\dagger\hat{c}\hat{\rho} + \hat{\rho}\hat{c}^\dagger\hat{c}\right). \tag{4.10}$$

Physically, the unconditioned state, ρ, represents our knowledge of the quantum system if we are ignorant of the measurement outcome (or we choose to ignore it), i.e. we do not know the timings of the detection events.

We will be using the master equation and the density operator formalism in the context of measurement. However, the exact same methods are also applied to a different class of open systems, namely dissipative systems [153]. A dissipative system is an open system that couples to an external bath in an uncontrolled way. The behaviour of such a system is similar to a system subject under observation in which we ignore all the results. One can even think of this external coupling as a measurement who's outcome record is not accessible and thus must be represented as an average over all possible trajectories. However, there is a crucial difference between measurement and dissipation. When we perform a measurement we use

the master equation to describe system evolution if we ignore the measurement outcomes, but at any time we can look at the detection times and obtain a conditioned pure state for this current experimental run. On the other hand, for a dissipative system we simply have no such record of results and thus the density matrix predicted by the master equation, which in general will be a mixed state, represents our best knowledge of the system. In order to obtain a pure state, it would be necessary to perform an actual measurement.

A definite advantage of using the master equation for measurement is that it includes the effect of any possible measurement outcome. Therefore, it is useful when extracting features that are common to many trajectories, regardless of the exact timing of the events. In this case we do not want to impose any specific trajectory on the system as we are not interested in a specific experimental run, but we would still like to identify the set of possible outcomes and their common properties. Unfortunately, calculating the inverse of Eq. (4.9) is not an easy task. In fact, the decomposition of a density matrix into pure states might not even be unique. However, if a measurement leads to a projection, i.e. the final state becomes confined to some subspace of the Hilbert space, then this will be visible in the final state of the density matrix. We will show this on an example of a qubit in the quantum state

$$|\psi\rangle = \alpha|0\rangle + \beta|1\rangle, \tag{4.11}$$

where $|0\rangle$ and $|1\rangle$ represent the two basis states of the qubit and we consider performing a measurement in the basis $\{|0\rangle, |1\rangle\}$, but we don't check the outcome. The quantum state will have collapsed now to the state $|0\rangle$ with probability $|\alpha|^2$ and $|1\rangle$ with probability $|\beta|^2$. The corresponding density matrix is given by

$$\hat{\rho} = \begin{pmatrix} |\alpha|^2 & 0 \\ 0 & |\beta|^2 \end{pmatrix}, \tag{4.12}$$

which is a mixed state as opposed to the initial state. We note that there are no off-diagonal terms as the system is not in a superposition between the two basis states. Therefore, the diagonal terms represent classical probabilities of the system being in either of the basis states. This is in contrast to their original interpretation when the state was given by Eq. (4.11) when they could not be interpreted as in such a way. The initial state was in a quantum superposition and thus the state was indeterminate due to the quantum uncertainty in our knowledge of the state which would have manifested itself in the density matrix as non-zero off-diagonal terms. The significance of these values being classical probabilities is that now we know that the measurement has already happened and we know with certainty that the state must be either $|0\rangle$ or $|1\rangle$. We just don't know which one until we check the result of the measurement.

We have assumed that it was a discrete wave function collapse that lead to the state in Eq. (4.12) in which case the conclusion we reached was obvious. However, the nature of the process that takes us from the initial state to the final state with classical uncertainty does not matter. The key observation is that regardless of the trajectory taken, if the final state is given by Eq. (4.12) we will definitely know that our state is either in the state $|0\rangle$ or $|1\rangle$ and not in some superposition of the two basis states. Therefore, if we obtained this density matrix as a result of applying the time evolution given by the master equation we would be able to identify the final states of individual trajectories even though we have no information about the individual trajectories themselves. This is analogous to an approach in which decoherence due to coupling to the environment is used to model the wave function collapse [53], but here we will be looking at projective effects due to weak measurement.

Here we have considered a very simple case of a Hilbert space with two non-degenerate basis states. In the following chapters we will generalise the above result to larger Hilbert spaces with multiple degenerate subspaces which are of much greater interest as they reveal nontrivial dynamics in the system.

4.4 Global Measurement and "Which-Way" Information[1]

We have already mentioned that one of the key features of our model is the global nature of the measurement operators. A single light mode couples to multiple lattice sites from where atoms scatter the light coherently into a single mode which we enhance and collect with a cavity. If atoms at different lattice sites scatter light with a different phase or magnitude we will be able to identify which atoms contributed to the light we detected. However, if they scatter the photons in phase and with the same amplitude then we have no way of knowing which atom emitted the photon, we have no "which-way" information. When we were considering nondestructive measurements and looking at expectation values, this had no consequence on our results as we were simply interested in probing the quantum correlations of a given ground state and whether two sites were distinguishable or not was irrelevant. Now, on the other hand, we are interested in the effect of these measurements on the dynamics of the system. The effect of measurement backaction will depend on the information that is encoded in the detected photon. If a scattered mode cannot distinguish between two different lattice sites then we have no information about the distribution of atoms between those two sites. Therefore, all quantum correlations between the atoms in these sites are unaffected by the backaction whilst their correlations with the rest of the system will change as the result of the quantum jumps.

The quantum jump operator for our model is given by $\hat{c} = \sqrt{2\kappa}C\hat{F}$ and we know from Eq. (2.24) that we have a large amount of flexibility in tuning $\hat{F}$ via the geometry of the optical setup. A cavity aligned at a different angle will correspond to a different measurement. We will consider the case when $\hat{F} = \hat{D}$ given by Eq. (2.25), but since the argument depends on geometry rather than the exact nature of the operator it straightforwardly generalises to other measurement operators, including the case when $\hat{F} = \hat{B}$ where the bonds (inter-site operators)

[1] The results of this section were first published in Ref. [91]

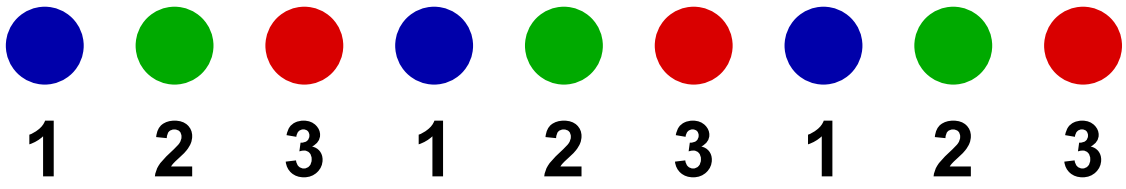

Fig. 4.2 The coefficients, and thus the operator $\hat{D}$ is made periodic with a period of three lattice sites. Therefore, the coefficients $J_{i,i}$ will repeat every third site making atoms in those sites indistinguishable to the measurement. Physically, this is due to the fact that this periodic arrangement causes the atoms within a single mode to scatter light with the same phase and amplitude. The scattered light contains no information which can be used to determine the atom distribution.

play the role of lattice sites. The operator $\hat{D}$ is given by

$$\hat{D} = \sum_i J_{i,i}\hat{n}_i, \tag{4.13}$$

where the coefficients $J_{i,i}$ are determined from Eq. (2.48). These coefficients represent the coupling strength between the atoms and the light modes and thus their spatial variation can be easily tuned by the geometry of the optical fields. We are in particular interested in making these coefficients degenerate across a number of lattice sites as shown in Figs. 4.2 and 4.3. Note that they do not have to be periodic, but it is much easier to make them so. This makes all lattice sites with the same value of $J_{i,i}$ indistinguishable to the measurement thus partitioning the lattice into a number of distinct zones which we will refer to as modes. It is crucial to note that these partitions in general are not neighbours of each other, they are not localised, they overlap in a nontrivial way, and the patterns can be made more complex in higher dimensions as shown in Fig. 4.3 or with a more sophisticated optical setup [87]. This has profound consequences as it can lead to the creation of long-range nonlocal correlations between lattice sites [93, 94]. The measurement does not know which atom within a certain mode scattered the light, there is no “which-way” information. Therefore, from the point of view of the observer’s knowledge all atoms within a mode are identical regardless of their

spatial separation. This effect can be used to create virtual lattices on top of the physical lattice.

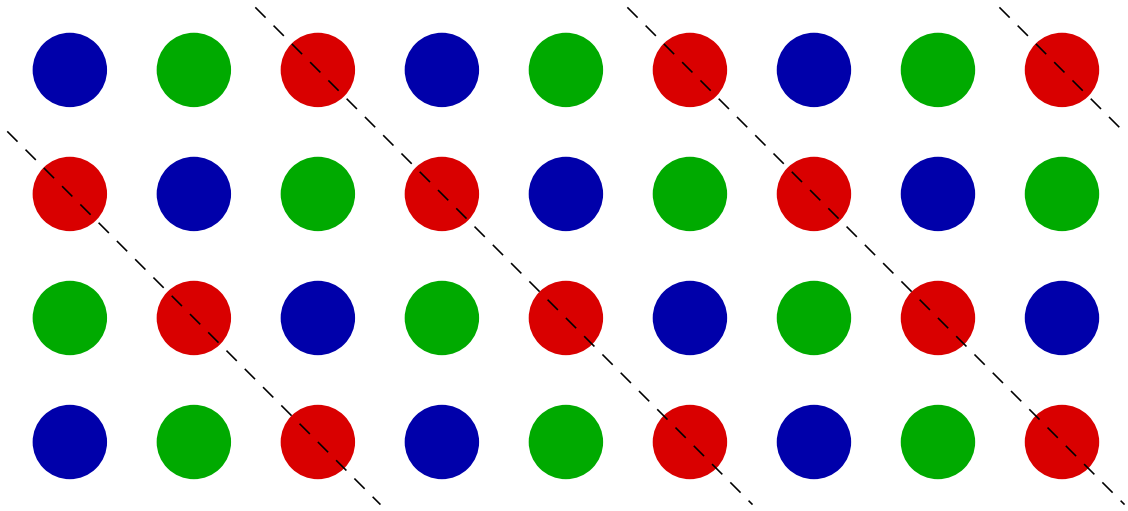

Fig. 4.3 More complex patterns of virtual lattice can be created in higher dimensions. With a more complicated setup even more complicated geometries are possible.

We will now look at a few practical examples. The simplest case is to measure in the diffraction maximum such that $a_1 = C\hat{N}_K$, where $\hat{N}_K = \sum_j^K \hat{n}_j$ is the number of atoms in the illuminated area. If the whole lattice is illuminated we effectively have a single mode as $J_{i,i} = 1$ for all sites. If only a subset of lattice sites is illuminated $K < M$ then we have two modes corresponding to the illuminated and unilluminated sites. It is actually possible to perform such a measurement in a nonlocal way by arranging every other site (e.g. all the even sites) to be at a node of both the cavity and the probe. The resulting field measures the number of atoms in the remaining sites (all the odd sites) in a global manner. It does not know how these atoms are distributed among these sites as we do not have access to the individual sites. This two mode arrangement is shown in the top panel of Fig. 4.4. A different two-mode arrangement is possible by measuring in the diffraction minimum such that each site scatters in anti-phase with its neighbours as shown in the bottom panel of Fig. 4.4.

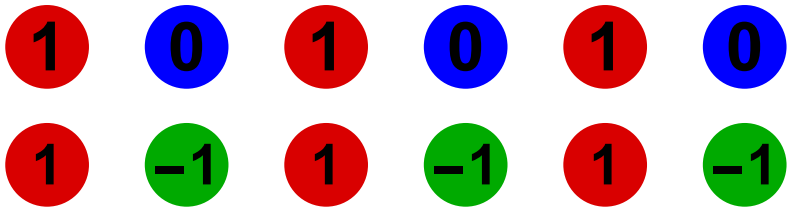

Fig. 4.4 Top: only the odd sites scatter light leading to a measurement of $\hat{N}_{\text{odd}}$ and an effective partitioning into even and odd sites. Bottom: this also partitions the lattice into odd and even sites, but this time atoms at all sites scatter light, but in anti-phase with their neighbours.

This approach can be generalised to an arbitrary number of modes, Z. For this we will consider a deep lattice such that $J_{i,i} = u_1^*(\mathbf{r})u_0(\mathbf{r})$. We will take the probe beam to be incident normally at a 1D lattice so that $u_0(\mathbf{r}) = 1$. Therefore, the final form of the scattered light field is given by

$$a_1 = C\hat{D} = C\sum_m^K \exp\left[-ik_1 md\sin\theta_1\right]\hat{n}_m. \tag{4.14}$$

From this equation we see that it can be made periodic with a period Z when

$$k_1 d\sin\theta_1 = 2\pi R/Z, \tag{4.15}$$

where R is just some integer and R/Z are is a fraction in its simplest form. Therefore, we can rewrite the Eq. (4.14) as a sum of the indistinguishable contributions from the Z modes

$$a_1 = C\hat{D} = C\sum_l^Z \exp\left[-i2\pi lR/Z\right]\hat{N}_l, \tag{4.16}$$

where $\hat{N}_l = \sum_{m\in l}\hat{n}_m$ is the sum of single site atom number operators that belong to the same mode. $\hat{N}_K$ and $\hat{N}_{\text{odd}}$ are the simplest examples of these modes. This partitions the 1D lattice in exactly $Z > 1$ modes by making every Zth lattice site scatter light with exactly the same phase. It is interesting to note that these angles correspond to the $K-1$ classical diffraction minima.

Chapter 5

Density Measurement Induced Dynamics[1]

5.1 Introduction

In the previous chapter we have introduced a theoretical framework which will allow us to study measurement backaction using discontinuous quantum jumps and non-Hermitian evolution due to null outcomes using quantum trajectories. We have also wrapped our quantum gas model in this formalism by considering ultracold bosons in an optical lattice coupled to a cavity which collects and enhances light scattered in one particular direction. One of the most important conclusions of the previous chapter was that the introduction of measurement introduces a new energy and time scale into the picture which competes with the intrinsic dynamics of the bosons.

In this chapter, we investigate the effect of quantum measurement backaction on the many-body state and dynamics of atoms. In particular, we will focus on the competition between the backaction and the two standard short-range processes, tunnelling and on-site interactions, in optical lattices. We show that the possibility to spatially structure the

[1]The results of this chapter were first published in Refs. [93–95]

measurement at a microscopic scale comparable to the lattice period without the need for single site resolution enables us to engineer efficient competition between the three processes in order to generate new nontrivial dynamics. However, unlike tunnelling and on-site interactions our measurement scheme is global in nature which makes it capable of creating long-range correlations which enable nonlocal dynamical processes. Furthermore, global light scattering from multiple lattice sites creates nontrivial spatially nonlocal coupling to the environment, as seen in section 4.4, which is impossible to obtain with local interactions [44, 146, 150]. These spatial modes of matter fields can be considered as designed systems and reservoirs opening the possibility of controlling dissipation in ultracold atomic systems without resorting to atom losses and collisions which are difficult to manipulate. Thus the continuous measurement of the light field introduces a controllable decoherence channel into the many-body dynamics. Such a quantum optical approach can broaden the field even further allowing quantum simulation models unobtainable using classical light and the design of novel systems beyond condensed matter analogues.

In the weak measurement limit, where the quantum jumps do not occur frequently compared to the tunnelling rate, this can lead to global macroscopic oscillations of bosons between odd and even sites. These oscillations occur coherently across the whole lattice enabled by the fact that measurement is capable of generating nonlocal spatial modes. When on-site interactions are included we obtain a system with three competing energy scales of which two correspond to local processes and one is global. This complicates the picture immensely. We show how under certain circumstances interactions prevent measurement from generating globally coherent dynamics, but on the other hand when the measurement is strong both processes collaborate in squeezing the atomic distribution.

On the other end of the spectrum, when measurement is strong we enter the regime of quantum Zeno dynamics. Frequent measurements can slow the evolution of a quantum system leading to the quantum Zeno effect where a quantum state is frozen in its initial

configuration [65, 66]. One can also devise measurements with multi-dimensional projections which lead to quantum Zeno dynamics where unitary evolution is uninhibited within this degenerate subspace, usually called the Zeno subspace [66, 74–76]. Our flexible setup where global light scattering can be engineered allows us to suppress or enhance specific dynamical processes thus realising spatially nonlocal quantum Zeno dynamics. This unconventional variation occurs when measurement is near, but not in, its projective limit. The system is still confined to Zeno subspaces, but intermediate transitions are allowed via virtual Raman-like processes. We show that this result can, in general (i.e. beyond the ultracold gas model), be approximated by a non-Hermitian Hamiltonian thus extending the notion of quantum Zeno dynamics into the realm of non-Hermitian quantum mechanics joining the two paradigms.

5.2 Quantum Measurement Induced Dynamics

5.2.1 Large-Scale Dynamics due to Weak Measurement

We start by considering the weak measurement limit when photon scattering does not occur frequently compared to the tunnelling rate of the atoms, i.e. $\gamma \ll J$. When the system is probed in this way, the measurement is unable to project the quantum state of the bosons to an eigenspace as postulated by the Copenhagen interpretation of quantum mechanics. The backaction of the photodetections is simply not strong or frequent enough to confine the atoms. However, instead of confining the evolution of the quantum state, it has been shown in Refs. [93, 95] that the measurement leads to coherent global oscillations between the modes generated by the spatial profile of the light field which we have seen in section 4.4. Fig. 5.1 illustrates the atom number distributions in the odd sites for $Z = 2$ and one of the three modes for $Z = 3$. These oscillations correspond to atoms flowing from one mode to another. We only observe a small number of well defined components which means that this flow happens in phase, all the atoms are tunnelling between the modes together in unison.

Furthermore, this exchange of population is macroscopic in scale. The trajectories reach a state where the maximum displacement point corresponds to all the atoms being entirely within a single mode. Finally, we note that these oscillating distributions are squeezed by the measurement and the individual components have a width smaller than the initial state. By contrast, in the absence of the external influence of measurement these distributions would spread out significantly and the centre of the broad distribution would oscillate with an amplitude comparable to the initial imbalance, i.e. small oscillations for a small initial imbalance.

In Figs. 5.1(b,c) we also see that the system is composed of multiple components. This depends on the quantity that is being measured and it is a consequence of the fact that the detected light intensity $a_1^\dagger a_1$ is not sensitive to the light phase. The measurement will not distinguish between permutations of mode occupations that scatter light with the same intensity, but with a different phase. For example, when measuring $\hat{D} = \hat{N}_{\text{odd}} - \hat{N}_{\text{even}}$, the light intensity will be proportional to $\hat{D}^\dagger \hat{D} = (\hat{N}_{\text{odd}} - \hat{N}_{\text{even}})^2$ and thus it cannot distinguish between a positive and negative imbalance leading to the two components seen in Fig. 5.1. More generally, the number of components of the atomic state, i.e. the degeneracy of $a_1^\dagger a_1$, can be computed from the eigenvalues of Eq. (4.16),

$$\hat{D} = \sum_l^Z \exp[-i2\pi lR/Z]\hat{N}_l. \tag{5.1}$$

Each eigenvalue can be represented as the sum of the individual terms in the above sum which are vectors on the complex plane with phases that are integer multiples of $2\pi/Z$: $N_1 e^{-i2\pi R/Z}$, $N_2 e^{-i4\pi R/Z}$, ..., N_Z. Since the set of possible sums of these vectors is invariant under rotations by $2\pi lR/Z$, $l \in \mathbb{Z}$, and reflection in the real axis, the state of the system is 2-fold degenerate for $Z = 2$ (reflections leave $Z = 2$ unchanged) and $2Z$-fold degenerate for $Z > 2$. Fig. 5.1 shows the three mode case, where there are in fact 6 components ($2Z = 6$), but in this case they all occur in pairs resulting in only three visible components.

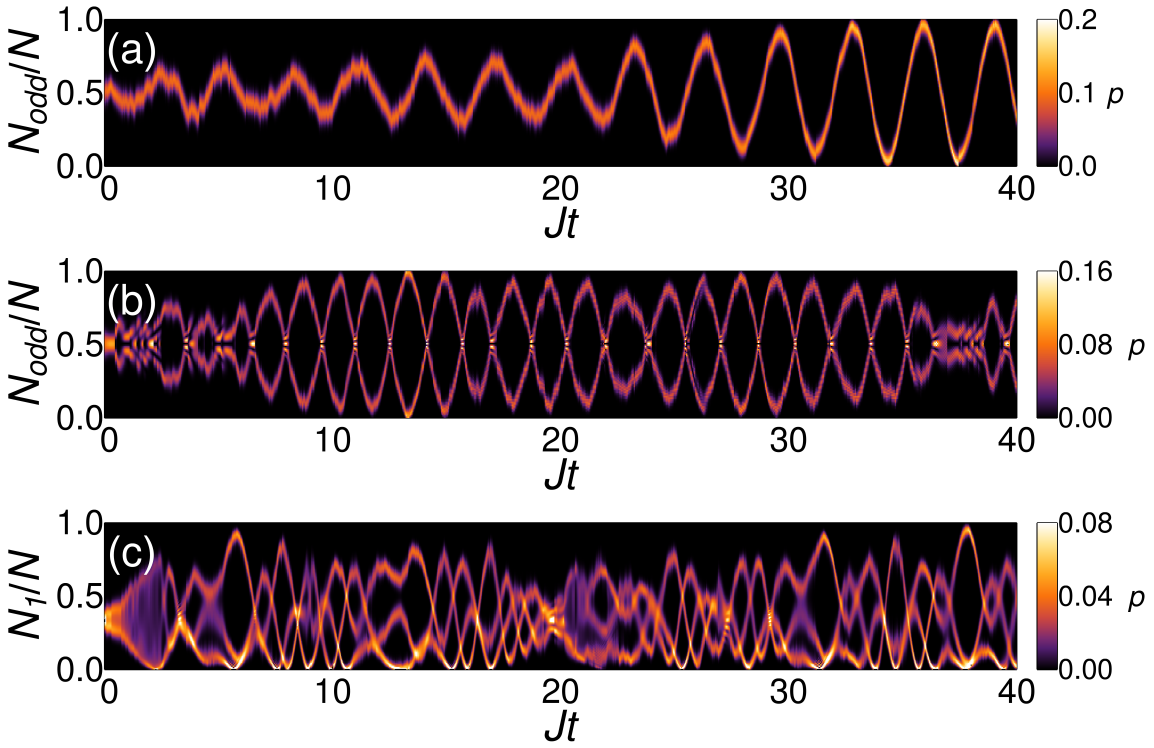

Fig. 5.1 Large oscillations between the measurement-induced spatial modes resulting from the competition between tunnelling and weak measurement induced backaction. The plots show the atom number distributions $p(N_l)$ in one of the modes in individual quantum trajectories. These distributions show various numbers of well-squeezed components reflecting the creation of macroscopic superposition states depending on the measurement configuration. $U/J = 0$, $\gamma/J = 0.01$, $M = N$, initial states: bosonic superfluid. (a) Measurement of the atom number at odd sites $\hat{N}_{\rm odd}$ creates one strongly oscillating component in $p(N_{\rm odd})$ ($N = 100$ bosons, $J_{j,j} = 1$ if j is odd and 0 otherwise). (b) Measurement of $(\hat{N}_{\rm odd} - \hat{N}_{\rm even})^2$ introduces $Z = 2$ modes and preserves the superposition of positive and negative atom number differences in $p(N_{\rm odd})$ ($N = 100$ bosons, $J_{j,j} = (-1)^{j+1}$). (c) Measurement for $Z = 3$ modes preserves three components in $p(N_1)$ ($N = 108$ bosons, $J_{j,j} = e^{i2\pi j/3}$).

We will now limit ourselves to a specific illumination pattern with $\hat{D} = \hat{N}_{\text{odd}}$ as this leads to the simplest multimode dynamics with $Z = 2$ and only a single component as seen in Fig. 5.1(a), i.e. no multiple peaks like in Figs. 5.1(b,c). This pattern can be obtained by crossing two beams such that their projections on the lattice are identical and the even sites are positioned at their nodes. However, even though this is the simplest possible case and we are only dealing with non-interacting atoms solving the full dynamics of the Bose-Hubbard Hamiltonian combined with measurement is nontrivial. The backaction introduces a highly nonlinear global term. However, it has been shown in Ref. [95] that the non-interacting dynamics with quantum measurement backaction for Z-modes reduce to an effective Bose-Hubbard Hamiltonian with Z-sites provided the initial state is a superfluid. In this simplified model the N_j atoms in the j-th site correspond to a superfluid of N_j atoms within a single spatial mode as defined in section 4.4. Therefore, we now proceed to study the dynamics for $\hat{D} = \hat{N}_{\text{odd}}$ using this reduced effective double-well model.

The atomic state can be written as

$$|\psi\rangle = \sum_{l}^{N} q_l |l, N-l\rangle, \tag{5.2}$$

where the ket $|l, N-l\rangle$, represents a superfluid with l atoms in the odd sites and $N-l$ atoms in the even sites. The non-Hermitian Hamiltonian describing the time evolution in between the jumps is given by

$$\hat{H} = -J\left(b_o^\dagger b_e + b_o b_e^\dagger\right) - i\gamma\hat{n}_o^2 \tag{5.3}$$

and the quantum jump operator which is applied at each photodetection is $\hat{c} = \sqrt{2\kappa}C\hat{n}_o$. b_o ($b_o^\dagger$) is the annihilation (creation) operator in the left site of the effective double-well corresponding to the superfluid at odd sites of the physical lattice. b_e ($b_e^\dagger$) is defined similarly, but for the right site and the superfluid at even sites of the physical lattice. $\hat{n}_o = b_o^\dagger b_o$ is the atom number operator in the left site.

Even though Eq. (5.3) is relatively simple as it is only a non-interacting two-site model, the non-Hermitian term complicates the situation making the system difficult to solve. However, a semiclassical approach to boson dynamics in a double-well in the limit of many atoms $N \gg 1$ has been developed in Ref. [154]. It was originally formulated to treat squeezing in a weakly interacting bosonic gas, but it can easily be applied to our system as well. In the limit of large atom number, the wave function in Eq. (5.2) can be described using continuous variables by defining $\psi(x = l/N) = \sqrt{N}q_l$. Note that this requires the coefficients q_l to vary smoothly which is the case for a superfluid state. We now rescale the Hamiltonian in Eq. (5.3) to be dimensionless by dividing by NJ and define the relative population imbalance between the two wells $z = 2x - 1$. Finally, by taking the expectation value of the Hamiltonian and looking for the stationary points of $\langle\psi|\hat{H}|\psi\rangle - E\langle\psi|\psi\rangle$ we obtain the semiclassical Schrödinger equation

$$ih\partial_t\psi(z,t) = \mathcal{H}\psi(z,t), \tag{5.4}$$

$$\mathcal{H} \approx -2h^2\partial_z^2\psi(z,t) + \left[\frac{\omega^2 z^2}{8} - \frac{i\Gamma}{4}(z+1)^2\right]\psi(z,t), \tag{5.5}$$

where $\Gamma = N\kappa|C|^2/J$, $h = 1/N$, $\omega = 2\sqrt{1+\Lambda-h}$, and $\Lambda = NU/(2J)$. The full derivation is not straightforward, but the introduction of the non-Hermitian term requires only a minor modification to the original formalism presented in detail in Ref. [154] so we have omitted it here. We will also be considering $U = 0$ as the effective model is only valid in this limit, thus $\Lambda = 0$. However, this model is valid for an actual physical double-well setup in which case interacting bosons can also be considered. The equation is defined on the interval $z \in [-1,1]$, but $z \ll 1$ has been assumed in order to simplify the kinetic term and approximate the potential as parabolic. This does mean that this approximation is not valid for the maximum amplitude oscillations seen in Fig. 5.1(a), but since they already appear

early on in the trajectory we are able to obtain a valid analytic description of the oscillations and their growth.

A superfluid state in our continuous variable approximation corresponds to a Gaussian wave function ψ. Furthermore, since the potential is parabolic, even with the inclusion of the non-Hermitian term, it will remain Gaussian during subsequent time evolution. Therefore, we will use a very general Gaussian wave function of the form

$$\psi(z,t) = \frac{1}{\pi b^2} \exp\left[i\varepsilon - \frac{(z-z_0)^2}{2b^2} + \frac{i\phi(z-z_\phi)^2}{2b^2} \right] \tag{5.6}$$

as our ansatz to Eq. (5.4). The parameters b, ϕ, z_0, and z_ϕ are real-valued functions of time whereas ε is a complex-valued function of time. Physically, the value b^2 denotes the width, z_0 the position of the centre, ϕ and z_ϕ contain the local phase information, and ε only affects the global phase and norm of the Gaussian wave packet.

The non-Hermitian Hamiltonian and an ansatz are not enough to describe the full dynamics due to measurement. We also need to know the effect of each quantum jump. Within the continuous variable approximation, our quantum jump become $\hat{c} \propto 1+z$. We neglect the constant prefactors, because the wave function is normalised after a quantum jump. Expanding around the peak of the Gaussian ansatz we get

$$1+z \approx \exp\left[\ln(1+z_0) + \frac{z-z_0}{1+z_0} - \frac{(z-z_0)^2}{2(1+z_0)^2} \right]. \tag{5.7}$$

Multiplying the wave function in Eq. (5.6) with the jump operator above yields a Gaussian wave function as well, but the parameters change discontinuously according to

$$b^2 \to \frac{b^2(1+z_0)^2}{(1+z_0)^2+b^2}, \tag{5.8}$$

$$\phi \to \frac{\phi(1+z_0)^2}{(1+z_0)^2+b^2}, \tag{5.9}$$

$$z_0 \to z_0 + \frac{b^2(1+z_0)}{(1+z_0)^2+b^2}, \tag{5.10}$$

$$z_\phi \to z_\phi, \tag{5.11}$$

$$\varepsilon \to \varepsilon. \tag{5.12}$$

The fact that the wave function remains Gaussian after a photodetection is a huge advantage, because it means that the combined time evolution of the system can be described with a single Gaussian ansatz in Eq. (5.6) subject to non-Hermitian time evolution according to Eq. (5.4) with discontinuous changes to the parameter values at each quantum jump.

Having identified an appropriate ansatz and the effect of quantum jumps we proceed with solving the dynamics of wave function in between the photodetections. The initial values of the parameters for a superfluid state of N atoms across the whole lattice are $b^2 = 2h$, $\phi = 0$, $a_0 = 0$, $a_\phi = 0$, $\varepsilon = 0$. However, we use the most general initial conditions at time $t = t_0$ which we denote by $b(t_0) = b_0$, $\phi(t_0) = \phi_0$, $z_0(t_0) = a_0$, $z_\phi(t_0) = a_\phi$, and $\varepsilon(t_0) = \varepsilon_0$. The reason for keeping them as general as possible is that after every quantum jump the system changes discontinuously. The subsequent time evolution is obtained by solving the Schrödinger equation with the post-jump parameter values as the new initial conditions.

By plugging the ansatz in Eq. (5.6) into the Schrödinger equation in Eq. (5.4) we obtain three differential equations

$$-2h^2p^2 + \left(\frac{\omega^2}{8} - \frac{i\Gamma}{4}\right) + \frac{ih}{2}\frac{\mathrm{d}p}{\mathrm{d}t} = 0, \tag{5.13}$$

$$4h^2pq - \frac{i\Gamma}{2} - ih\frac{\mathrm{d}q}{\mathrm{d}t} = 0 \tag{5.14}$$

$$-2h^2(q^2-p) - \frac{i\Gamma}{4} - ih\left(\frac{1}{4x}\frac{\mathrm{d}x}{\mathrm{d}t} + i\frac{\mathrm{d}\varepsilon}{\mathrm{d}t} - \frac{1}{2}\frac{\mathrm{d}r}{\mathrm{d}t}\right) = 0, \tag{5.15}$$

where $x = 1/b^2$, $p = (1-i\phi)/b^2$, $q = (z_0 - i\phi z_\phi)/b^2$, and $r = (z_0^2 - \phi z_\phi^2)/b^2$. The corresponding initial conditions are $x(t_0) = x_0 = 1/b_0^2$, $p(t_0) = p_0 = (1-i\phi_0)/b_0^2$, $q(t_0) = q_0 =$

$(a_0 - \phi_0 a_\phi)/b_0^2$, and $r(t_0) = r_0 = (a_0^2 - \phi_0 a_\phi^2)/b_0^2$. The original parameters can be extracted from these auxiliary variables by $b^2 = 1/\Re\{p\}$, $\phi = -\Im\{p\}/\Re\{p\}$, $z_0 = \Re\{q\}/\Re\{p\}$, $z_\phi = \Im\{q\}/\Im\{p\}$, and ε appears explicitly in the equations above.

First, it is worth noting that all parameters of interest can be extracted from $p(t)$ and $q(t)$ alone. We are not interested in $\varepsilon(t)$ as it is only related to the global phase and the norm of the wave function and it contains little physical information. Furthermore, an interesting and incredibly convenient feature of these equations is that the Eq. (5.13) is a function of $p(t)$ alone and Eq. (5.14) is a function of $p(t)$ and $q(t)$ only. Therefore, we only need to solve first two equations and we can neglect Eq. (5.15). However, in order to actually perform Monte-Carlo simulations of quantum trajectories Eq. (5.15) would need to be solved in order to obtain correct jump statistics.

We start with Eq. (5.13) and we note it can be rearranged into the form

$$\frac{\mathrm{d}p}{(\zeta\omega/4h)^2 - p^2} = i4h\mathrm{d}t, \tag{5.16}$$

where $\zeta^2 = (\alpha - i\beta)^2 = 1 - i2\Gamma/\omega^2$, and

$$\alpha = \sqrt{\frac{1}{2} + \frac{1}{2}\sqrt{1 + \frac{4\Gamma^2}{\omega^4}}}, \tag{5.17}$$

$$\beta = -\sqrt{-\frac{1}{2} + \frac{1}{2}\sqrt{1 + \frac{4\Gamma^2}{\omega^4}}}. \tag{5.18}$$

This is a standard integral[2]and thus yields

$$p(t) = \frac{\zeta\omega}{4h}\frac{(\zeta\omega + 4hp_0)e^{i\zeta\omega t} - (\zeta\omega - 4hp_0)e^{-i\zeta\omega t}}{(\zeta\omega + 4hp_0)e^{i\zeta\omega t} + (\zeta\omega - 4hp_0)e^{-i\zeta\omega t}}. \tag{5.19}$$

[2] $$\int \frac{\mathrm{d}x}{a^2 - x^2} = \frac{1}{2a}\ln\left(\frac{a+x}{a-x}\right) + \text{const.}$$

Having found an expression for $p(t)$ we can now solve Eq. (5.14) for $q(t)$. To do that we first define the integrating factor

$$I(t) = \exp\left[i4h\int p\mathrm{d}t\right] = (\zeta\omega + 4hp_0)e^{i\zeta\omega t} + (\zeta\omega - 4hp_0)e^{-i\zeta\omega t}, \tag{5.20}$$

which lets us rewrite Eq. (5.14) as

$$\frac{\mathrm{d}}{\mathrm{d}t}(Iq) = -\frac{\Gamma}{2h}I. \tag{5.21}$$

Upon integrating and the substitution of the explicit form of the integration factor into this equation we obtain the solution

$$q(t) = \frac{1}{2h\zeta\omega}\frac{4h\zeta^2\omega^2 q_0 - i8h\Gamma p_0 + i\Gamma[(\zeta\omega + 4hp_0)e^{i\zeta\omega t} - (\zeta\omega - 4hp_0)e^{-i\zeta\omega t}]}{(\zeta\omega + 4hp_0)e^{i\zeta\omega t} + (\zeta\omega - 4hp_0)e^{-i\zeta\omega t}}. \tag{5.22}$$

The solutions we have obtained to $p(t)$ in Eq. (5.19) and $q(t)$ in Eq. (5.22) are sufficient to completely describe the physics of the system. Unfortunately, these expressions are fairly complex and it is difficult to extract the physically meaningful parameters in a form that is easy to analyse. Therefore, we instead consider the case when $\Gamma = 0$, but we do not neglect the effect of quantum jumps. It may seem counter-intuitive to neglect the term that appears due to measurement, but we are considering the weak measurement regime where $\gamma \ll J$ and thus the dynamics between the quantum jumps are actually dominated by the tunnelling of atoms rather than the null outcomes. Furthermore, the effect of the quantum jump is independent of the value of Γ (Γ only determined their frequency). However, this is only true at times shorter than the average time between two consecutive quantum jumps. Therefore, this approach will not yield valid answers on the time scale of a whole quantum trajectory, but it will give good insight into the dynamics immediately after a quantum jump. The

solutions for $\Gamma = 0$ are

$$b^2(t) = \frac{b_0^2}{2}\left[\left(1+\frac{16h^2(1+\phi_0^2)}{b_0^4\omega^2}\right)+\left(1-\frac{16h^2(1+\phi_0^2)}{b_0^4\omega^2}\right)\cos(2\omega t)+\frac{8h\phi_0}{b_0^2\omega}\sin(2\omega t)\right], \tag{5.23}$$

$$\phi(t) = \frac{b_0^2\omega}{8h}\left[\left(\frac{16h^2(1+\phi_0^2)}{b_0^4\omega^2}-1\right)\sin(2\omega t)+\frac{8h\phi_0}{b_0^2\omega}\cos(2\omega t)\right], \tag{5.24}$$

$$z_0(t) = a_0\cos(\omega t)+\frac{4h\phi_0}{b_0^2\omega}(a_0-a_\phi)\sin(\omega t), \tag{5.25}$$

$$\phi(t)z_\phi(t) = \phi_0 a_\phi\cos(\omega t)+\frac{4h}{b_0^2\omega}(a_0-\phi_0^2 a_\phi)\sin(\omega t). \tag{5.26}$$

First, these equations show that all quantities oscillate with a frequency ω or 2ω. We are in particular interested in the quantity $z_0(t)$ as it represents the position of the peak of the wave function and we see that it oscillates with an amplitude $\sqrt{a_0^2+16h^2\phi_0^2(a_0-a_\phi)^2/(b_0^4\omega^2)}$. Thus we have obtained a solution that clearly shows oscillations of a single Gaussian wave packet. The fact that this appears even when $\Gamma = 0$ shows that the oscillations are a property of the Bose-Hubbard model itself. However, they also depend on the initial conditions and for these oscillations to occur, a_0 and a_ϕ cannot be zero, but this is exactly the case for an initial superfluid state. We have seen in Eq. (5.10) that the effect of a photodetection is to displace the wave packet by approximately b^2, i.e. the width of the Gaussian, in the direction of the positive z-axis. Therefore, even though the atoms can oscillate in the absence of measurement it is the quantum jumps that are the driving force behind this phenomenon. Furthermore, these oscillations grow because the quantum jumps occur at an average instantaneous rate proportional to $\langle\hat{c}^\dagger\hat{c}\rangle(t)$ which itself is proportional to $(1+z)^2$. This means they are most likely to occur at the point of maximum displacement in the positive z direction at which point a quantum jump provides positive feedback and further increases the amplitude of the wave function leading to the growth seen in Fig. 5.1(a). The oscillations themselves are essentially due to the natural dynamics of coherently displaced atoms in a lattice , but it is the measurement that causes the initial and more importantly coherent displacement and the

positive feedback drive which causes the oscillations to continuously grow. Furthermore, it is by engineering the measurement, and through it the geometry of the modes, that we have control over the nature of the correlated dynamics of the oscillations.

We have now seen the effect of the quantum jumps and how that leads to oscillations between odd and even sites in a lattice. However, we have neglected the effect of null outcomes on the dynamics. Even though it is small, it will not be negligible on the time scale of a quantum trajectory with multiple jumps. First, we note that all the oscillatory terms $p(t)$ and $q(t)$ actually appear as $\zeta\omega = (\alpha - i\beta)\omega$. Therefore, we can see that the null outcomes lead to two effects: an increase in the oscillation frequency by a factor of α to $\alpha\omega$ and a damping term with a time scale $1/(\beta\omega)$. For weak measurement, both α and β will be close to 1 so the effects are not visible on short time scales. Instead, we look at the long time limit. Unfortunately, since all the quantities are oscillatory a stationary long time limit does not exist especially since the quantum jumps provide a driving force. However, the width of the Gaussian, b^2, is unique in that it does not oscillate around $b^2 = 0$. Furthermore, from Eq. (5.8) we see that even though it will decrease discontinuously at every jump, this effect is fairly small since $b^2 \ll 1$ generally. Therefore, we expect b^2 to oscillate, but with an amplitude that decreases approximately monotonically with time due to quantum jumps and the $1/(\beta\omega)$ decay terms, because unlike for z_0 the quantum jumps do not cause further displacement in this quantity. Thus, neglecting the effect of quantum jumps and taking the long time limit yields

$$b^2(t \to \infty) = \frac{4h}{\gamma\omega} \approx b_{\mathrm{SF}}^2 \left(1 - \frac{\Gamma^2}{32}\right), \tag{5.27}$$

where the approximation on the right-hand side follows from the fact that $\omega \approx 2$ since we are considering the $N \gg 1$ limit, and because we are considering the weak measurement limit $\Gamma^2/\omega^4 \ll 1$. $b_{\mathrm{SF}}^2 = 2h$ denotes the width of the initial superfluid state. This result is interesting, because it shows that the width of the Gaussian distribution is squeezed as compared with its initial state which is exactly what we see in Fig. 5.1(a). However, if we

substitute the parameter values used in that trajectory we only get a reduction in width by about 3%, but the maximum amplitude oscillations look like they have a significantly smaller width than the initial distribution. This discrepancy is due to the fact that the continuous variable approximation is only valid for $z \ll 1$ and thus it cannot explain the final behaviour of the system. Furthermore, it has been shown that the width of the distribution b^2 does not actually shrink to a constant value, but rather it keeps oscillating around the value given in Eq. (5.27) [95]. However, what we do see is that during the early stages of the trajectory, which are well described by this model, is that the width does in fact stay roughly constant. It is only in the later stages when the oscillations reach maximal amplitude that the width becomes visibly reduced.

5.2.2 Three-Way Competition

Now it is time to turn on the inter-atomic interactions, $U/J \neq 0$. As a result the atomic dynamics will change as the measurement now competes with both the tunnelling and the on-site interactions. A common approach to study such open systems is to map a dissipative phase diagram by finding the steady state of the master equation for a range of parameter values [155]. However, here we adopt a quantum optical approach in which we focus on the conditional dynamics of a single quantum trajectory as this corresponds to a single realisation of an experiment. The resulting evolution does not necessarily reach a steady state and usually occurs far from the ground state of the system.

A key feature of the quantum trajectory approach is that each trajectory evolves differently as it is conditioned on the photodetection times which are determined stochastically. Furthermore, even states in the same measurement subspace, i.e. indistinguishable to the measurement , can have minimal overlap. This is in contrast to the unconditioned solutions obtained with the master equation which only yields a single outcome that is an average

taken over all possible outcomes. However, this makes it difficult to study the three-way competition in some meaningful way across the whole parameter range.

Ultimately, regardless of its strength measurement always tries to project the quantum state onto one of its eigenstates (or eigenspaces if there are degeneracies). If the probe is strong enough this will succeed, but we have seen in the previous section that when this is not the case, measurement leads to new dynamical phenomena. However, despite this vast difference in behaviour, there is a single quantity that lets us determine the degree of success of the projection, namely the fluctuations, σ_D^2 (or equivalently the standard deviation, σ_D), of the observable that is being measured, $\hat{D}$. For a perfect projection this value is exactly zero, because the system at that point is in the corresponding eigenstate. When the system is unable to project the state into such a state, the variance will be non-zero. However, the smaller its value is the closer it is to being in such an eigenstate and on the other hand a large variance means that the internal processes dominate the competition. Finally, this quantity is perfect to study quantum trajectories, because its value in the long-time limit it is only a function of γ, J, and U. It does not depend on the explicit history of photodetections. Fig. 5.2 shows a plot of this quantity for $\hat{D} = \hat{N}_{\text{odd}}$ averaged over multiple trajectories, $\langle \sigma_D^2 \rangle_{\text{traj}}$, as a function of γ/J and U/J for a lattice of six atoms on six sites (we cannot use the effective double-well model, because $U \neq 0$). We use a ground state for the corresponding U and J values as this provides a realistic starting point and a reference for comparing the measurement induced dynamics. We will also consider only $\hat{D} = \hat{N}_{\text{odd}}$ unless stated otherwise.

First, it is important to note that even though we are dealing with an average over many trajectories this information cannot be extracted from a master equation solution. This is because the variance of $\hat{D}$ as calculated from the density matrix would be dominated by the uncertainty of the final state. In other words, the fact that the final value of $\hat{D}$ is undetermined is included in this average and thus the fluctuations obtained this way are representative of the variance in the final outcome rather than the squeezing of an individual conditioned

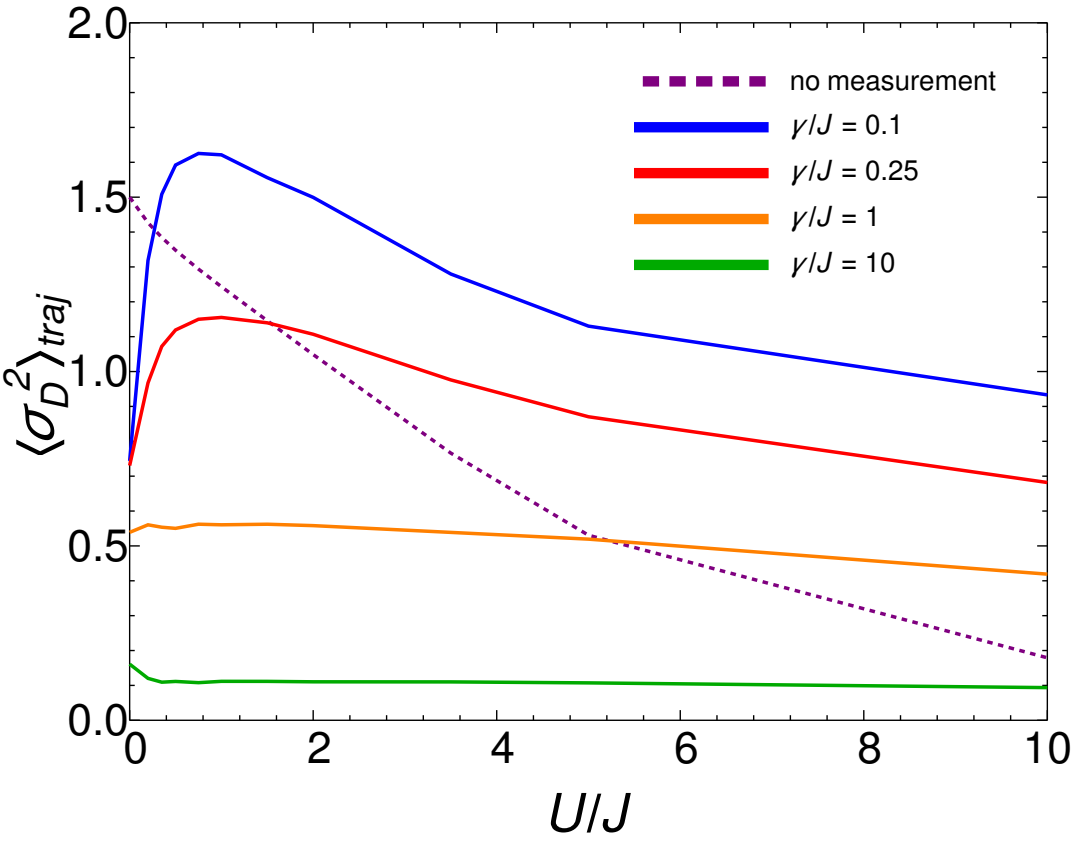

Fig. 5.2 Atom number fluctuations at odd sites for $N = 6$ atoms at $M = 6$ sites subject to a $\hat{D} = \hat{N}_{\text{odd}}$ measurement demonstrating the competition of global measurement with local interactions and tunnelling. Number variances are averaged over 100 trajectories. Error bars are too small to be shown ($\sim 1\%$) which emphasizes the universal nature of the squeezing. The initial state used was the ground state for the corresponding U and J value. The fluctuations in the ground state without measurement decrease as U/J increases, reflecting the transition between the superfluid and Mott insulator phases. For weak measurement values $\langle \sigma_D^2 \rangle_{\text{traj}}$ is squeezed below the ground state value for $U = 0$, but it subsequently increases and reaches its maximum as the atom repulsion prevents the accumulation of atoms prohibiting coherent oscillations thus making the squeezing less effective. In the strongly interacting limit, the Mott insulator state is destroyed and the fluctuations are larger than in the ground state as weak measurement is not strong enough to project into a state with smaller fluctuations than the ground state.

trajectory. This highlights the fact that interesting physics happens on a single trajectory level which would be lost if we studied an ensemble average.

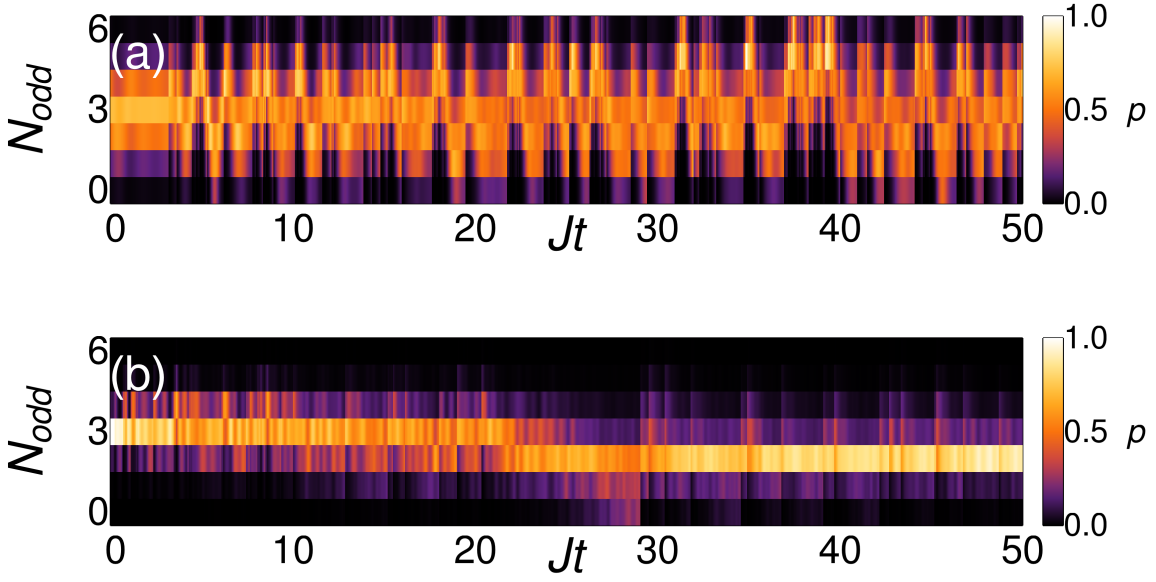

Fig. 5.3 Conditional dynamics of the atom-number distributions at odd sites illustrating competition of the global measurement with local interactions and tunnelling. The plots are for single quantum trajectories starting from the ground state for $N = 6$ atoms on $M = 6$ sites with $\hat{D} = \hat{N}_{\text{odd}}$, $\gamma/J = 0.1$. (a) Weakly interacting bosons $U/J = 1$: the on-site repulsion prevents the formation of well-defined oscillation in the population of the mode. As states with different imbalance evolve with different frequencies, the squeezing is not as efficient for the non-interacting case. (b) Strongly interacting bosons $U/J = 10$: oscillations are completely suppressed and the number of atoms in the mode is rather well-defined although clearly worse than in a Mott insulator.

Looking at Fig. 5.2 we see many interesting things happening suggesting different regimes of behaviour. For the ground state (i.e. no measurement) we see that the fluctuations decrease monotonically as U increases reflecting the superfluid to Mott insulator quantum phase transition. The measured state on the other hand behaves very differently and $\langle \sigma_D^2 \rangle_{\text{traj}}$ varies non-monotonically. For weak interactions the fluctuations are strongly squeezed below those of the ground state followed by a rapid increase as U is increased before peaking and eventually decreasing. We have already seen in the previous section and in particular Fig. 5.1

that the macroscopic oscillations at $U = 0$ are well squeezed when compared to the initial state and this is the case over here as well. However, as U is increased the interactions prevent the atoms from accumulating in one place thus preventing oscillations with a large amplitude which effectively makes the squeezing less effective as seen in Fig. 5.3(a). In fact, we have seen towards the end of the last section how for small amplitude oscillations that can be described by the effective double-well model the width of the number distribution does not change by much. Even though that model is not valid for $U \neq 0$ we should not be surprised that without macroscopic oscillations the fluctuations cannot be significantly reduced.

On the other end of the spectrum, for weak measurement, but strong on-site interactions we note that the backaction leads to a significant increase in fluctuations compared to the ground state. This is simply due to the fact that the measurement destroys the Mott insulating state, which has small fluctuations due to strong local interactions, but then subsequently is not strong enough to squeeze the resulting dynamics as shown in Fig. 5.3(b). To see why this is so easy for the quantum jumps to do we look at the ground state in first-order perturbation theory given by

$$|\Psi_{J/U}\rangle = \left[1 + \frac{J}{U}\sum_{\langle i,j\rangle} b_i^\dagger b_j\right]|\Psi_0\rangle, \tag{5.28}$$

where we have neglected the non-Hermitian term as we're in the weak measurement regime and $|\Psi_0\rangle$ is the Mott insulator state and the second term in the brackets represents a uniform distribution of particle-hole excitation pairs across the lattice. In the $U \to \infty$ limit a quantum jump has no effect as $|\Psi_0\rangle$ is already an eigenstate of $\hat{D}$. However, for finite U, each photocount will amplify the present excitations increasing the fluctuations in the system. In fact, consecutive detections lead to an exponential growth of these excitations. For $K \gg 1$ illuminated sites and unit filling of the lattice, the atomic state after m consecutive quantum jumps becomes $\hat{c}^m|\Psi_{J/U}\rangle \propto |\Psi_{J/U}\rangle + |\Phi_m\rangle$ where

$$|\Phi_m\rangle = \frac{2^m J}{KU}\sum_{i\in\text{odd}}\left(b_i^\dagger b_{i-1} - b_{i-1}^\dagger b_i - b_{i+1}^\dagger b_i + b_i^\dagger b_{i+1}\right)|\Psi_0\rangle. \tag{5.29}$$

In the weak measurement regime the effect of non-Hermitian decay is negligible compared to the local atomic dynamics combined with the quantum jumps so there is minimal dissipation occurring. Therefore, because of the exponential growth of the excitations, even a small number of photons arriving in succession can destroy the ground state. We have neglected all dynamics in between the jumps which would distribute the new excitations in a way which will affect and possibly reduce the effects of the subsequent quantum jumps. However, due to the lack of any serious decay channels they will remain in the system and subsequent jumps will still amplify them further destroying the ground state and thus quickly leading to a state with large fluctuations.

In the strong measurement regime ($\gamma \gg J$) the measurement becomes more significant than the local dynamics and the system will freeze the state in the measurement operator eigenstates. In this case, the squeezing will always be better than in the ground state, because measurement and on-site interaction cooperate in suppressing fluctuations. This cooperation did not exist for weak measurement, because it tried to induce dynamics which produced squeezed states (either successfully as seen with the macroscopic oscillations or unsuccessfully as seen with the Mott insulator). This suffered heavily from the effects of interactions as they would prevent this dynamics by dephasing different components of the coherent excitations. Strong measurement, on the other hand, squeezes the quantum state by trying to project it onto an eigenstate of the observable [57, 58]. For weak interactions where the ground state is a highly delocalised superfluid it is obvious that projections onto $\hat{D} = \hat{N}_{\text{odd}}$ will suppress fluctuations significantly. However, the strongly interacting regime is much less evident, especially since we have just demonstrated how sensitive the Mott insulating phase is to the quantum jumps when the measurement is weak.

To understand the strongly interacting case we will again use first-order perturbation theory and consider a postselected $\langle \hat{D}^\dagger \hat{D} \rangle = 0$ trajectory. This corresponds to a state that scatters no photons and thus is fully described by the non-Hermitian Hamiltonian alone.

Squeezing depends on the measurement and interaction strengths and is common to all the possible trajectories so we can gain insight into the general behaviour by considering a specific special case. However, we will instead consider $\hat{D} = \Delta\hat{N} = \hat{N}_{\text{odd}} - \hat{N}_{\text{even}}$, because this measurement also has only $Z = 2$ modes, but its $\langle\hat{D}^\dagger\hat{D}\rangle = 0$ trajectory would be very close to the Mott insulating ground state, because $\hat{D}^\dagger\hat{D}|\Psi_0\rangle = 0$ and we can expand around the Mott insulating state. Applying perturbation theory to obtain the modified ground state we get

$$|\Psi_{J,U,\gamma}\rangle = \left[1 + \frac{J}{U - i4\gamma}\sum_{\langle i,j\rangle} b_i^\dagger b_j\right]|\Psi_0\rangle. \tag{5.30}$$

The variance of the measurement operator for this state is given by

$$\sigma^2_{\Delta N} = \frac{16J^2M}{U^2 + 16\gamma^2}. \tag{5.31}$$

From the form of the denominator we immediately see that both interaction and measurement squeeze with the same quadratic dependence and that the squeezing is always better than in the ground state ($\gamma = 0$) regardless of the value of U. Also, depending on the ratio of γ/U the squeezing can be dominated by measurement ($\gamma/U \gg 1$) or by interactions ($\gamma/U \ll 1$) or both processes can contribute equally ($\gamma/U \approx 1$). The $\hat{D} = \hat{N}_{\text{odd}}$ measurement will behave similarly since the geometry is exactly the same. Furthermore, the Mott insulator state is also an eigenstate of this operator, just not the zero eigenvalue vector and thus the final state would need to be described using a balance of quantum jumps and non-Hermitian evolution complicating the picture. However, the particle-hole excitation term would be proportional to $(U^2 + \gamma^2)^{-1}$ instead since the γ coefficient in the perturbative expansion depends on $(J_{i,i} - J_{i\pm1,i\pm1})^2$. We can see the system transitioning into the strong measurement regime in Fig. 5.2 as the U-dependence flattens out with increasing measurement strength as the $\gamma/U \gg 1$ regime is reached.

5.2.3 Emergent Long-Range Correlated Tunnelling

When $\gamma \to \infty$ the measurement becomes projective. This means that as soon as the probing begins, the system collapses into one of the observable's eigenstates. Furthermore, since this measurement is continuous and does not stop after the projection the system will be frozen in this state. This effect is called the quantum Zeno effect [65, 66] from Zeno's classical paradox in which a "watched arrow never moves" that stated that since an arrow in flight is not seen to move during any single instant, it cannot possibly be moving at all. Classically the paradox was resolved with a better understanding of infinity and infinitesimal changes, but in the quantum world a watched quantum arrow will in fact never move. The system is being continuously projected into its initial state before it has any chance to evolve. If degenerate eigenspaces exist then we can observe quantum Zeno dynamics where unitary evolution is uninhibited within such a degenerate subspace, called the Zeno subspace [66, 74–76].

These effects can be easily seen in our model when $\gamma \to \infty$. The system will be projected into one or more degenerate eigenstates of $\hat{c}^\dagger \hat{c}$, $|\psi_i\rangle$, for which we define the projector $P_\varphi = \sum_{i \in \varphi} |\psi_i\rangle\langle\psi_i|$ where φ denotes a single degenerate subspace. The Zeno subspace is determined randomly as per the Copenhagen postulates and thus it depends on the initial state. If the projection is into the subspace φ, the subsequent evolution is described by the projected Hamiltonian $P_\varphi \hat{H}_0 P_\varphi$. We have used the original Hamiltonian, $\hat{H}_0$, without the non-Hermitian term or the quantum jumps as their combined effect is now described by the projectors. Physically, in our model of ultracold bosons trapped in a lattice this means that tunnelling between different spatial modes is completely suppressed since this process couples eigenstates belonging to different Zeno subspaces. If a small connected part of the lattice was illuminated uniformly such that $\hat{D} = \hat{N}_K$ then tunnelling would only be prohibited between the illuminated and unilluminated areas, but dynamics proceeds normally within each zone separately. However, the geometric patterns we have in which the modes are spatially delocalised in such a way that neighbouring sites never belong to the same mode,

e.g. $\hat{D} = \hat{N}_{\text{odd}}$, would lead to a complete suppression of tunnelling across the whole lattice as there is no way for an atom to tunnel within this Zeno subspace without first having to leave it.

This is an interesting example of the quantum Zeno effect and dynamics and it can be used to prohibit parts of the dynamics of the Bose-Hubbard Model in order to engineer desired Hamiltonians for quantum simulations or other applications. However, the infinite projective limit is uninteresting in the context of a global measurement scheme. The same effects and Hamiltonians can be achieved using multiple independent measurements which address a few sites each. In order to take advantage of the nonlocal nature of the measurement it turns out that we need to consider a finite limit for $\gamma \gg J$. By considering a non-infinite γ we observe additional dynamics while the usual atomic tunnelling is still heavily Zeno-suppressed. These new effects are shown in Fig. 5.4.

There are two crucial features of the resulting dynamics that are of note. First, just like in the infinite quantum Zeno limit the evolution between nearest neighbours within the same mode is unperturbed whilst tunnelling between different modes is heavily suppressed by the measurement. Therefore, we see the usual quantum Zeno dynamics within a single Zeno subspace and just like before, it is also possible to use the global probing scheme to engineer these eigenspaces and select which tunnelling processes should be uninhibited and which should be suppressed. However, there is a second effect that was not present before. In Fig. 5.4 we can observe tunnelling that violates the boundaries established by the spatial modes. When γ is finite, second-order processes, i.e. two correlated tunnelling events, can now occur via an intermediate (virtual) state outside of the Zeno subspace as long as the Zeno subspace of the final state remains the same. Crucially, these tunnelling events are only correlated in time, but not in space. This means that the two events do not have to occur for the same atom or even at the same site in the lattice. As long as the Zeno subspace is preserved, these processes can occur anywhere in the system. That is, a pair of atoms separated by many sites

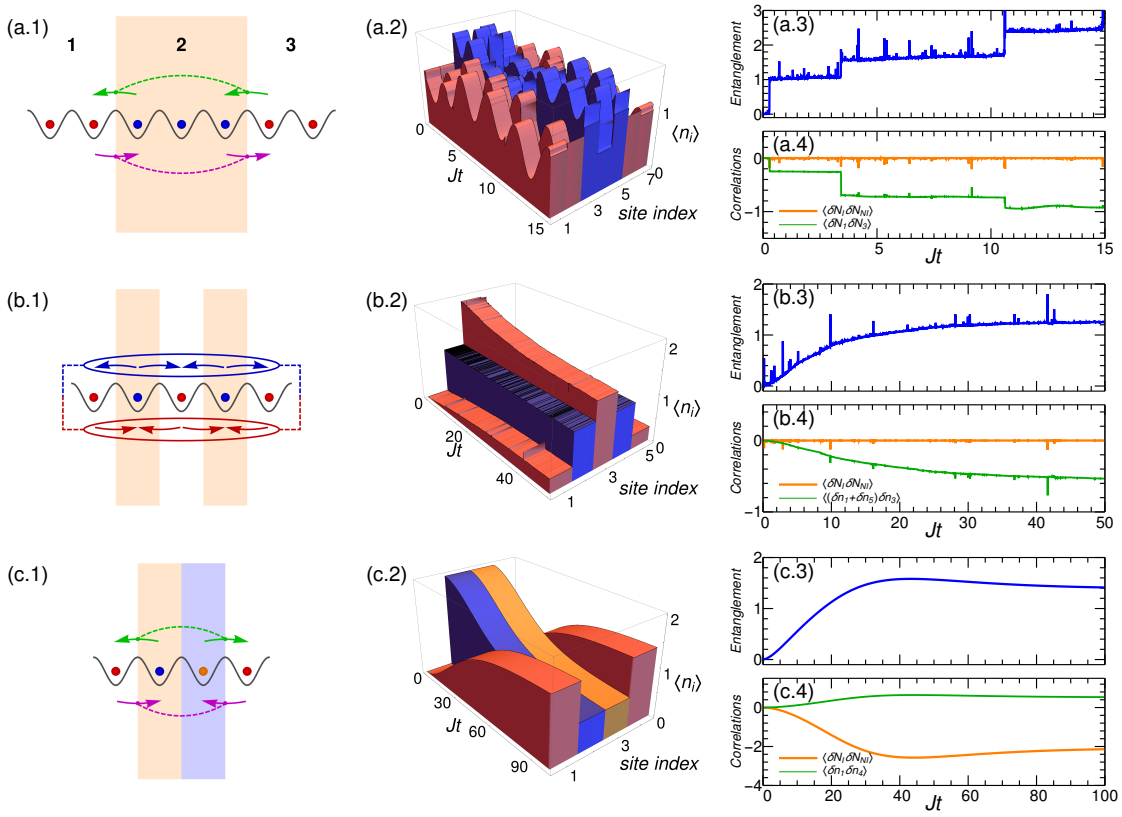

Fig. 5.4 Long-range correlated tunnelling and entanglement, dynamically induced by strong global measurement in a single quantum trajectory. (a),(b),(c) show different measurement geometries, implying different constraints. Panels (1): schematic representation of the long-range tunnelling processes. Panels (2): evolution of on-site densities. Panels (3): entanglement entropy growth between illuminated and non-illuminated regions. Panels (4): correlations between different modes (orange) and within the same mode (green); N_I (N_{NI}) is the atom number in the illuminated (non-illuminated) mode. (a) (a.1) Atom number in the central region is frozen: system is divided into three regions. (a.2) Standard dynamics happens within each region, but not between them. (a.3) Entanglement build up. (a.4) Negative correlations between non-illuminated regions (green) and zero correlations between the N_I and N_{NI} modes (orange). Initial state: $|1,1,1,1,1,1,1\rangle$, $\gamma/J = 100$, $J_{jj} = [0,0,1,1,1,0,0]$. (b) (b.1) Even sites are illuminated, freezing N_{even} and N_{odd}. Long-range tunnelling is represented by any pair of one blue and one red arrow. (b.2) Correlated tunnelling occurs between non-neighbouring sites without changing mode populations. (b.3) Entanglement build up. (b.4) Negative correlations between edge sites (green) and zero correlations between the modes defined by N_{even} and N_{odd} (orange). Initial state: $|0,1,2,1,0\rangle$, $\gamma/J = 100$, $J_{jj} = [0,1,0,1,0]$. (c) (c.1,2) Atom number difference between two central sites is frozen. (c.3) Entanglement build up. (c.4) In contrast to previous examples, sites in the same zones are positively correlated (green), while atoms in different zones are negatively correlated (orange). Initial state: $|0,2,2,0\rangle$, $\gamma/J = 100$, $J_{jj} = [0,-1,1,0]$. 1D lattice, $U/J = 0$.

is able to tunnel in a correlated manner. This is only possible due to the ability of creating extensive and spatially nonlocal modes as described in section 4.4 which in turn is enabled by the global nature of the measurement. This would not be possible to achieve with local measurements as the Zeno subspaces would be described entirely by local variables which cannot be preserved by such delocalised tunnelling events.

In the subsequent sections we will rigorously derive the following Hamiltonian for the non-interacting dynamics within a single Zeno subspace, $\varphi = 0$, for a lattice where the measurement defines $Z = 2$ distinct modes, e.g. $\hat{D} = \hat{N}_K$ or $\hat{D} = \hat{N}_{\text{odd}}$

$$\hat{H}_\varphi = P_0 \left[-J \sum_{\langle i,j \rangle} b_i^\dagger b_j - i \frac{J^2}{A\gamma} \sum_{\varphi} \sum_{\substack{\langle i \in \varphi, j \in \varphi' \rangle \\ \langle k \in \varphi', l \in \varphi \rangle}} b_i^\dagger b_j b_k^\dagger b_l \right] P_0, \tag{5.32}$$

where $A = (J_{\varphi,\varphi} - J_{\varphi',\varphi'})^2$ is a constant that depends on the measurement scheme, φ denotes a set of sites belonging to a single mode and φ' is the set's complement (e.g. odd and even or illuminated and non-illuminated sites). We see that this Hamiltonian consists of two parts. The first term corresponds to the standard quantum Zeno first-order dynamics that occurs within a Zeno subspace, i.e. tunnelling between neighbouring sites that belong to the same mode. Otherwise, if i and j belong to different modes $P_0 b_i^\dagger b_j P_0 = 0$. When $\gamma \to \infty$ we recover the quantum Zeno Hamiltonian where this would be the only remaining term. It is the second term that shows the second-order correlated tunnelling terms. This is evident from the inner sum which requires that pairs of sites (i, j) and (k, l) between which atoms tunnel must be nearest neighbours, but these pairs can be anywhere on the lattice within the constraints of the mode structure. This is in particular explicitly shown in Figs. 5.4(a,b). The imaginary coefficient means that the tunnelling behaves like an exponential decay (overdamped oscillations). This also implies that the norm will decay, but this does not mean that there are physical losses in the system. Instead, the norm itself represents the probability of the system remaining in the $\varphi = 0$ Zeno subspace. Since γ is not infinite

there is now a finite probability that the stochastic nature of the measurement will lead to a discontinuous change in the system where the Zeno subspace rapidly changes which can be seen in Fig. 5.4(a). However, later in this chapter we will see that steady states of this Hamiltonian exist which will no longer change Zeno subspaces.

Crucially, what sets this effect apart from usual many-body dynamics with short-range interactions is that first order processes are selectively suppressed by the global conservation of the measured observable and not by the prohibitive energy costs of doubly-occupied sites, as is the case in the t-J model [156]. This has profound consequences as this is the physical origin of the long-range correlated tunnelling events represented in Eq. (5.32) by the fact that the pairs $(i,\ j)$ and $(k,\ l)$ can be very distant. The projection P_0 is not sensitive to individual site occupancies, but instead enforces a fixed value of the observable, i.e. a single Zeno subspace. This is a striking difference with the t-J and other strongly interacting models. The strong interaction also leads to correlated events in which atoms can tunnel over each other by creating an unstable doubly occupied site during the intermediate step. However, these correlated events are by their nature localised. Due to interactions the doubly-occupied site cannot be present in the final state which means that any tunnelling event that created this unstable configuration must be followed by another tunnelling event which takes an atom away. In the case of global measurement this process is delocalised, because since the modes consist of many sites the stable configuration can be restored by a tunnelling event from a completely different lattice site that belongs to the same mode.

In Fig. 5.4(a) we consider illuminating only the central region of the optical lattice and detecting light in the diffraction maximum, thus we freeze the atom number in the K illuminated sites $\hat{N}_{\mathrm{K}}$ [57, 58]. The measurement scheme defines two different spatial modes: the non-illuminated zones 1 and 3 and the illuminated one 2. Figure 5.4(a.2) illustrates the evolution of the mean density at each lattice site: typical dynamics occurs within each region but the standard tunnelling between different modes is suppressed. Importantly, second-order

processes that do not change N_K are still possible since an atom from 1 can tunnel to 2, if simultaneously one atom tunnels from 2 to 3. Therefore, effective long-range tunnelling between two spatially disconnected zones 1 and 3 happens due to the two-step processes $1 \to 2 \to 3$ or $3 \to 2 \to 1$. These transitions are responsible for the negative (anti-)correlations $\langle \delta N_1 \delta N_3 \rangle = \langle N_1 N_3 \rangle - \langle N_1 \rangle \langle N_3 \rangle$ showing that an atom disappearing from zone 1 appears in zone 3, while there are no number correlations between illuminated and non-illuminated regions, $\langle (\delta N_1 + \delta N_3) \delta N_2 \rangle = 0$ as shown in Fig. 5.4(a.4). In contrast to fully-projective measurement, the existence of an intermediate (virtual) step in the correlated tunnelling process builds long-range entanglement between illuminated and non-illuminated regions as shown in Fig. 5.4(a.3).

To make correlated tunnelling visible even in the mean atom number, we suppress the standard Bose-Hubbard dynamics by illuminating only the even sites of the lattice in Fig. 5.4(b). Even though this measurement scheme freezes both N_{even} and N_{odd}, atoms can slowly tunnel between the odd sites of the lattice, despite them being spatially disconnected. This atom exchange spreads correlations between non-neighbouring lattice sites on a time scale $\sim \gamma/J^2$ as seen in Eq. (5.32). The schematic explanation of long-range correlated tunnelling is presented in Fig. 5.4(b.1): the atoms can tunnel only in pairs to assure the globally conserved values of N_{even} and N_{odd}, such that one correlated tunnelling event is represented by a pair of one red and one blue arrow. Importantly, this scheme is fully applicable for a lattice with large atom and site numbers, well beyond the numerical example in Fig. 5.4(b.1), because as we can see in Eq. (5.32) it is the geometry of quantum measurement that assures this mode structure (in this example, two modes at odd and even sites) and thus the underlying pairwise global tunnelling.

The scheme in Fig. 5.4(b.1) can help design a nonlocal reservoir for the tunnelling (or "decay") of atoms from one region to another. For example, if the atoms are placed only at odd sites, according to Eq. (5.32) their tunnelling is suppressed since the multi-tunnelling

event must be successive, i.e. an atom tunnelling into a different mode, φ', must then also tunnel back into its original mode, φ. If, however, one adds some atoms to even sites (even if they are far from the initial atoms), the correlated tunnelling events become allowed and their rate can be tuned by the number of added atoms. This resembles the repulsively bound pairs created by local interactions [157, 158]. In contrast, here the atom pairs are nonlocally correlated due to the global measurement. Additionally, these long-range correlations are a consequence of the dynamics being constrained to a Zeno subspace: the virtual processes allowed by the measurement entangle the spatial modes nonlocally. Since the measurement only reveals the total number of atoms in the illuminated sites, but not their exact distribution, these multi-tunnelling events cause the build-up of long-range entanglement. This is in striking contrast to the entanglement caused by local processes which can be very confined, especially in 1D where it is typically short range. This makes numerical calculations of our system for large atom numbers really difficult, since well-known methods such as DMRG and MPS [159] (which are successful for short-range interactions) rely on the limited extent of entanglement.

The negative number correlations are typical for systems with constraints (superselection rules) such as fixed atom number. The effective dynamics due to our global, but spatially structured, measurement introduces more general constraints to the evolution of the system. For example, in Fig. 5.4(c) we show the generation of positive number correlations shown in Fig. 5.4(c.4) by freezing the atom number difference between the sites ($N_{\text{odd}} - N_{\text{even}}$). Thus, atoms can only enter or leave this region in pairs, which again is possible due to correlated tunnelling as seen in Figs. 5.4(c.1,c.2) and manifests positive correlations. As in the previous example, two edge modes in Fig. 5.4(c) can be considered as a nonlocal reservoir for two central sites, where a constraint is applied. Note that, using more modes, the design of higher-order multi-tunnelling events is possible.

This global pair tunnelling may play a role of a building block for more complicated many-body effects. For example, a pair tunnelling between the neighbouring sites has been recently shown to play important role in the formation of new quantum phases, e.g., pair superfluid [160] and lead to formulation of extended Bose-Hubbard models [161]. The search for novel mechanisms providing long-range interactions is crucial in many-body physics. One of the standard candidates is the dipole-dipole interaction in, e.g., dipolar molecules, where the mentioned pair tunnelling between even neighbouring sites is already considered to be long-range [160, 161]. In this context, our work suggests a fundamentally different mechanism originating from quantum optics: the backaction of global and spatially structured measurement, which as we prove can successfully compete with other short-range processes in many-body systems. This opens promising opportunities for future research.

5.3 Non-Hermitian Dynamics in the Quantum Zeno Limit

In the previous section we provided a rather high-level analysis of the strong measurement limit in our quantum gas model. We showed that global measurement in the strong, but not projective, limit leads to correlated tunnelling events which can be highly delocalised. Multiple examples for different optical geometries and measurement operators demonstrated the incredible flexibility and potential in engineering dynamics for ultracold gases in an optical lattice. We also claimed that the behaviour of the system is described by the Hamiltonian given in Eq. (5.32). Having developed a physical and intuitive understanding of the dynamics in the quantum Zeno limit we will now provide a more rigorous, low-level and fundamental understanding of the process.

5.3.1 Suppression of Coherences in the Density Matrix

At this point we deviate from the quantum trajectory approach and we resort to a master equation as introduced in section 4.3. We do this, because we have seen that the emergent long-range correlated tunnelling is a feature of all trajectories and mostly depends on the geometry of the measurement. Therefore, a general approach starting from an unconditioned state should be able to reveal these features. However, we will later make use of the fact that we are in possession of a measurement record and obtain a conditioned state. Furthermore, we first consider the most general case of an open system subject to a quantum measurement and only limit ourselves to the quantum gas model later on. This demonstrates that the dynamics we observed in the previous section are a feature of measurement rather than our specific model.

As introduced in section 4.3 we consider a state described by the density matrix $\hat{\rho}$ whose isolated behaviour is described by the Hamiltonian $\hat{H}_0$ and when measured the jump operator $\hat{c}$ is applied to the state at each detection [23]. The master equation describing its time evolution when we ignore the measurement outcomes is given by

$$\dot{\hat{\rho}} = -i[\hat{H}_0, \hat{\rho}] + \hat{c}\hat{\rho}\hat{c}^\dagger - \frac{1}{2}(\hat{c}^\dagger\hat{c}\hat{\rho} + \hat{\rho}\hat{c}^\dagger\hat{c}). \tag{5.33}$$

We also define $\hat{c} = \lambda\hat{o}$ and $\hat{H}_0 = \nu\hat{h}$. The exact definition of λ and ν is not so important as long as these coefficients can be considered to be some measure of the relative size of these operators. They would have to be determined on a case-by-case basis, because the operators $\hat{c}$ and $\hat{H}_0$ may be unbounded. If these operators are bounded, one can simply define them such that $||\hat{o}|| \sim O(1)$ and $||\hat{h}|| \sim O(1)$. If they are unbounded, one possible approach would be to identify the relevant subspace of which dynamics we are interested in and scale the operators such that the eigenvalues of $\hat{o}$ and $\hat{h}$ in this subspace are $\sim O(1)$.

We will once again use projectors P_m which have no effect on states within a degenerate subspace of $\hat{c}$ ($\hat{o}$) with eigenvalue c_m (o_m), but annihilate everything else. For convenience we will also use the following definition $\hat{\rho}_{mn} = P_m \hat{\rho} P_n$. Note that these are submatrices of the density matrix, which in general are not single matrix elements. Therefore, we can write the master equation that describes this open system as a set of equations

$$\dot{\hat{\rho}}_{mn} = -i\nu P_m \left[\hat{h} \sum_r \hat{\rho}_{rn} - \sum_r \hat{\rho}_{mr} \hat{h} \right] P_n + \lambda^2 \left[o_m o_n^* - \frac{1}{2} \left(|o_m|^2 + |o_n|^2 \right) \right] \hat{\rho}_{mn}, \tag{5.34}$$

where the first term describes coherent evolution whereas the second term causes dissipation.

First, note that for the density submatrices for which $m = n$, $\hat{\rho}_{mm}$, the dissipative term vanishes. This means that these submatrices are subject to coherent evolution only and do not experience losses and they are thus decoherence free subspaces. It is crucial to note that these submatrices are simply the density matrices of the individual degenerate Zeno subspaces. Interestingly, any state that consists only of these decoherence free subspaces, i.e. $\hat{\rho} = \sum_m \hat{\rho}_{mm}$, and that commutes with the Hamiltonian, $[\hat{\rho}, \hat{H}_0] = 0$, will be a steady state. This can be seen by substituting this ansatz into Eq. (5.34) which yields $\dot{\hat{\rho}}_{mn} = 0$ for all m and n. These states can be prepared dissipatively using known techniques [44], but it is not required that the state be a dark state of the dissipative operator as is usually the case.

Second, we consider a large detection rate, $\lambda^2 \gg \nu$, for which the coherences, i.e. the density submatrices $\hat{\rho}_{mn}$ for which $m \neq n$, will be heavily suppressed by dissipation. We can adiabatically eliminate these cross-terms by setting $\dot{\hat{\rho}}_{mn} = 0$, to get

$$\hat{\rho}_{mn} = \frac{\nu}{\lambda^2} \frac{i P_m \left[\hat{h} \sum_r \hat{\rho}_{rn} - \sum_r \hat{\rho}_{mr} \hat{h} \right] P_n}{o_m o_n^* - \frac{1}{2} \left(|o_m|^2 + |o_n|^2 \right)} \tag{5.35}$$

which tells us that they are of order $\nu/\lambda^2 \ll 1$. Therefore, the resulting density matrix will be given by $\hat{\rho} \approx \sum_m \hat{\rho}_{mm}$ which consists solely of the individual Zeno subspace density matrices. One can easily recover the projective Zeno limit by considering $\lambda \to \infty$ when all

the subspaces completely decouple. This is exactly the $\gamma \to \infty$ limit discussed in the previous section. However, we have seen that it is crucial we only consider $\lambda^2 \gg \nu$, but not infinite. If the subspaces do not decouple completely, then transitions within a single subspace can occur via other subspaces in a manner similar to Raman transitions. In Raman transitions population is transferred between two states via a third, virtual, state that remains empty throughout the process. By avoiding the infinitely projective Zeno limit we open the option for such processes to happen in our system where transitions within a single Zeno subspace occur via a second, different, Zeno subspace even though the occupation of the intermediate states will remain negligible at all times.

A single quantum trajectory results in a pure state as opposed to the density matrix and in general, there are many density matrices that have non-zero and non-negligible $m = n$ submatrices, $\hat{\rho}_{mm}$, even when the coherences are small. They correspond to a mixed states containing many Zeno subspaces and it is not clear what the pure states that make up these density matrices are. However, we note that for a single pure state the density matrix can consist of only a single diagonal submatrix $\hat{\rho}_{mm}$. To understand this, consider the state $|\Phi\rangle$ and take it to span exactly two distinct subspaces P_a and P_b ($a \neq b$). This wave function can thus be written as $|\Phi\rangle = P_a|\Phi\rangle + P_b|\Phi\rangle$. The corresponding density matrix is given by

$$\hat{\rho}_\Psi = P_a|\Phi\rangle\langle\Phi|P_a + P_a|\Phi\rangle\langle\Phi|P_b + P_b|\Phi\rangle\langle\Phi|P_a + P_b|\Phi\rangle\langle\Phi|P_b. \tag{5.36}$$

If the wave function has significant components in both subspaces then in general the density matrix will not have negligible coherences, $\hat{\rho}_{ab} = P_a|\Phi\rangle\langle\Phi|P_b$. A density matrix with just diagonal components must be in either subspace a, $|\Phi\rangle = P_a|\Phi\rangle$, or in subspace b, $|\Phi\rangle = P_b|\Phi\rangle$. Therefore, a density matrix of the form $\hat{\rho} = \sum_m \hat{\rho}_{mm}$ without any cross-terms between different Zeno subspaces can only be composed of pure states that each lie predominantly within a single subspace. However, because we will not be dealing with the projective limit, the wave function will in general not be entirely confined to a single

Zeno subspace. We have seen that the coherences are of order ν/λ^2. This would require the wave function components to satisfy $P_a|\Phi\rangle \approx O(1)$ and $P_b|\Phi\rangle \approx O(\nu/\lambda^2)$ (or vice-versa). This in turn implies that the population of the states outside of the dominant subspace (and thus the submatrix $\hat{\rho}_{bb}$) will be of order $\langle\Phi|P_b^2|\Phi\rangle \approx O(\nu^2/\lambda^4)$. Therefore, these pure states, even though they span multiple Zeno subspaces, cannot exist in a meaningful coherent superposition in this limit. This means that a density matrix that spans multiple Zeno subspaces has only classical uncertainty about which subspace is currently occupied as opposed to the uncertainty due to a quantum superposition. This is analogous to the simple qubit example we considered in section 4.3.

5.3.2 Quantum Measurement vs. Dissipation

This is where quantum measurement deviates from dissipation. If we have access to a measurement record we can infer which Zeno subspace is occupied, because we know that only one of them can be occupied at any time. We have seen that since the density matrix cross-terms are small we know *a priori* that the individual wave functions comprising the density matrix mixture will not be coherent superpositions of different Zeno subspaces and thus we only have classical uncertainty which means we can resort to classical probability methods. Each individual experiment will at any time be predominantly in a single Zeno subspace with small cross-terms and negligible occupations in the other subspaces. With no measurement record our density matrix would be a mixture of all these possibilities. We can try and determine the Zeno subspace around which the state evolves in a single experiment from the number of detections, m, in time t.

The detection distribution on time-scales shorter than dissipation (so we can approximate as if we were in a fully Zeno regime) can be obtained by integrating over the detection times [58] to get

$$P(m,t) = \sum_n \frac{[|c_n|^2 t]^m}{m!} e^{-|c_n|^2 t} \mathrm{Tr}(\rho_{nn}). \tag{5.37}$$

For a state that is predominantly in one Zeno subspace, the distribution will be approximately Poissonian (up to $O(\nu^2/\lambda^4)$, the population of the other subspaces). Therefore, in a single experiment we will measure $m = |c_0|^2 t \pm \sqrt{|c_0|^2 t}$ detections (note, we have assumed $|c_0|^2 t$ is large enough to approximate the distribution as normal. This is not necessary, we simply use it here to not have to worry about the asymmetry in the deviation around the mean value). The uncertainty does not come from the fact that λ is not infinite. The jumps are random events with a Poisson distribution. Therefore, even in the full projective limit we will not observe the same detection trajectory in each experiment even though the system evolves in exactly the same way and remains in a perfectly pure state.

If the basis of $\hat{c}$ is continuous (e.g. free particle position or momentum) then the deviation around the mean will be our upper bound on the deviation of the system from a pure state evolving around a single Zeno subspace. However, continuous systems are beyond the scope of this work and we will confine ourselves to discrete systems. Though it is important to remember that continuous systems can be treated this way, but the error estimate (and thus the mixedness of the state) will be different.

For a discrete system it is easier to exclude all possibilities except for one. The error in our estimate of $|c_0|^2$ in a single experiment decreases as $1/\sqrt{t}$ and thus it can take a long time to confidently determine $|c_0|^2$ to a sufficient precision this way. However, since we know that it can only take one of the possible values from the set $\{|c_n|^2\}$ it is much easier to instead exclude all the other values.

In an experiment we can use Bayes' theorem to infer the state of our system as follows

$$p(c_n = c_0|m) = \frac{p(m|c_n = c_0)p(c_n = c_0)}{p(m)}, \tag{5.38}$$

where $p(x)$ denotes the probability of the discrete event x and $p(x|y)$ the conditional probability of x given y. We know that $p(m|c_n = c_0)$ is simply given by a Poisson distribution with mean $|c_0|^2 t$. $p(m)$ is just a normalising factor and $p(c_n = c_0)$ is our *a priori* knowledge of

the state. Therefore, one can get the probability of being in the right Zeno subspace from

$$p(c_n = c_0|m) = \frac{p_0(c_n = c_0)\frac{\left(|c_0|^2 t\right)^{2m}}{m!}e^{-|c_0|^2 t}}{\sum_n p_0(c_n)\frac{\left(|c_n|^2 t\right)^{2m}}{m!}e^{-|c_n|^2 t}}$$
$$= p_0(c_n = c_0)\left[\sum_n p_0(c_n)\left(\frac{|c_n|^2}{|c_0|^2}\right)^{2m} e^{\left(|c_0|^2-|c_n|^2\right)t}\right]^{-1}, \tag{5.39}$$

where p_0 denotes probabilities at $t = 0$. In a real experiment one could prepare the initial state to be close to the Zeno subspace of interest and thus it would be easier to deduce the state. Furthermore, in the middle of an experiment if we have already established the Zeno subspace this will be reflected in these *a priori* probabilities again making it easier to infer the correct subspace. However, we will consider the worst case scenario which might be useful if we don't know the initial state or if the Zeno subspace changes during the experiment, a uniform $p_0(c_n)$.

This probability is a rather complicated function as m is a stochastic quantity that also increases with t. We want it to be as close to 1 as possible. In order to devise an appropriate condition for this we note that in the first line all terms in the denominator are Poisson distributions of m. Therefore, if the mean values $|c_n|^2 t$ are sufficiently spaced out, only one of the terms in the sum will be significant for a given m and if this happens to be the one that corresponds to c_0 we get a probability close to unity. Therefore, we set the condition such that it is highly unlikely that our measured m could be produced by two different distributions

$$\sqrt{|c_0|^2 t} \ll ||c_0|^2 - |c_n|^2|t, \forall n \neq 0 \tag{5.40}$$
$$\sqrt{|c_n|^2 t} \ll ||c_0|^2 - |c_n|^2|t, \forall n \neq 0 \tag{5.41}$$

The left-hand side is the standard deviation of m if the system was in subspace P_0 or P_n. The right-hand side is the difference in the mean detections between the subspace n and the one we are interested in. The condition becomes more strict if the subspaces become less

distinguishable as it becomes harder to confidently determine the correct state. Once again, using $\hat{c} = \lambda\hat{o}$ where $\hat{o} \sim O(1)$ we get

$$t \gg \frac{1}{\lambda^2}\frac{|o_{0,n}|^2}{(|o_0|^2 - |o_n|^2|)^2}. \tag{5.42}$$

Since detections happen on average at an average rate of order λ^2 we only need to wait for a few detections to satisfy this condition. Therefore, we see that even in the worst case scenario of complete ignorance of the state of the system we can very easily determine the correct subspace. Once it is established for the first time, the *a priori* information can be updated and it will become even easier to monitor the system.

However, it is important to note that physically once the quantum jumps deviate too much from the mean value the system is more likely to change the Zeno subspace (due to measurement backaction) and the detection rate will visibly change. Therefore, if we observe a consistent detection rate it is extremely unlikely that it can be produced by two different Zeno subspaces so in fact it is even easier to determine the correct state, but the above estimate serves as a good lower bound on the necessary detection time.

Having derived the necessary conditions to confidently determine which Zeno subspace is being observed in the experiment we can make another approximation thanks to measurement which would be impossible in a purely dissipative open system. If we observe a number of detections consistent with the subspace $P_m = P_0$ we can set $\hat{\rho}_{mn} \approx 0$ for all cases when both $m \neq 0$ and $n \neq 0$ leaving our density matrix in the form

$$\hat{\rho} = \hat{\rho}_{00} + \sum_{r\neq 0}(\hat{\rho}_{0r} + \hat{\rho}_{r0}). \tag{5.43}$$

We can do this, because the other states are inconsistent with the measurement record. We know from the previous section that the system must lie predominantly in only one of the Zeno subspaces and when that is the case, $\hat{\rho}_{0r} \approx O(\nu/\lambda^2)$ and for $m \neq 0$ and $n \neq 0$ we

have $\hat{\rho}_{mn} \approx O(\nu^2/\lambda^4)$. Therefore, this amounts to keeping first order terms in ν/λ^2 in our approximation.

This is a crucial step as all $\hat{\rho}_{mm}$ matrices are decoherence free subspaces and thus they can all coexist in a mixed state decreasing the purity of the system without measurement. Physically, this means we exclude trajectories in which the Zeno subspace has changed (measurement is not fully projective). By substituting Eq. (5.35) into Eq. (5.34) we see that this happens at a rate of ν^2/λ^2. However, since the two measurement outcomes cannot coexist any transition between them happens in discrete transitions (which we know about from the change in the detection rate as each Zeno subspace will correspond to a different rate) and not as continuous coherent evolution. Therefore, we can postselect in a manner similar to Refs. [82–84], but our requirements are significantly more relaxed - we do not require a specific single trajectory, only that it remains within a Zeno subspace. Furthermore, upon reaching a steady state, these transitions become impossible as the coherences vanish. This approximation is analogous to optical Raman transitions where the population of the excited state is neglected. Here, we can make a similar approximation and neglect all but one Zeno subspace thanks to the additional knowledge we gain from knowing the measurement outcomes.

5.3.3 The Non-Hermitian Hamiltonian

Rewriting the master equation using $\hat{c} = c_0 + \delta\hat{c}$, where c_0 is the eigenvalue corresponding to the eigenspace defined by the projector P_0 which we used to obtain the density matrix in Eq. (5.43), we get

$$\dot{\hat{\rho}} = -i\left(\hat{H}_{\text{eff}}\hat{\rho} - \hat{\rho}\hat{H}_{\text{eff}}^{\dagger}\right) + \delta\hat{c}\hat{\rho}\,\delta\hat{c}^{\dagger}, \tag{5.44}$$

$$\hat{H}_{\text{eff}} = \hat{H}_0 + i\left(c_0^*\hat{c} - \frac{|c_0|^2}{2} - \frac{\hat{c}^{\dagger}\hat{c}}{2}\right). \tag{5.45}$$

The first term in Eq. (5.44) describes coherent evolution due to the non-Hermitian Hamiltonian $\hat{H}_{\text{eff}}$ and the second term is decoherence due to our ignorance of measurement outcomes. When we substitute our approximation of the density matrix $\hat{\rho} = \hat{\rho}_{00} + \sum_{r\neq 0}(\hat{\rho}_{0r} + \hat{\rho}_{r0})$ into Eq. (5.44), the last term vanishes, $\delta\hat{c}\hat{\rho}\,\delta\hat{c}^\dagger = 0$. This happens, because $\delta\hat{c}P_0\hat{\rho} = \hat{\rho}P_0\delta\hat{c}^\dagger = 0$. The projector annihilates all states except for those with eigenvalue c_0 and so the operator $\delta\hat{c} = \hat{c} - c_0$ will always evaluate to $c_0 - c_0 = 0$. Recall that we defined $\hat{\rho}_{mn} = P_m\hat{\rho}P_n$ which means that every term in our approximate density matrix contains the projector P_0. However, it is important to note that this argument does not apply to other second order terms in the master equation, because some terms only have the projector P_0 applied from one side, e.g. $\hat{\rho}_{0m}$. The term $\delta\hat{c}\hat{\rho}\,\delta\hat{c}^\dagger$ applies the fluctuation operator from both sides so it does not matter in this case, but it becomes relevant for terms such as $\hat{\rho}\,\delta\hat{c}^\dagger\delta\hat{c}$. It is important to note that this term does not automatically vanish, but when the explicit form of our approximate density matrix is inserted, it is in fact zero. Therefore, we can omit this term using the information we gained from measurement, but keep other second order terms, such as $\delta\hat{c}^\dagger\delta\hat{c}\rho$ in the Hamiltonian which are the origin of other second-order dynamics. This could not be the case in a dissipative system.

Ultimately we find that a system under continuous measurement for which $\lambda^2 \gg \nu$ in the Zeno subspace P_0 is described by the deterministic non-Hermitian Hamiltonian $\hat{H}_{\text{eff}}$ in Eq. (5.45) and thus obeys the following Schrödinger equation

$$i\frac{\mathrm{d}|\Psi\rangle}{\mathrm{d}t} = \left[\hat{H}_0 + i\left(c_0^*\hat{c} - \frac{|c_0|^2}{2} - \frac{\hat{c}^\dagger\hat{c}}{2}\right)\right]|\Psi\rangle. \tag{5.46}$$

Of the three terms in the parentheses the first two represent the effects of quantum jumps due to detections (which one can think of as 'reference frame' shifts between different degenerate eigenspaces) and the last term is the non-Hermitian decay due to information gain from no detections. It is important to emphasize that even though we obtained a deterministic equation, we have not neglected the stochastic nature of the detection events. The detection

trajectory seen in an experiment will have fluctuations around the mean determined by the Zeno subspace, but there simply are many possible measurement records with the same outcome. This is just like the fully projective Zeno limit where the system remains perfectly pure in one of the possible projections, but the detections remain randomly distributed in time.

One might then be concerned that purity is preserved even though we might be averaging over many trajectories within this Zeno subspace. We have neglected the small terms $\hat{\rho}_{m,n}$ $(m,n \neq 0)$ which are $O(\nu^2/\lambda^4)$ and thus they are not correctly accounted for by our approximation. This means that we have an $O(\nu^2/\lambda^4)$ error in our density matrix. The purity given by

$$\mathrm{Tr}(\hat{\rho}^2) = \mathrm{Tr}(\hat{\rho}_{00}^2 + \sum_{m\neq 0} \hat{\rho}_{0m}\hat{\rho}_{m0}) + \mathrm{Tr}(\sum_{m,n\neq 0} \hat{\rho}_{mn}\hat{\rho}_{nm}) \tag{5.47}$$

where the second term contains the terms not accounted for by our approximation thus introduces an $O(\nu^4/\lambda^8)$ error. Therefore, this discrepancy is negligible in our approximation. The pure state predicted by $\hat{H}_{\mathrm{eff}}$ is only an approximation, albeit a good one, and the real state will be mixed to a small extent. Whilst perfect purity within the Zeno subspace $\hat{\rho}_{00}$ is expected due to the measurement's strong decoupling effect, the nearly perfect purity when transitions outside the Zeno subspace are included is a nontrivial result. Similarly, in Raman transitions the population of the neglected excited state is also non-zero, but negligible. Furthermore, this equation does not actually require the adiabatic elimination used in Eq. (5.35) (we only used it to convince ourselves that the coherences are small) and such situations may be considered provided all approximations remain valid. In a similar way the limit of linear optics is derived from the physics of a two-level nonlinear medium, when the population of the upper state is neglected and the adiabatic elimination of coherences is not required.

5.3.4 Non-Hermitian Dynamics in Ultracold Gases

We finally return to our quantum gas model inside of a cavity. We start by considering the simplest case of a global multi-site measurement of the form $\hat{D} = \hat{N}_K = \sum_i^K \hat{n}_i$, where the sum is over K illuminated sites. The effective Hamiltonian becomes

$$\hat{H}_{\text{eff}} = \hat{H}_0 - i\gamma\left(\delta\hat{N}_K\right)^2, \tag{5.48}$$

where $\delta\hat{N}_K = \hat{N}_K - N_K^0$ and N_K^0 is the Zeno subspace eigenvalue. It is now obvious that continuous measurement squeezes the fluctuations in the measured quantity, as expected, and that the only competing process is the system's own dynamics.

In this case, if we adiabatically eliminate the density matrix cross-terms and substitute Eq. (5.35) into Eq. (5.34) for this system we obtain an effective Hamiltonian within the Zeno subspace defined by N_K

$$\hat{H}_\varphi = P_0\left[\hat{H}_0 - i\frac{J^2}{\gamma}\sum_\varphi \sum_{\substack{\langle i\in\varphi, j\in\varphi'\rangle \\ \langle k\in\varphi', l\in\varphi\rangle}} b_i^\dagger b_j b_k^\dagger b_l\right] P_0, \tag{5.49}$$

where φ denotes a set of sites belonging to a single mode and φ' is the set's complement (e.g. odd and even or illuminated and non-illuminated sites) and P_0 is the projector onto the eigenspace with N_K^0 atoms in the illuminated area. We focus on the case when the second term is not only significant, but also leads to dynamics within a Zeno subspace that are not allowed by conventional quantum Zeno dynamics accounted for by the first term. The second term represents second-order transitions via other subspaces which act as intermediate states much like virtual states in optical Raman transitions. This is in contrast to the conventional understanding of the Zeno dynamics for infinitely frequent projective measurements (corresponding to $\gamma \to \infty$) where such processes are forbidden [66]. Thus, it is the weak quantum measurement that effectively couples the states. Note that this is a special

case of the equation in Eq. (5.32) which can be obtained by considering a more general two mode setup.

5.3.5 Small System Example

To get clear physical insight, we initially consider three atoms in three sites and choose our measurement operator such that $\hat{D} = \hat{n}_2$, i.e. only the middle site is subject to measurement, and the Zeno subspace defined by $n_2 = 1$. Such an illumination pattern can be achieved with global addressing by crossing two beams and placing the nodes at the odd sites and the antinodes at even sites. This means that $P_0\hat{H}_0P_0 = 0$. However, the first and third sites are connected via the second term. Diagonalising the Hamiltonian reveals that out of its ten eigenvalues all but three have a significant negative imaginary component of the order γ which means that the corresponding eigenstates decay on a time scale of a single quantum jump and thus quickly become negligible. The three remaining eigenvectors are dominated by the linear superpositions of the three Fock states $|2,1,0\rangle$, $|1,1,1\rangle$, and $|0,1,2\rangle$. Whilst it is not surprising that these components are the only ones that remain as they are the only ones that actually lie in the Zeno subspace $n_2 = 1$, it is impossible to solve the full dynamics by just considering these Fock states alone as they are not coupled to each other in $\hat{H}_0$. The components lying outside of the Zeno subspace have to be included to allow intermediate steps to occur via states that do not belong in this subspace, much like virtual states in optical Raman transitions.

An approximate solution for $U = 0$ can be written for the $\{|2,1,0\rangle, |1,1,1\rangle, |0,1,2\rangle\}$ subspace by multiplying each eigenvector with its corresponding time evolution

$$|\Psi(t)\rangle \propto \begin{pmatrix} z_1 + \sqrt{2}z_2 e^{-6J^2t/\gamma} + z_3 e^{-12J^2t/\gamma} \\ -\sqrt{2}\left(z_1 - z_3 e^{-12J^2t/\gamma}\right) \\ z_1 - \sqrt{2}z_2 e^{-6J^2t/\gamma} + z_3 e^{-12J^2t/\gamma} \end{pmatrix}, \tag{5.50}$$

where z_i denote the overlap between the eigenvectors and the initial state, $z_i = \langle v_i|\Psi(0)\rangle$, with $|v_1\rangle = (1,-\sqrt{2},1)/2$, $|v_2\rangle = (1,0,-1)/\sqrt{2}$, and $|v_3\rangle = (1,\sqrt{2},1)/2$. The steady state as $t \to \infty$ is given by $|v_1\rangle = (1,-\sqrt{2},1)/2$. This solution is illustrated in Fig. 5.5 which clearly demonstrates dynamics beyond the canonical understanding of quantum Zeno dynamics as tunnelling occurs between states coupled via a different Zeno subspace.

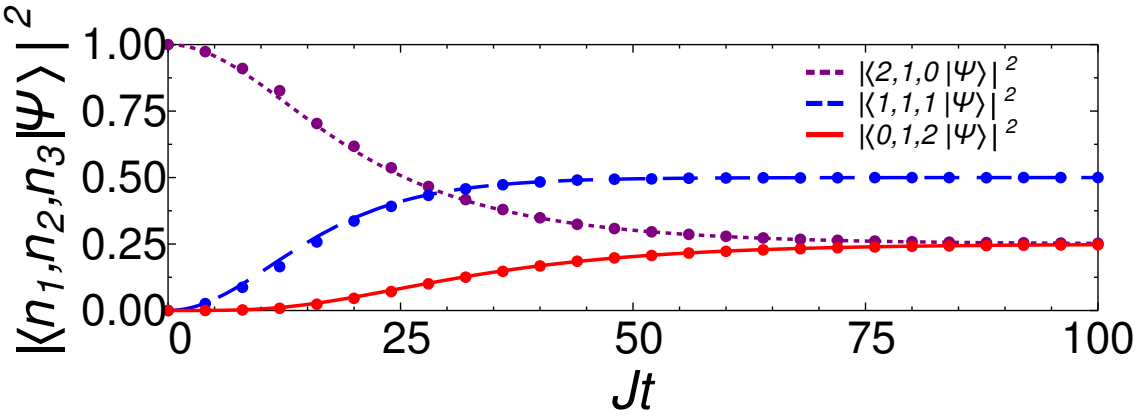

Fig. 5.5 Populations of the Fock states in the Zeno subspace for $\gamma/J = 100$ and initial state $|2,1,0\rangle$. It is clear that quantum Zeno dynamics occurs via Raman-like processes even though none of these states are connected in $\hat{H}_0$. The dynamics occurs via virtual intermediate states outside the Zeno subspace. The system also tends to a steady state which minimises tunnelling effectively suppressing fluctuations. The lines are solutions to the non-Hermitian Hamiltonian, and the dots are points from a stochastic trajectory calculation.

5.3.6 Steady State of non-Hermitian Dynamics

A distinctive difference between Bose-Hubbard model ground states and the final steady state, $|\Psi\rangle = [|2,1,0\rangle - \sqrt{2}|1,1,1\rangle + |0,1,2\rangle]/2$, is that its components are not in phase. Squeezing due to measurement naturally competes with inter-site tunnelling which tends to spread the atoms. However, from Eq. (5.48) we see the final state will always be the eigenvector with the smallest fluctuations as it will have an eigenvalue with the largest imaginary component. This naturally corresponds to the state where tunnelling between Zeno subspaces (here between every site) is minimised by destructive matter-wave interference, i.e. the tunnelling dark

state defined by $\hat{T}|\Psi\rangle = 0$, where $\hat{T} = \sum_{\langle i,j\rangle} b_i^\dagger b_j$. This is simply the physical interpretation of the steady states we predicted for Eq. (5.34). Crucially, this state can only be reached if the dynamics are not fully suppressed by measurement and thus, counter-intuitively, the atomic dynamics cooperate with measurement to suppress itself by destructive interference. Therefore, this effect is beyond the scope of traditional quantum Zeno dynamics and presents a new perspective on the competition between a system's short-range dynamics and global measurement backaction.

We now consider a one-dimensional lattice with M sites so we extend the measurement to $\hat{D} = \hat{N}_{\text{even}}$ where every even site is illuminated. The wave function in a Zeno subspace must be an eigenstate of $\hat{c}$ and we combine this with the requirement for it to be in the dark state of the tunnelling operator (eigenstate of $\hat{H}_0$ for $U = 0$) to derive the steady state. These two conditions in momentum space are

$$\hat{T}|\Psi\rangle = \sum_{\text{RBZ}} \left[b_k^\dagger b_k - b_q^\dagger b_q \right] \cos(ka)|\Psi\rangle = 0, \tag{5.51}$$

$$\Delta\hat{N}|\Psi\rangle = \sum_{\text{RBZ}} \left[b_k^\dagger b_{-q} + b_{-q}^\dagger b_k \right] |\Psi\rangle = \Delta N|\Psi\rangle, \tag{5.52}$$

where $b_k = \frac{1}{\sqrt{M}} \sum_j e^{ikja} b_j$, $\Delta\hat{N} = \hat{D} - N/2$, $q = \pi/a - k$, a is the lattice spacing, N the total atom number, and we perform summations over the reduced Brillouin zone (RBZ), $-\pi/2a < k \leq \pi/2a$, as the symmetries of the system are clearer this way. Now we define

$$\hat{\alpha}_k^\dagger = b_k^\dagger b_q^\dagger - b_{-k}^\dagger b_{-q}^\dagger, \tag{5.53}$$

$$\hat{\beta}_\varphi^\dagger = b_{\pi/2a}^\dagger + \varphi b_{-\pi/2a}^\dagger, \tag{5.54}$$

where $\varphi = \Delta N/|\Delta N|$, which create the smallest possible states that satisfy the two equations for $\Delta N = 0$ and $\Delta N \neq 0$ respectively. Therefore, by noting that

$$\left[\hat{T}, \hat{\alpha}_k^\dagger\right] = 0, \tag{5.55}$$

$$\left[\hat{T}, \hat{\beta}_\varphi^\dagger\right] = 0, \tag{5.56}$$

$$\left[\Delta\hat{N}, \hat{\alpha}_k^\dagger\right] = 0, \tag{5.57}$$

$$\left[\Delta\hat{N}, \hat{\beta}_\varphi^\dagger\right] = \varphi\hat{\beta}_\varphi^\dagger, \tag{5.58}$$

we can now write the equation for the N-particle steady state

$$|\Psi\rangle \propto \left[\prod_{i=1}^{(N-|\Delta N|)/2}\left(\sum_{k=0}^{\pi/2a}\phi_{i,k}\hat{\alpha}_k^\dagger\right)\right]\left(\hat{\beta}_\varphi^\dagger\right)^{|\Delta N|}|0\rangle, \tag{5.59}$$

where $\phi_{i,k}$ are coefficients that depend on the trajectory taken to reach this state and $|0\rangle$ is the vacuum state defined by $b_k|0\rangle = 0$. Since this a dark state (an eigenstate of $\hat{H}_0$) of the atomic dynamics, this state will remain stationary even with measurement switched-off. Interestingly, this state is very different from the ground states of the Bose-Hubbard Hamiltonian, it is even orthogonal to the superfluid state, and thus it cannot be obtained by cooling or projecting from an initial ground state. The combination of tunnelling with measurement is necessary.

In order to prepare the steady state one has to run the experiment and wait until the photocount rate remains constant for a sufficiently long time. Such a trajectory is illustrated in Fig. 5.6 and compared to a deterministic trajectory calculated using the non-Hermitian Hamiltonian. It is easy to see from Fig. 5.6(a) how the stochastic fluctuations around the mean value of the observable have no effect on the general behaviour of the system in the strong measurement regime. By discarding these fluctuations we no longer describe a pure state, but we showed how this only leads to a negligible error. Fig. 5.6(b) shows the local density variance in the lattice. Not only does it grow showing evidence of tunnelling between

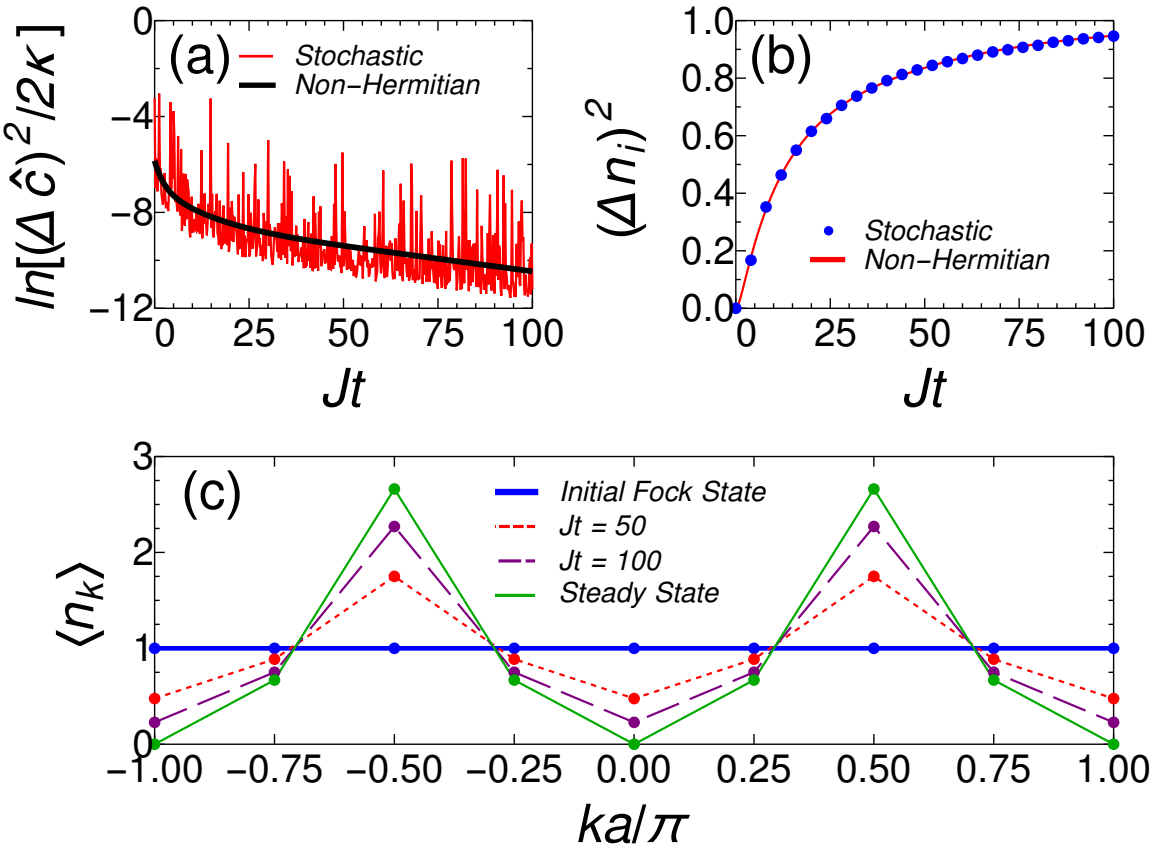

Fig. 5.6 A trajectory simulation for eight atoms in eight sites, initially in $|1,1,1,1,1,1,1,1\rangle$, with periodic boundary conditions and $\gamma/J = 100$. (a), The fluctuations in $\hat{c}$ where the stochastic nature of the process is clearly visible on a single trajectory level. However, the general trend is captured by the non-Hermitian Hamiltonian. (b), The local density variance. Whilst the fluctuations in the global measurement operator decrease, the fluctuations in local density increase due to tunnelling via states outside the Zeno subspace. (c), The momentum distribution. The initial Fock state has a flat distribution which with time approaches the steady state distribution of two identical and symmetric distributions centred at $k = \pi/2a$ and $k = -\pi/2a$.

illuminated and non-illuminated sites, but it grows to significant values. This is in contrast to conventional quantum Zeno dynamics where no tunnelling would be allowed at all. Finally, Fig. 5.6(c) shows the momentum distribution of the trajectory. We can clearly see that it deviates significantly from the initial flat distribution of the Fock state. Furthermore, the steady state does not have any atoms in the $k = 0$ state and thus is orthogonal to the superfluid state as discussed.

To obtain a state with a specific value of ΔN postselection may be necessary, but otherwise it is not needed. The process can be optimised by feedback control since the state is monitored at all times [123, 162, 163]. Furthermore, the form of the measurement operator is very flexible and it can easily be engineered by the geometry of the optical setup [91, 93] which can be used to design a state with desired properties.

5.4 Conclusions

In this chapter we have demonstrated that global quantum measurement backaction can efficiently compete with standard local processes in many-body systems. This introduces a completely new energy and time scale into quantum many-body research. This is made possible by the ability to structure the spatial profile of the measurement on a microscopic scale comparable to the lattice period without the need for single site addressing. The extreme flexibility of the setup considered allowed us to effectively tailor long-range entanglement and correlations present in the system. We showed that the competition between the global backaction and usual atomic dynamics leads to the production of spatially multimode macroscopic superpositions which exhibit large-scale oscillatory dynamics which could be used for quantum information and metrology. We subsequently demonstrated that when on-site atomic interactions are introduced the dynamics become much more complicated with different regimes of behaviour where measurement and interactions can either compete or cooperate. In the strong measurement regime we showed that conventional quantum Zeno

dynamics can be realised, but more interestingly, by considering a strong, but not projective, limit of measurement we observe a new type of nonlocal dynamics. It turns out that a global measurement scheme leads to correlations between spatially separated tunnelling events which conserve the Zeno subspace via Raman-like processes which would be forbidden in the canonical fully projective limit. We subsequently presented a rigorous analysis of the underlying process of this new type of quantum Zeno dynamics in which we showed that in this limit quantum trajectories can be described by a deterministic non-Hermitian Hamiltonian. In contrast to previous works, it is independent of the underlying system and there is no need to postselect a particular exotic trajectory [83, 84]. Finally, we have shown that the system will always tend towards the eigenstate of the Hamiltonian with the best squeezing of the observable and the atomic dynamics, which normally tend to spread the distribution, cooperates with measurement to produce a state in which tunnelling is suppressed by destructive matter-wave interference. A dark state of the tunnelling operator will have zero fluctuations and we provided an expression for the steady state which is significantly different from the ground state of the Hamiltonian. This is in contrast to previous works on dissipative state preparation where the steady state had to be a dark state of the measurement operator [44].

Such globally paired tunnelling due to a fundamentally new phenomenon, global quantum measurement backaction, can enrich the physics of long-range correlated systems beyond relatively short-range interactions expected from standard dipole-dipole interactions [160, 161]. These nonlocal high-order processes entangle regions of the optical lattice that are disconnected by the measurement. Using different detection schemes, we showed how to tailor density-density correlations between distant lattice sites. Quantum optical engineering of nonlocal coupling to environment, combined with quantum measurement, can allow the design of nontrivial system-bath interactions, enabling new links to quantum simulations [164] and thermodynamics [165] and extend these directions to the field of non-Hermitian quantum

mechanics, where quantum optical setups are particularly promising [84]. Importantly, both systems and baths, designed by our method, can be strongly correlated systems with internal long-range entanglement.

Chapter 6

Phase Measurement Induced Dynamics[1]

6.1 Introduction

Light scatters due to its interaction with the dipole moment of the atoms which for off-resonant light results in an effective coupling with atomic density, not the matter-wave amplitude. Therefore, it is challenging to couple light to the phase of the matter-field, as is typical in quantum optics for optical fields. In the previous chapter we only considered measurement that couples directly to atomic density operators just like most of the existing work [19, 32, 40, 63, 64]. However, we have shown in section 2.5 that it is possible to couple to the relative phase differences between sites in an optical lattice by illuminating the bonds between them. Furthermore, we have also shown how it can be applied to probe the Bose-Hubbard order parameter or even matter-field quadratures in Chapter 3. This concept has also been applied to the study of quantum optical potentials formed in a cavity and shown to lead to a host of interesting quantum phase diagrams [85–88]. This is a multi-site generalisation of previous double-well schemes [54–56, 116, 117], although the physical mechanism is fundamentally different as it involves direct coupling to the interference terms caused by atoms tunnelling rather than combining light scattered from different sources.

[1] The results of this chapter were first published in Ref. [96]

We have already mentioned that there are three primary avenues in which the field of quantum optics with ultracold gases can be taken: nondestructive measurement, quantum measurement backaction, and quantum optical potentials. All three have been covered in the context of density-based measurement either here or in other works. However, coupling to phase observables in lattices has only been proposed and considered in the context of nondestructive measurements (see Chapter 3) and quantum optical potentials [85–88]. In this chapter, we go in a new direction by considering the effect of measurement backaction on the atomic gas that results from such coupling. We investigate this mechanism using light scattered from these phase-related observables. The novel combination of measurement backaction as the physical mechanism driving the dynamics and phase coherence as the observable to which the optical fields couple to provides a completely new opportunity to affect and manipulate the quantum state. We first show how this scheme enables us to prepare energy eigenstates of the lattice Hamiltonian. Furthermore, in the second part we also demonstrate a novel type of a projection due to measurement which occurs even when there is significant competition with the Hamiltonian dynamics. This projection is fundamentally different to the standard formulation of the Copenhagen postulate projection or the quantum Zeno effect [65, 66, 74–76] thus providing an extension of the measurement postulate to dynamical systems subject to weak measurement.

6.2 Diffraction Maximum and Energy Eigenstates

In this chapter we will only consider measurement backaction when $a_1 = C\hat{B}$ and $\hat{c} = \sqrt{2\kappa}a_1$ as introduced in section 2.5. We have seen that there are two ways of engineering the spatial profile of the measurement such that the density contribution from $\hat{D}$ is suppressed. We will first consider the case when the profile is uniform, i.e. the diffraction maximum of scattered

light, when our measurement operator is given by

$$\hat{B} = \hat{B}_{\max} = J^B_{\max} \sum_j^K \left(b_j^\dagger b_{j+1} + b_j b_{j+1}^\dagger \right) = 2J^B_{\max} \sum_k b_k^\dagger b_k \cos(ka), \tag{6.1}$$

where the second equality follows from converting to momentum space, denoted by index k, via $b_m = \frac{1}{\sqrt{M}} \sum_k e^{-ikma} b_k$ and b_k annihilates an atom in the Brillouin zone. Note that this operator is diagonal in momentum space which means that its eigenstates are simply momentum Fock states. We have also seen in Chapter 4 how the global nature of the jump operators introduces a nonlocal quadratic term to the Hamiltonian, $\hat{H} = \hat{H}_0 - i\hat{c}^\dagger \hat{c}/2$. In order to focus on the competition between tunnelling and measurement backaction we again consider non-interacting atoms, $U = 0$. Therefore, $\hat{B}$ is proportional to the Hamiltonian and both operators have the same eigenstates.

The combined Hamiltonian for the non-interacting gas subject to measurement of the from $a_1 = C\hat{B}$ is thus

$$\hat{H} = -J \sum_j \left(b_j^\dagger b_{j+1} + b_j b_{j+1}^\dagger \right) - i\gamma \hat{B}^\dagger_{\max} \hat{B}_{\max}. \tag{6.2}$$

Furthermore, whenever a photon is detected, the operator $\hat{c} = \sqrt{2\kappa} C \hat{B}_{\max}$ is applied to the wave function. We can rewrite the above equation as

$$\hat{H} = -\frac{J}{J^B_{\max}} \hat{B}_{\max} - i\gamma \hat{B}^\dagger_{\max} \hat{B}_{\max}. \tag{6.3}$$

The eigenstates of this operator will be exactly the same as of the isolated Hamiltonian which we will label as $|h_l\rangle$, where h_l denotes the corresponding eigenvalue. Therefore, for an initial state

$$|\Psi\rangle = \sum_l z_l^0 |h_l\rangle \tag{6.4}$$

it is easy to show that the state after m photocounts and time t is given by

$$|\Psi(m,t)\rangle = \frac{1}{\sqrt{F(t)}} \sum_l h_l^m z_l^0 e^{[ih_l - \gamma(J^B_{\max}/J)^2 h_l^2]t} |h_l\rangle, \tag{6.5}$$

where $\sqrt{F(t)}$ is the normalisation factor. Therefore, the probability of being in state $|h_l\rangle$ at time t after m photocounts is given by

$$p(h_l,m,t) = \frac{h_l^{2m}}{F(t)} \exp\left[-2\gamma\left(\frac{J^B_{\max}}{J}\right)^2 h_l^2 t\right] |z_l^0|^2. \tag{6.6}$$

As a lot of eigenstates are degenerate, we are actually more interested in the probability of being in eigenspace with the eigenvalue $h_l = (J/J^B_{\max})B_{\max}$. This probability is given by

$$p(B_{\max},m,t) = \frac{B^{2m}_{\max}}{F(t)} \exp\left[-2\gamma B^2_{\max} t\right] p_0(B_{\max}), \tag{6.7}$$

where $p_0(B_{\max}) = \sum_{J_{\max} h_l = J B_{\max}} |z_l^0|^2$. This distribution will have two distinct peaks at $B_{\max} = \pm\sqrt{m/2\kappa|C|^2 t}$ and an initially broad distribution will narrow down around these two peaks with successive photocounts. The final state is in a superposition, because we measure the photon number, $a_1^\dagger a_1$ and not field amplitude. Therefore, the measurement is insensitive to the phase of $a_1 = C\hat{B}$ and we get a superposition of $\pm B_{\max}$. This is exactly the same situation that we saw for the macroscopic oscillations of two distinct components when the atom number difference between two modes is measured as seen in Fig. 5.1(b). However, this means that the matter is still entangled with the light as the two states scatter light with different phase which the photocount detector cannot distinguish. Fortunately, this is easily mitigated at the end of the experiment by switching off the probe beam and allowing the cavity to empty out or by measuring the light phase (quadrature) to isolate one of the components [19, 58, 92].

Unusually, we do not have to worry about the timing of the quantum jumps, because the measurement operator commutes with the Hamiltonian. This highlights an important feature of this measurement - it does not compete with atomic tunnelling, and represents a quantum non-demolition (QND) measurement of the phase-related observable [36]. Eq. (6.7) shows that regardless of the initial state or the photocount trajectory the system will project onto a superposition of eigenstates of the $\hat{B}_{\max}$ operator. In fact, the final state probability distribution would be exactly the same if we were to simply employ a projective measurement of the same operator. What is unusual in our case is that this has been achieved with weak measurement in the presence of significant atomic dynamics. The conditions for such a measurement have only recently been rigorously derived in Ref. [166] and here we provide a practical realisation using in ultracold bosonic gases.

This projective behaviour is in contrast to conventional density based measurements which squeeze the atom number in the illuminated region and thus are in direct competition with the atom dynamics (which spreads the atoms), effectively requiring strong couplings for a projection as seen in the previous chapter. Here a projection is achieved at any measurement strength which allows for a weaker probe and thus effectively less heating and a longer experimental lifetime. This is in contrast to the quantum Zeno effect which requires a very strong probe to compete effectively with the Hamiltonian [65, 66, 74–76]. Interestingly, the $\hat{B}_{\max}$ measurement will even establish phase coherence across the lattice, $\langle b_j^\dagger b_j \rangle \neq 0$, in contrast to density based measurements where the opposite is true: Fock states with no coherences are favoured.

6.3 General Model for Weak Measurement Projection

6.3.1 Projections for Incompatible Dynamics and Measurement

In section 2.5 we have also shown that it is possible to achieve a more complicated spatial profile of the $\hat{B}$-measurement. The optical geometry can be adjusted such that each bond scatters light in anti-phase with its neighbours leading to a diffraction minimum where the expectation value of the amplitude is zero. In this case the $\hat{B}$ operator is given by

$$\hat{B} = \hat{B}_{\min} = J^B_{\min} \sum_m^K (-1)^m \hat{B}_m = 2iJ^B_{\min} \sum_k b^\dagger_k b_{k-\pi/a} \sin(ka). \tag{6.8}$$

Note how the measurement operator now couples the momentum mode k with mode $k-\pi/a$. This measurement operator no longer commutes with the Hamiltonian so it is no longer QND and we do not expect there to be a steady state as before. In order to understand the measurement it will be easier to work in a basis in which it is diagonal. We perform the transformation $\beta_k = \frac{1}{\sqrt{2}}\left(b_k + ib_{k-\pi/a}\right)$, $\tilde{\beta}_k = \frac{1}{\sqrt{2}}\left(b_k - ib_{k-\pi/a}\right)$, which yields the following forms of the measurement operator and the Hamiltonian:

$$\hat{B}_{\min} = 2J^B_{\min} \sum_{\mathrm{RBZ}} \sin(ka) \left(\beta^\dagger_k \beta_k - \tilde{\beta}^\dagger_k \tilde{\beta}_k\right), \tag{6.9}$$

$$\hat{H}_0 = -2J \sum_{\mathrm{RBZ}} \cos(ka) \left(\beta^\dagger_k \tilde{\beta}_k + \tilde{\beta}^\dagger_k \beta_k\right), \tag{6.10}$$

where the summations are performed over the reduced Brillouin Zone (RBZ), $0 < k \leq \pi/a$, to ensure the transformation is canonical. We see that the measurement operator now consists of two types of modes, β_k and $\tilde{\beta}_k$, which are superpositions of two momentum states, k and $k-\pi/a$. Note how a spatial pattern with a period of two sites leads to a basis with two modes whilst a uniform pattern had only one mode, b_k. Furthermore, note the similarities to $\hat{D} = \Delta\hat{N} = \hat{N}_{\mathrm{even}} - \hat{N}_{\mathrm{odd}}$ which is the density measurement operator obtained by illuminated

the lattice such that neighbouring sites scatter light in anti-phase. This further highlights the importance of geometry for global measurement.

Trajectory simulations confirm that there is no steady state. However, unexpectedly, for each trajectory we observe that the dynamics always ends up confined to some subspace as seen in Fig. 6.1. In general, this subspace is neither an eigenspace of the measurement operator or the Hamiltonian. In Fig. 6.1(b) it in fact clearly consists of multiple measurement eigenspaces. This clearly distinguishes it from the fundamental projections predicted by the Copenhagen postulates. It is also not the quantum Zeno effect which predicts that strong measurement can confine the evolution of a system as this subspace must be an eigenspace of the measurement operator [65, 66, 74–76]. Furthermore, the projection we see in Fig. 6.1 occurs for even weak measurement strengths compared to the Hamiltonian's own evolution, a regime in which the quantum Zeno effect does not happen. It is also possible to dissipatively prepare quantum states in an eigenstate of a Hamiltonian provided it is also a dark state of the jump operator, $\hat{c}|\Psi\rangle = 0$ [44]. However, this is also clearly not the case as the final state in Fig. 6.1(c) is not only not confined to a single measurement operator eigenspace, it also spans multiple Hamiltonian eigenspaces. Therefore, the dynamics induced by $a_1 = C\hat{B}_{\min}$ project the system into some subspace, but since this does not happen via any of the mechanisms described above it is not immediately obvious what this subspace is.

To understand this dynamics we will look at the master equation for open systems described by the density matrix, $\hat{\rho}$,

$$\dot{\hat{\rho}} = -i\left[\hat{H}_0, \hat{\rho}\right] + \left[\hat{c}\hat{\rho}\hat{c}^\dagger - \frac{1}{2}\left(\hat{c}^\dagger\hat{c}\hat{\rho} + \hat{\rho}\hat{c}^\dagger\hat{c}\right)\right]. \tag{6.11}$$

The following results will not depend on the nature nor the exact form of the jump operator $\hat{c}$. However, whenever we refer to our simulations or our model we will be considering $\hat{c} = \sqrt{2\kappa}C(\hat{D} + \hat{B})$ as before, but the results are more general and can be applied to their setups. This equation describes the state of the system if we discard all knowledge of the

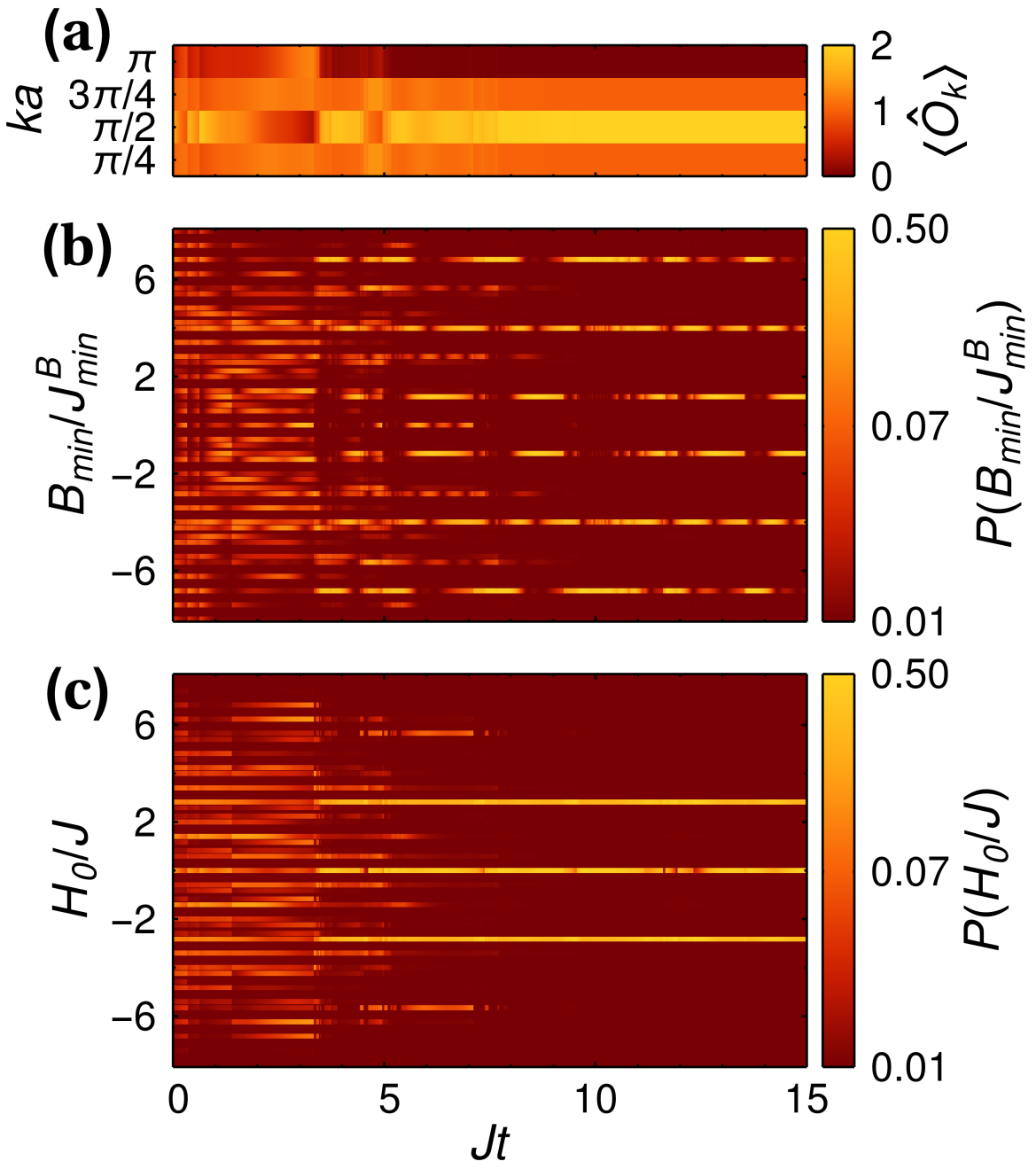

Fig. 6.1 Subspace projections. Projection to a $\mathcal{P}_M$ space for four atoms on eight sites with periodic boundary conditions. The parameters used are $J = 1$, $U = 0$, $\gamma = 0.1$, and the initial state was $|0,0,1,1,1,1,0,0\rangle$. (a) The $\langle \hat{O}_k \rangle = \langle \hat{n}_k + \hat{n}_{k-\pi/a} \rangle$ distribution reaches a steady state at $Jt \approx 8$ indicating the system has been projected. (b) Populations of the $\hat{B}_{\min}$ eigenspaces. (c) Population of the $\hat{H}_0$ eigenspaces. Once the projection is achieved at $Jt \approx 8$ we can see from (b-c) that the system is not in an eigenspace of either $\hat{B}_{\min}$ or $\hat{H}_0$, but it becomes confined to some subspace. The system has been projected onto a subspace, but it is neither that of the measurement operator or the Hamiltonian.

outcome. The commutator describes coherent dynamics due to the isolated Hamiltonian and the remaining terms are due to measurement. This is a convenient way to find features of the dynamics common to every measurement trajectory.

Just like in the preceding chapter we define the projectors of the measurement eigenspaces, P_m, which have no effect on any of the (possibly degenerate) eigenstates of $\hat{c}$ with eigenvalue c_m, but annihilate everything else, thus $P_m = \sum_{c_n=c_m} |c_n\rangle\langle c_n|$, where $|c_n\rangle$ is an eigenstate of $\hat{c}$ with eigenvalue c_n. Note that in the specific case of our quantum gas model $\hat{c} = \sqrt{2\kappa}C(\hat{D}+\hat{B})$ so these projectors act on the matter state. Recall from the previous chapter that this allows us to decompose the master equation in terms of the measurement basis as a series of equations $P_m\dot{\hat{\rho}}P_n$. We have seen that for $m = n$ we obtain decoherence free subspaces, $P_m\dot{\hat{\rho}}P_m = -iP_m\left[\hat{H}_0, \hat{\rho}\right]P_m$, where the measurement terms disappear which shows that a state in a single eigenspace is unaffected by observation. On the other hand, for $m \neq n$ the Hamiltonian evolution actively competes against measurement. In general, if $\hat{c}$ does not commute with the Hamiltonian then a projection to a single eigenspace P_m is impossible unless the measurement is strong enough for the quantum Zeno effect to occur.

We now go beyond what we previously did and define a new type of projector

$$\mathcal{P}_M = \sum_{m\in M} P_m, \tag{6.12}$$

such that

$$\mathcal{P}_M\mathcal{P}_N = \delta_{M,N}\mathcal{P}_M \tag{6.13}$$

$$\sum_M \mathcal{P}_M = \hat{1} \tag{6.14}$$

where M denotes some arbitrary subspace. The first equation implies that the subspaces can be built from P_m whilst the second and third equation are properties of projectors and specify that these projectors do not overlap and that they cover the whole Hilbert space. Furthermore,

we will also require that

$$[\mathcal{P}_M, \hat{H}_0] = 0, \tag{6.15}$$

$$[\mathcal{P}_M, \hat{c}] = 0. \tag{6.16}$$

The second commutator simply follows from the definition $\mathcal{P}_M = \sum_{m\in M} P_m$, but the first one is non-trivial. However, if we can show that $\mathcal{P}_M = \sum_{m\in M} |h_m\rangle\langle h_m|$, where $|h_m\rangle$ is an eigenstate of $\hat{H}_0$ then the commutator is guaranteed to be zero. This is a complex set of requirements and it is unclear if it is possible to satisfy all of them at once. However, we note that there exists a trivial case where all these conditions are satisfied and that is when there is only one such projector $\mathcal{P}_M = \hat{1}$.

Assuming that it is possible to have non-trivial cases where $\mathcal{P}_M \neq \hat{1}$ we can write the master equation as

$$\mathcal{P}_M\dot{\hat{\rho}}\mathcal{P}_N = -i\left[\hat{H}_0, \mathcal{P}_M\hat{\rho}\mathcal{P}_N\right] + \left[\hat{c}\mathcal{P}_M\hat{\rho}\mathcal{P}_N\hat{c}^\dagger - \frac{1}{2}\left(\hat{c}^\dagger\hat{c}\mathcal{P}_M\hat{\rho}\mathcal{P}_N + \mathcal{P}_M\hat{\rho}\mathcal{P}_N\hat{c}^\dagger\hat{c}\right)\right]. \tag{6.17}$$

Crucially, thanks to the commutation relations we were able to divide the density matrix in such a way that each submatrix's time evolution depends only on itself. Every submatrix $\mathcal{P}_M\dot{\hat{\rho}}\mathcal{P}_N$ depends only on the current state of itself and its evolution is ignorant of anything else in the total density matrix. This is in contrast to the partitioning we achieved with P_m. Previously we only identified subspaces that were decoherence free, i.e. unaffected by measurement. However, those submatrices could still couple with the rest of the density matrix via the coherent term $P_m[\hat{H}_0, \hat{\rho}]P_n$.

We note that when $M = N$ the equations for $\mathcal{P}_M\hat{\rho}\mathcal{P}_M$ will include decoherence free subspaces, i.e. $P_m\hat{\rho}P_m$. Therefore, parts of the $\mathcal{P}_M\hat{\rho}\mathcal{P}_M$ submatrices will also remain unaffected by measurement. However, the submatrices $\mathcal{P}_M\hat{\rho}\mathcal{P}_N$, for which $M \neq N$, are guaranteed to not contain any of these measurement free subspaces thanks to the orthogonality of $\mathcal{P}_M$. Therefore, for $M \neq N$ all elements of $\mathcal{P}_M\hat{\rho}\mathcal{P}_N$ will experience a non-zero measurement term

whose effect is always dissipative/lossy. Furthermore, these coherence submatrices $\mathcal{P}_M\hat{\rho}\mathcal{P}_N$ are not coupled to any other part of the density matrix as seen from Eq. (6.17) and so they can never increase in magnitude; the remaining coherent evolution is unable to counteract the dissipative term without an 'external pump' from other parts of the density matrix. The combined effect is such that all $\mathcal{P}_M\hat{\rho}\mathcal{P}_N$ for which $M \neq N$ will always go to zero due to dissipation.

When all these cross-terms vanish, we are left with a density matrix that is a mixed state of the form $\hat{\rho} = \sum_M \mathcal{P}_M\hat{\rho}\mathcal{P}_M$. Since there are no coherences, $\mathcal{P}_M\hat{\rho}\mathcal{P}_N$, this state contains only classical uncertainty about which subspace, $\mathcal{P}_M$, is occupied - there are no quantum superpositions between different $\mathcal{P}_M$ spaces. Therefore, in a single measurement run we are guaranteed to have a state that lies entirely within a subspace defined by $\mathcal{P}_M$. This is once again analogous to the qubit example from section 4.3.

Such a non-trivial case is indeed possible for our $\hat{H}_0$ and $a_1 = C\hat{B}_{\min}$ and we can see the effect in Fig. 6.1. We can clearly see how a state that was initially a superposition of a large number of eigenstates of both operators becomes confined to some small subspace that is neither an eigenspace of a_1 or $\hat{H}_0$. In this case the projective spaces, $\mathcal{P}_M$, are defined by the parities (odd or even) of the combined number of atoms in the β_k and $\tilde{\beta}_k$ modes for different momenta $0 < k < \pi/a$ that are distinguishable to $\hat{B}_{\min}$. The explanation requires careful consideration of where the eigenstates of the two operators overlap.

6.3.2 Determining the Projection Subspace

To find $\mathcal{P}_M$ we need to identify the subspaces M which satisfy the following relation

$$\mathcal{P}_M = \sum_{m\in M} P_m = \sum_{m\in M} |h_m\rangle\langle h_m|. \tag{6.18}$$

This can be done iteratively by

1. selecting some P_m,
2. identifying the $|h_m\rangle$ which overlap with this subspace,
3. identifying any other P_m which also overlap with these $|h_m\rangle$ from step (ii).
4. Repeat 2-3 for all the P_m found in 3 until we have identified all the subspaces P_m linked in this way and they will form one of our $\mathcal{P}_M$ projectors. If $\mathcal{P}_M \neq 1$ then there will be other subspaces P_m which we have not included so far and thus we repeat this procedure on the unused projectors until we identify all $\mathcal{P}_M$.

Computationally this can be straightforwardly solved with some basic algorithm that can compute the connected components of a graph.

The above procedure, whilst mathematically correct and always guarantees to generate the projectors $\mathcal{P}_M$, is very unintuitive and gives poor insight into the nature or physical meaning of $\mathcal{P}_M$. In order to get a better understanding of these subspaces we need to define a new operator $\hat{O}$, with eigenspace projectors R_m, which commutes with both $\hat{H}_0$ and $\hat{c}$,

$$[\hat{O}, \hat{H}_0] = 0, \tag{6.19}$$

$$[\hat{O}, \hat{c}] = 0. \tag{6.20}$$

Physically this means that $\hat{O}$ is a compatible observable with $\hat{c}$ and corresponds to a quantity conserved by the Hamiltonian. The fact that $\hat{O}$ commutes with the Hamiltonian implies that the projectors can be written as a sum of Hamiltonian eigenstates

$$R_m = \sum_{h_i = h_m} |h_i\rangle\langle h_i| \tag{6.21}$$

and thus a projector

$$\mathcal{P}_M = \sum_{m \in M} R_m \tag{6.22}$$

is guaranteed to commute with the Hamiltonian and similarly since $[\hat{O},\hat{c}] = 0$ $\mathcal{P}_M$ will also commute with $\hat{c}$ as required. Therefore,

$$\mathcal{P}_M = \sum_{m\in M} R_m = \sum_{m\in M} P_m \tag{6.23}$$

will satisfy all the necessary prerequisites. This is illustrated in Fig. 6.2.

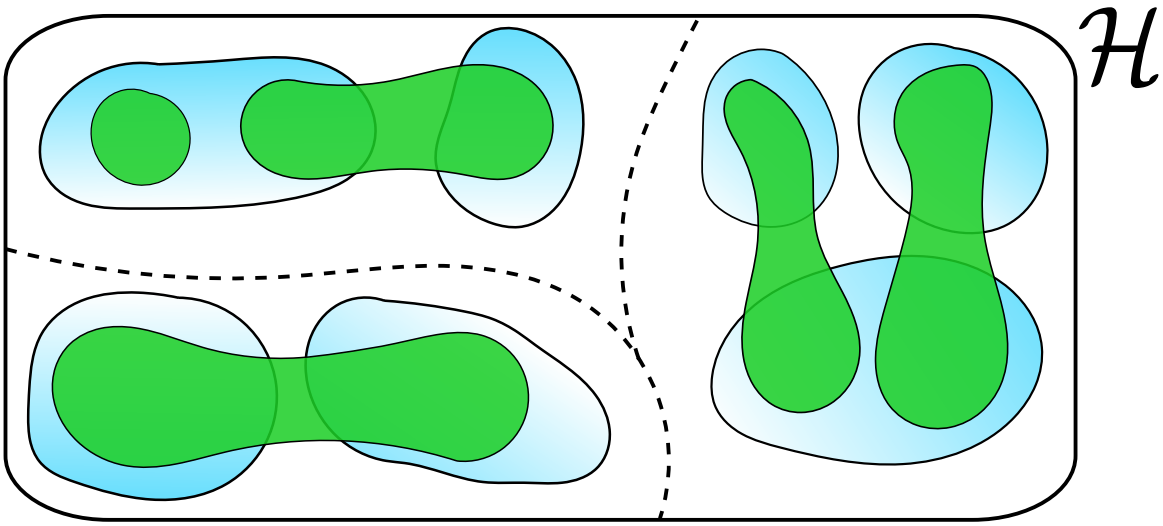

Fig. 6.2 A visual representation of the projection spaces of the measurement. The light blue areas (bottom layer) are R_m, the eigenspaces of $\hat{O}$. The green areas are measurement eigenspaces, P_m, and they overlap non-trivially with the R_m subspaces. The $\mathcal{P}_M$ projection space boundary (dashed line) runs through the Hilbert space, $\mathcal{H}$, where there is no overlap between P_m and R_m.

In the simplest case the projectors $\mathcal{P}_M$ can consist of only single eigenspaces of $\hat{O}$, $\mathcal{P}_M = R_m$. The interpretation is straightforward - measurement projects the system onto a eigenspace of an observable $\hat{O}$ which is a compatible observable with a_1 and corresponds to a quantity conserved by the coherent Hamiltonian evolution. However, this may not be possible and we have the more general case when $\mathcal{P}_M = \sum_{m\in M} R_m$. In this case, one can simply think of all $R_{m\in M}$ as degenerate just like eigenstates of the measurement operator, a_1, that are degenerate, can form a single eigenspace P_m. However, these subspaces correspond

to different eigenvalues of $\hat{O}$ distinguishing it from conventional projections. Instead, the degeneracies are identified by some other feature.

In our case, it is apparent from the form of $\hat{B}_{\min}$ and $\hat{H}_0$ in Eqs. (6.9) and (6.10) that

$$\hat{O}_k = \beta_k^\dagger \beta_k + \tilde{\beta}_k^\dagger \tilde{\beta}_k = \hat{n}_k + \hat{n}_{k-\pi/a} \tag{6.24}$$

commutes with both operators for all k. Thus, we can easily construct

$$\hat{O} = \sum_{\text{RBZ}} g_k \hat{O}_k \tag{6.25}$$

for any arbitrary g_k. Its eigenspaces, R_m, can then be easily constructed and their relationship with P_m and $\mathcal{P}_M$ is illustrated in Fig. 6.2 whilst the time evolution of $\langle \hat{O}_k \rangle$ for a sample trajectory is shown in Fig. 6.1(a). Note that unlike the $\hat{c}$ or $\hat{H}_0$ we can actually see that this observable's distribution does indeed freeze. These eigenspaces are composed of Fock states in momentum space that have the same number of atoms within each pair of k and $k - \pi/a$ modes.

Having identified an appropriate $\hat{O}$ operator we proceed to identifying $\mathcal{P}_M$ subspaces for the operator $\hat{B}_{\min}$. Firstly, since $\hat{B}_{\min}$ contains $\sin(ka)$ coefficients atoms in different k modes that have the same $\sin(ka)$ value are indistinguishable to the measurement and will lie in the same P_m eigenspaces. This will happen for the pairs $(k, \pi/a - k)$. Therefore, the R_m spaces that have the same $\hat{O}_k + \hat{O}_{\pi/a-k}$ eigenvalues must belong to the same $\mathcal{P}_M$.

Secondly, if we re-write $\hat{O}$ in terms of the β_k and $\tilde{\beta}_k$ modes we get

$$\hat{O} = \sum_{\text{RBZ}} g_k \left(\beta_k^\dagger \beta_k + \tilde{\beta}_k^\dagger \tilde{\beta}_k \right), \tag{6.26}$$

and so it's not hard to see that $\hat{B}_{\min,k} = (\beta_k^\dagger \beta_k - \tilde{\beta}_k^\dagger \tilde{\beta}_k)$ can have the same eigenvalues for different values of $\hat{O}_k = \beta_k^\dagger \beta_k + \tilde{\beta}_k^\dagger \tilde{\beta}_k$. Specifically, if a given subspace R_m corresponds to the

eigenvalue O_k of $\hat{O}_k$ then the possible values of $B_{\min,k}$ will be $\{-O_k, -O_k+2, ..., O_k-2, O_k\}$ just like $\Delta N = N_{\text{even}} - N_{\text{odd}}$ can have multiple possible values for a fixed $N = N_{\text{even}} + N_{\text{odd}}$. Therefore, we can see that all R_m with even values of O_k will share $B_{\min,k}$ eigenvalues and thus they will overlap with the same P_m subspaces. The same is true for odd values of O_k. However, R_m with an even value of O_k will never have the same value of $B_{\min,k}$ as a subspace with an odd value of O_k. Therefore, a single $\mathcal{P}_M$ will contain all R_m that have the same parities of O_k for all k, e.g. if it includes the R_m with $O_k = 6$, it will also include the R_m for which $O_k = 0, 2, 4, 6, ..., N$, but not any of $O_k = 1, 3, 5, 7, ..., N$, where N is the total number of atoms.

Finally, the $k = \pi/a$ mode is special, because $\sin(\pi) = 0$ which means that $B_{\min,k=\pi/a} = 0$ always. This in turn implies that all possible values of $O_{\pi/a}$ are degenerate to the measurement. Therefore, we exclude this mode when matching the parities of the other modes.

To illustrate the above let us consider a specific example. Let us consider two atoms, $N = 2$, on eight sites $M = 8$. This particular configuration has eight momentum modes $ka = \{-\frac{3\pi}{4}, -\frac{\pi}{2}, -\frac{\pi}{4}, 0, \frac{\pi}{4}, \frac{\pi}{2}, \frac{3\pi}{4}, \pi\}$ and so the RBZ has only four modes, RBZ $:= \{\frac{\pi}{4}, \frac{\pi}{2}, \frac{3\pi}{4}, \pi\}$. There are 10 different ways of splitting two atoms into these four modes and thus we have 10 different $R_m = \{O_{\pi/4a}, O_{\pi/2a}, O_{3\pi/4a}, O_{\pi/a}\}$ eigenspaces of $\hat{O}$ In the third column we have also listed the eigenvalues of the $\hat{B}_{\min}$ eigenstates that lie within the given R_m.

We note that $ka = \pi/4$ will be degenerate with $ka = 3\pi/4$ since $\sin(ka)$ is the same for both. Therefore, we already know that we can combine (R_0, R_2, R_7), (R_1, R_5), and (R_3, R_8), because those combinations have the same $O_{\pi/4a} + O_{3\pi/4a}$ values. This is very clear in the table as these subspaces span exactly the same values of $B_{\min}$, i.e. they have exactly the same values in the third column.

Now we have to match the parities. Subspaces that have the same parity combination for the pair $(O_{\pi/4a} + O_{3\pi/4a}, O_{\pi/2a})$ will be degenerate in $\mathcal{P}_M$. Note that we excluded $O_{\pi/a}$, because as we discussed earlier they are all degenerate due to $\sin(\pi) = 0$. Therefore, the

m	R_m	Possible values of $B_{\min}$
0	$\{2,0,0,0\}$	$-\sqrt{2},0,\sqrt{2}$
1	$\{1,1,0,0\}$	$-\frac{1+\sqrt{2}}{\sqrt{2}},-\frac{1-\sqrt{2}}{\sqrt{2}},\frac{1-\sqrt{2}}{\sqrt{2}},\frac{1+\sqrt{2}}{\sqrt{2}}$
2	$\{1,0,1,0\}$	$-\sqrt{2},0,\sqrt{2}$
3	$\{1,0,0,1\}$	$-\frac{1}{\sqrt{2}},\frac{1}{\sqrt{2}}$
4	$\{0,2,0,0\}$	$-2,0,2$
5	$\{0,1,1,0\}$	$-\frac{1+\sqrt{2}}{\sqrt{2}},-\frac{1-\sqrt{2}}{\sqrt{2}},\frac{1-\sqrt{2}}{\sqrt{2}},\frac{1+\sqrt{2}}{\sqrt{2}}$
6	$\{0,1,0,1\}$	$-1,1$
7	$\{0,0,2,0\}$	$-\sqrt{2},0,\sqrt{2}$
8	$\{0,0,1,1\}$	$-\frac{1}{\sqrt{2}},\frac{1}{\sqrt{2}}$
9	$\{0,0,0,2\}$	0

Table 6.1 A list of all R_m eigenspaces for $N=2$ atoms at $M=8$ sites. The third column displays the eigenvalues of all the eigenstates of $\hat{B}_{\min}$ that lie in the given R_m.

(even,even) subspace will include (R_0,R_2,R_4,R_7,R_9), the (odd,even) will contain (R_3,R_8), the (even, odd) will contain (R_6) only, and the (odd, odd) contains (R_1,R_5). These overlaps should be evident from the table as we can see that these combinations combine all R_m that share any eigenstates of $\hat{B}_{\min}$ with the same eigenvalues.

Therefore, we have ended up with four distinct $\mathcal{P}_M$ subspaces

$$\begin{aligned}
\mathcal{P}_{\text{even,even}} &= R_0+R_2+R_4+R_7+R_9 \\
\mathcal{P}_{\text{odd,even}} &= R_3+R_8 \\
\mathcal{P}_{\text{even,odd}} &= R_6 \\
\mathcal{P}_{\text{odd,odd}} &= R_1+R_5.
\end{aligned}$$

At this point it should be clear that these projectors satisfy all our requirement. The conditions $\sum_M \mathcal{P}_M = 1$ and $\mathcal{P}_M\mathcal{P}_N = \delta_{M,N}\mathcal{P}_M$ should be evident from the form above. The commutator requirements are also easily satisfied since the subspaces R_m are of an operator that commutes with both the Hamiltonian and the measurement operator. And finally, one can also verify

using the table that all of these projectors are built from complete subspaces of $\hat{B}_{\text{min}}$ (i.e. each subspace P_m belongs to only one $\mathcal{P}_M$) and thus $\mathcal{P}_M = \sum_{m \in M} P_m$.

6.4 Conclusions

In summary we have investigated measurement backaction resulting from coupling light to an ultracold gas's phase-related observables. We demonstrated how this can be used to prepare the Hamiltonian eigenstates even if significant tunnelling is occurring as the measurement can be engineered to not compete with the system's dynamics. Furthermore, we have shown that when the observable of the phase-related quantities does not commute with the Hamiltonian we still project to a specific subspace of the system that is neither an eigenspace of the Hamiltonian or the measurement operator. This is in contrast to quantum Zeno dynamics [65, 66, 74–76] or dissipative state preparation [44]. We showed how this projection is essentially an extension of the measurement postulate to weak measurement on dynamical systems where the competition between the two processes is significant.

Chapter 7

Summary and Conclusions

Quantum optics of quantum gases explores the ultimate quantum regime of light-matter interactions where both the optical and matter fields are fully quantised. It provides a very rich system in which new phenomena can be observed, engineered, and controlled beyond what would be possible in condensed matter. Combined with rapid and promising experimental progress in this field the theoretical proposals have the potential of directing the research in the foreseeable future [24–28].

In this thesis we focused on the coupling between global quantised optical fields and an ultracold bosonic quantum gas. By considering global fields as opposed to localised light-matter interactions we were able to introduce several nonlocal properties to the Hamiltonian in a controllable manner which would otherwise be impossible to implement. We showed how this can be useful in the context of nondestructive probing by showing that it can easily distinguish between a highly delocalised quantum state such as a superfluid and insulating states such as the Mott insulator and the Bose glass phases which is currently a challenge [132]. Furthermore, we have seen how the correlation length, which would be inaccessible in localised measurements, was immediately visible in our scheme and lead to an angular scattering pattern that was far richer than it was for the classical case. This is best highlighted

by the fact that it would be visible even when classically no light would scatter coherently at all.

More interestingly, the global nature of the measurement was also capable of creating such long-range correlations itself when we considered measurement backaction. This was most visible when we saw how weak measurement was capable of driving global macroscopic multimode oscillations between different spatial modes, such as odd and even sites, across the whole lattice which could be used for quantum information and metrology. Such dynamical states show spatial density-density correlations with nontrivial periods and long-range coherence, thus having supersolid properties, but as an essentially dynamical version. Furthermore, the tunability of the optical arrangement meant that we had extreme flexibility in choosing our observables, effectively tailoring the long-range entanglement and correlations in the system. We have also shown how global measurement when combined with both atomic tunnelling and interactions leads to highly nontrivial dynamics in which backaction can either compete or cooperate with on-site repulsion in squeezing the atomic variables.

In the limit of strong measurement when quantum Zeno dynamics occurs we showed that these nonlocal spatial modes created by the global measurement lead to long-range correlated tunnelling events whilst suppressing any other dynamics between different spatial modes of the measurement. Such globally paired tunnelling due to a fundamentally novel phenomenon can enrich physics of long-range correlated systems beyond relatively short range interactions expected from standard dipole-dipole interactions [160, 161]. These nonlocal high-order processes entangle regions of the optical lattice that are disconnected by the measurement. Using different detection schemes, we showed how to tailor density-density correlations between distant lattice sites. Quantum optical engineering of nonlocal coupling to environment, combined with quantum measurement, can allow the design of nontrivial system-bath interactions, enabling new links to quantum simulations [164] and

thermodynamics [165]. Interestingly, these dynamics also provide a link to non-Hermitian quantum mechanics as this regime of measurement can be accurately described with a non-Hermitian Hamiltonian. Furthermore, we show that this allows for a rather novel type of competition between measurement and tunnelling where both processes actually cooperate to produce a steady state in which tunnelling is suppressed by destructive matter-wave interference.

A unique feature of our global measurement scheme meant that we could couple directly to the phase observables of the system by coupling to the interference between the lattice sites, which represents the shortest meaningful distance in an optical lattice, rather than their on-site density. This defines most processes in optical lattices. For example, matter-field phase changes may happen not only due to external gradients, but also due to intriguing effects such quantum jumps leading to phase flips at neighbouring sites and sudden cancellation of tunnelling [142], which should be accessible by this method. Furthermore, in mean-field one can measure the matter-field amplitude (which is also the order parameter), quadratures and their squeezing. This can link atom optics to areas where quantum optics has already made progress, e.g., quantum imaging [42, 43], using an optical lattice as an array of multimode nonclassical matter- field sources with a high degree of entanglement for quantum information processing. We have also shown how this scheme of coupling to phase observables can be used in the context of quantum measurement backaction to achieve a new degree of control. We used this result to show a generalisation of weak measurement on dynamical systems by showing that there is now a new class of projections available even when the measurement is not a compatible observable of the Hamiltonian. This an interesting result as the projections themselves are unlike those postulated by the Copenhagen interpretation, those present in quantum Zeno dynamic, or even those possible to engineer using dissipative methods.

In this thesis we have covered significant areas of the broad field that is quantum optics of quantum gases, but there is much more that has been left untouched. Here, we have only

considered spinless bosons, but the theory can also been extended to fermions [92, 93, 97] and molecules [143] and potentially even photonic circuits [95]. Furthermore, the question of quantum measurement and its properties has been a subject of heated debate since the very origins of quantum theory yet it is still as mysterious as it was at the beginning of the 20^{th} century. However, this work has hopefully demonstrated that coupling quantised light fields to many-body systems provides a very rich playground for exploring new quantum mechanical phenomena especially the competition between weak quantum measurement and many-body dynamics in ultracold bosonic gases.

References

[1] M. H. Anderson, J. R. Ensher, M. R. Matthews, C. E. Wieman, and E. A. Cornell. Observation of Bose-Einstein Condensation in a Dilute Atomic Vapor. *Science*, 269:14, 1995.

[2] Cl. C. Bradley, C. A. Sackett, J. J. Tollett, and Randall G. Hulet. Evidence of Bose-Einstein condensation in an atomic gas with attractive interactions. *Physical Review Letters*, 75(9):1687, 1995.

[3] K. B. Davis, M.-O. Mewes, M. R. Andrews, N. J. Van Druten, D. S. Durfee, D. M. Kurn, and W. Ketterle. Bose-Einstein condensation in a gas of sodium atoms. *Physical Review Letters*, 75(22):3969, 1995.

[4] L. Pitaevskii and S. Stringari. *Bose-Einstein Condensation and Superfluidity*, volume 164. Oxford University Press, 2016.

[5] M. Lewenstein, A. Sanpera, V. Ahufinger, B. Damski, A. Sen, and U. Sen. Ultracold atomic gases in optical lattices: mimicking condensed matter physics and beyond. *Advances in Physics*, 56(2):243–379, 2007.

[6] I. Bloch, J. Dalibard, and W. Zwerger. Many-body physics with ultracold gases. *Reviews of Modern Physics*, 80(3):885, 2008.

[7] M. R. Andrews, C. G. Townsend, H.-J. Miesner, D. S. Durfee, D. M. Kurn, and W. Ketterle. Observation of interference between two Bose condensates. *Science*, 275(5300):637–641, 1997.

[8] I. Bloch, Th. W. Hänsch, and T. Esslinger. Measurement of the spatial coherence of a trapped Bose gas at the phase transition. *Nature*, 403(6766):166–170, 2000.

[9] M. R. Matthews, B. P. Anderson, P. C. Haljan, D. S. Hall, C. E. Wieman, and E. A. Cornell. Vortices in a Bose-Einstein condensate. *Physical Review Letters*, 83(13):2498, 1999.

[10] K. W. Madison, F. Chevy, W. Wohlleben, and J. Dalibard. Vortex formation in a stirred Bose-Einstein condensate. *Physical Review Letters*, 84(5):806, 2000.

[11] J. R. Abo-Shaeer, C. Raman, J. M. Vogels, and W. Ketterle. Observation of vortex lattices in Bose-Einstein condensates. *Science*, 292(5516):476–479, 2001.

[12] B. DeMarco and D. S. Jin. Onset of Fermi degeneracy in a trapped atomic gas. *Science*, 285(5434):1703–1706, 1999.

[13] F. Schreck, L. Khaykovich, K. L. Corwin, G. Ferrari, T. Bourdel, J. Cubizolles, and C. Salomon. Quasipure Bose-Einstein condensate immersed in a Fermi sea. *Physical Review Letters*, 87(8):080403, 2001.

[14] A. G. Truscott, K. E. Strecker, W. I. McAlexander, G. B. Partridge, and R. G. Hulet. Observation of Fermi pressure in a gas of trapped atoms. *Science*, 291(5513):2570–2572, 2001.

[15] D. Jaksch, C. Bruder, J. I. Cirac, C. W. Gardiner, and P. Zoller. Cold bosonic atoms in optical lattices. *Physical Review Letters*, 81(15):3108, 1998.

[16] M. Greiner, O. Mandel, T. Esslinger, Th. W. Hänsch, and I. Bloch. Quantum phase transition from a superfluid to a Mott insulator in a gas of ultracold atoms. *Nature*, 415(6867):39–44, 2002.

[17] M. P. A. Fisher, P. B. Weichman, G. Grinstein, and D. S. Fisher. Boson localization and the superfluid-insulator transition. *Physical Review B*, 40(1):546, 1989.

[18] F. Dalfovo, S. Giorgini, L. P. Pitaevskii, and Sandro Stringari. Theory of Bose-Einstein condensation in trapped gases. *Reviews of Modern Physics*, 71(3):463, 1999.

[19] I. B. Mekhov and H. Ritsch. Quantum optics with ultracold quantum gases: towards the full quantum regime of the light–matter interaction. *Journal of Physics B: Atomic, Molecular and Optical Physics*, 45(10):102001, 2012.

[20] H. Ritsch, P. Domokos, F. Brennecke, and T. Esslinger. Cold atoms in cavity-generated dynamical optical potentials. *Reviews of Modern Physics*, 85(2):553, 2013.

[21] M. Scully and S. Zubairy. *Quantum Optics*, chapter 10.1, page 293. Cambridge University Press, 1997.

[22] H. Carmichael. *An open systems approach to quantum optics: lectures presented at the Université Libre de Bruxelles, October 28 to November 4, 1991*, volume 18. Springer Science & Business Media, 2009.

[23] H. M. Wiseman and G. J. Milburn. *Quantum Measurement and Control*. Cambridge University Press, 2010.

[24] K. Baumann, C. Guerlin, F. Brennecke, and T. Esslinger. Dicke quantum phase transition with a superfluid gas in an optical cavity. *Nature*, 464(7293):1301–1306, 2010.

[25] M. Wolke, J. Klinner, H. Keßler, and A. Hemmerich. Cavity cooling below the recoil limit. *Science*, 337(6090):75–78, 2012.

[26] D. Schmidt, H. Tomczyk, S. Slama, and C. Zimmermann. Dynamical Instability of a Bose-Einstein Condensate in an Optical Ring Resonator. *Physical Review Letters*, 112(11):115302, 2014.

[27] J. Klinder, H. Keßler, M. R. Bakhtiari, M. Thorwart, and A. Hemmerich. Observation of a superradiant Mott insulator in the Dicke-Hubbard model. *Physical Review Letters*, 115(23):230403, 2015.

[28] R. Landig, L. Hruby, N. Dogra, M. Landini, R. Mottl, T. Donner, and T. Esslinger. Quantum phases from competing short-and long-range interactions in an optical lattice. *Nature*, 2016.

[29] I. B. Mekhov, C. Maschler, and H. Ritsch. Cavity-enhanced light scattering in optical lattices to probe atomic quantum statistics. *Physical Review Letters*, 98(10):100402, 2007.

[30] I. B. Mekhov, C. Maschler, and H. Ritsch. Light scattering from ultracold atoms in optical lattices as an optical probe of quantum statistics. *Physical Review A*, 76(5):053618, 2007.

[31] Igor B Mekhov, Christoph Maschler, and Helmut Ritsch. Probing quantum phases of ultracold atoms in optical lattices by transmission spectra in cavity quantum electrodynamics. *Nature Physics*, 3(5):319–323, 2007.

[32] I. B. Mekhov and H. Ritsch. Quantum optics with quantum gases. *Laser Physics*, 19(4):610–615, 2009.

[33] V. B. Braginsky. Topics in Theoretical and Experimental Gravitation Physics. 1977.

[34] W. G. Unruh. Analysis of quantum-nondemolition measurement. *Physical Review D*, 18(6):1764, 1978.

[35] M. Brune, S. Haroche, V. Lefevre, J. M. Raimond, and N. Zagury. Quantum nondemolition measurement of small photon numbers by Rydberg-atom phase-sensitive detection. *Physical Review Letters*, 65(8):976, 1990.

[36] M. Brune, S. Haroche, J. M. Raimond, L. Davidovich, and N. Zagury. Manipulation of photons in a cavity by dispersive atom-field coupling: Quantum-nondemolition measurements and generation of "Schrödinger cat" states. *Physical Review A*, 45(7):5193, 1992.

[37] K. Eckert, O. Romero-Isart, M. Rodriguez, M. Lewenstein, E. S. Polzik, and A. Sanpera. Quantum non-demolition detection of strongly correlated systems. *Nature Physics*, 4(1):50–54, 2008.

[38] T. Roscilde, M. Rodriguez, K. Eckert, O. Romero-Isart, M. Lewenstein, E. Polzik, and A. Sanpera. Quantum polarization spectroscopy of correlations in attractive fermionic gases. *New Journal of Physics*, 11(5):055041, 2009.

[39] P. Hauke, R. J. Sewell, M. W. Mitchell, and M. Lewenstein. Quantum control of spin correlations in ultracold lattice gases. *Physical Review A*, 87(2):021601, 2013.

[40] B. Rogers, M. Paternostro, J. F. Sherson, and G. De Chiara. Characterization of Bose-Hubbard models with quantum nondemolition measurements. *Physical Review A*, 90(4):043618, 2014.

[41] H. Miyake, G. A. Siviloglou, G. Puentes, D. E. Pritchard, W. Ketterle, and D. M. Weld. Bragg scattering as a probe of atomic wave functions and quantum phase transitions in optical lattices. *Physical Review Letters*, 107(17):175302, 2011.

[42] T. Golubeva, Yu. Golubev, K. Samburskaya, C. Fabre, N. Treps, and M. Kolobov. Entanglement measurement of the quadrature components without homodyne detection in the bright, spatially multimode far field. *Physical Review A*, 81:013831, 2010.

[43] M. I. Kolobov. The spatial behavior of nonclassical light. *Reviews of Modern Physics*, 71:1539–1589, 1999.

[44] S. Diehl, A. Micheli, A. Kantian, B. Kraus, H. P. Büchler, and P. Zoller. Quantum states and phases in driven open quantum systems with cold atoms. *Nature Physics*, 4(11):878–883, 2008.

[45] H. J. Carmichael. Analytical and numerical results for the steady state in cooperative resonance fluorescence. *Journal of Physics B: Atomic and Molecular Physics*, 13(18):3551, 1980.

[46] P. Werner, K. Völker, M. Troyer, and S. Chakravarty. Phase diagram and critical exponents of a dissipative Ising spin chain in a transverse magnetic field. *Physical Review Letters*, 94(4):047201, 2005.

[47] L. Capriotti, A. Cuccoli, A. Fubini, V. Tognetti, and R. Vaia. Dissipation-driven phase transition in two-dimensional Josephson arrays. *Physical Review Letters*, 94(15):157001, 2005.

[48] S. Morrison and A. S. Parkins. Dissipation-driven quantum phase transitions in collective spin systems. *Journal of Physics B: Atomic, Molecular and Optical Physics*, 41(19):195502, 2008.

[49] J. Eisert and T. Prosen. Noise-driven quantum criticality. *arXiv preprint arXiv:1012.5013*, 2010.

[50] M. J. Bhaseen, J. Mayoh, B. D. Simons, and J. Keeling. Dynamics of nonequilibrium Dicke models. *Physical Review A*, 85(1):013817, 2012.

[51] S. Diehl, A. Tomadin, A. Micheli, R. Fazio, and P. Zoller. Dynamical phase transitions and instabilities in open atomic many-body systems. *Physical Review Letters*, 105(1):015702, 2010.

[52] M. Žnidarič. Solvable quantum nonequilibrium model exhibiting a phase transition and a matrix product representation. *Physical Review E*, 83(1):011108, 2011.

[53] W. H. Zurek. Decoherence and the transition from quantum to classical-revisited. *Los Alamos Science*, 27:86–109, 2002.

[54] J. I. Cirac, C. W. Gardiner, M. Naraschewski, and P. Zoller. Continuous observation of interference fringes from Bose condensates. *Physical Review A*, 54(5):R3714, 1996.

[55] Y. Castin and J. Dalibard. Relative phase of two Bose-Einstein condensates. *Physical Review A*, 55(6):4330, 1997.

[56] J. Ruostekoski and D. F. Walls. Nondestructive optical measurement of relative phase between two Bose-Einstein condensates. *Physical Review A*, 56(4):2996, 1997.

[57] I. B. Mekhov and H. Ritsch. Quantum Nondemolition Measurements and State Preparation in Quantum Gases by Light Detection. *Physical Review Letters*, 102(2):020403, 2009.

[58] I. B. Mekhov and H. Ritsch. Quantum optics with quantum gases: Controlled state reduction by designed light scattering. *Physical Review A*, 80(1):013604, 2009.

[59] I. B. Mekhov and H. Ritsch. Quantum Optical Measurements in Ultracold Gases: Macroscopic Bose–Einstein Condensates. *Laser Physics*, 20:694, 2010.

[60] J. S. Douglas and K. Burnett. Scattering-induced spatial superpositions in multiparticle localization. *Physical Review A*, 86(5):052120, 2012.

[61] I. B. Mekhov and H. Ritsch. Atom State Evolution and Collapse in Ultracold Gases during Light Scattering into a Cavity. *Laser Physics*, 21:1486, 2011.

[62] J. S. Douglas and K. Burnett. Scattering distributions in the presence of measurement backaction. *Journal of Physics B: Atomic, Molecular and Optical Physics*, 46(20):205301, 2013.

[63] Y. Ashida and M. Ueda. Diffraction-Unlimited Position Measurement of Ultracold Atoms in an Optical Lattice. *Physical Review Letters*, 115(9):095301, 2015.

[64] Y. Ashida and M. Ueda. Multi-Particle Quantum Dynamics under Continuous Observation. *arXiv preprint arXiv:1510.04001*, 2015.

[65] B. Misra and E. C. G. Sudarshan. The Zeno's paradox in quantum theory. *Journal of Mathematical Physics*, 18(4):756–763, 1977.

[66] P. Facchi and S. Pascazio. Quantum Zeno dynamics: mathematical and physical aspects. *Journal of Physics A: Mathematical and Theoretical*, 41(49):493001, 2008.

[67] W. M. Itano, D. J. Heinzen, J. J. Bollinger, and D. J. Wineland. Quantum Zeno effect. *Physical Review A*, 41:2295–2300, 1990.

[68] B. Nagels, L. J. F. Hermans, and P. L. Chapovsky. Quantum Zeno Effect Induced by Collisions. *Physical Review Letters*, 79:3097–3100, 1997.

[69] P. G. Kwiat, A. G. White, J. R. Mitchell, O. Nairz, G. Weihs, H. Weinfurter, and A. Zeilinger. High-Efficiency Quantum Interrogation Measurements via the Quantum Zeno Effect. *Physical Review Letters*, 83:4725–4728, 1999.

[70] C. Balzer, R. Huesmann, W. Neuhauser, and P. E. Toschek. The quantum Zeno effect – evolution of an atom impeded by measurement. *Optics Communications*, 180(1–3):115–120, 2000.

[71] E. W. Streed, J. Mun, M. Boyd, G. K. Campbell, P. Medley, W. Ketterle, and D. E. Pritchard. Continuous and Pulsed Quantum Zeno Effect. *Physical Review Letters*, 97:260402, 2006.

[72] O. Hosten, M. T. Rakher, J. T. Barreiro, N. A. Peters, and P. G. Kwiat. Counterfactual quantum computation through quantum interrogation. *Nature*, 439:949–952, 2006.

[73] J. Bernu, S. Deléglise, C. Sayrin, S. Kuhr, I. Dotsenko, M. Brune, J. M. Raimond, and S. Haroche. Freezing Coherent Field Growth in a Cavity by the Quantum Zeno Effect. *Physical Review Letters*, 101:180402, 2008.

[74] J.-M. Raimond, C. Sayrin, S. Gleyzes, I. Dotsenko, M. Brune, S. Haroche, P. Facchi, and S. Pascazio. Phase space tweezers for tailoring cavity fields by quantum Zeno dynamics. *Physical Review Letters*, 105(21):213601, 2010.

[75] J.-M. Raimond, P. Facchi, B. Peaudecerf, S. Pascazio, C. Sayrin, I. Dotsenko, S. Gleyzes, M. Brune, and S. Haroche. Quantum Zeno dynamics of a field in a cavity. *Physical Review A*, 86(3):032120, 2012.

[76] A. Signoles, A. Facon, D. Grosso, I. Dotsenko, S. Haroche, J.-M. Raimond, M. Brune, and S. Gleyzes. Confined quantum Zeno dynamics of a watched atomic arrow. *Nature Physics*, 10(10):715–719, 2014.

[77] N. Hatano and D. R. Nelson. Localization Transitions in Non-Hermitian Quantum Mechanics. *Physical Review Letters*, 77:570–573, 1996.

[78] G. Refael, W. Hofstetter, and D. R. Nelson. Transverse Meissner physics of planar superconductors with columnar pins. *Physical Review B*, 74:174520, 2006.

[79] C. M. Bender and S. Boettcher. Real Spectra in Non-Hermitian Hamiltonians Having $\mathcal{PT}$ Symmetry. *Physical Review Letters*, 80:5243–5246, 1998.

[80] G. L. Giorgi. Spontaneous $\mathcal{PT}$ symmetry breaking and quantum phase transitions in dimerized spin chains. *Physical Review B*, 82:052404, 2010.

[81] X. Z. Zhang and Z. Song. Non-Hermitian anisotropic XY model with intrinsic rotation-time-reversal symmetry. *Physical Review A*, 87:012114, 2013.

[82] J. Otterbach and M. Lemeshko. Dissipative Preparation of Spatial Order in Rydberg-Dressed Bose-Einstein Condensates. *Physical Review Letters*, 113:070401, 2014.

[83] T. E. Lee and C.-K. Chan. Heralded Magnetism in Non-Hermitian Atomic Systems. *Physical Review X*, 4:041001, 2014.

[84] T. E. Lee, F. Reiter, and N. Moiseyev. Entanglement and Spin Squeezing in Non-Hermitian Phase Transitions. *Physical Review Letters*, 113:250401, 2014.

[85] S. F. Caballero-Benitez and I. B. Mekhov. Quantum optical lattices for emergent many-body phases of ultracold atoms. *Physical Review Letters*, 115(24):243604, 2015.

[86] S. F. Caballero-Benitez and I. B. Mekhov. Quantum properties of light scattered from structured many-body phases of ultracold atoms in quantum optical lattices. *New Journal of Physics*, 17(12):123023, 2015.

[87] S. F. Caballero-Benitez, G. Mazzucchi, and I. B. Mekhov. Quantum simulators based on the global collective light-matter interaction. *Physical Review A*, 93:063632, 2016.

[88] S. F. Caballero-Benitez and I. B. Mekhov. Bond Order via Light-Induced Synthetic Many-body Interactions of Ultracold Atoms in Optical Lattices. *arXiv preprint arXiv:1604.02563*, 2016.

[89] T. J. Elliott and I. B. Mekhov. Engineering many-body dynamics with quantum light potentials and measurements. *Phys. Rev. A*, 94:013614, 2016.

[90] W. Kozlowski, S. F. Caballero-Benitez, and I. B. Mekhov. Probing matter-field and atom-number correlations in optical lattices by global nondestructive addressing. *Physical Review A*, 92(1):013613, 2015.

[91] T. J. Elliott, W. Kozlowski, S. F. Caballero-Benitez, and I. B. Mekhov. Multipartite Entangled Spatial Modes of Ultracold Atoms Generated and Controlled by Quantum Measurement. *Physical Review Letters*, 114:113604, 2015.

[92] T. J. Elliott, G. Mazzucchi, W. Kozlowski, S. F. Caballero-Benitez, and I. B. Mekhov. Probing and Manipulating Fermionic and Bosonic Quantum Gases with Quantum Light. *Atoms*, 3(3):392–406, 2015.

[93] G. Mazzucchi, W. Kozlowski, S. F. Caballero-Benitez, T. J. Elliott, and I. B. Mekhov. Quantum measurement-induced dynamics of many-body ultracold bosonic and fermionic systems in optical lattices. *Physical Review A*, 93:023632, 2016.

[94] W. Kozlowski, S. F. Caballero-Benitez, and I. B. Mekhov. Non-Hermitian dynamics in the quantum Zeno limit. *Physical Review A*, 94:012123, 2016.

[95] G. Mazzucchi, W. Kozlowski, S. F. Caballero-Benitez, and I. B. Mekhov. Collective dynamics of multimode bosonic systems induced by weak quantum measurement. *New Journal of Physics*, 18(7):073017, 2016.

[96] W. Kozlowski, S. F. Caballero-Benitez, and I. B. Mekhov. Quantum State Reduction by Matter-Phase-Related Measurements in Optical Lattices. *arXiv preprint arXiv:1605.06000*, 2016.

[97] G. Mazzucchi, S. F. Caballero-Benitez, and I. B. Mekhov. Quantum measurement-induced antiferromagnetic order and density modulations in ultracold Fermi gases in optical lattices. *Scientific Reports*, 6:31196, 2016.

[98] S. Bux, H. Tomczyk, D. Schmidt, Ph. W. Courteille, N. Piovella, and C. Zimmermann. Control of matter-wave superradiance with a high-finesse ring cavity. *Physical Review A*, 87(2):023607, 2013.

[99] H. Keßler, J. Klinder, M. Wolke, and A. Hemmerich. Steering matter wave superradiance with an ultranarrow-band optical cavity. *Physical Review Letters*, 113(7):070404, 2014.

[100] R. Landig, F. Brennecke, R. Mottl, T. Donner, and T. Esslinger. Measuring the dynamic structure factor of a quantum gas undergoing a structural phase transition. *Nature Communications*, 6, 2015.

[101] C. Maschler, I. B. Mekhov, and H. Ritsch. Dicke quantum phase transition with a superfluid gas in an optical cavity. *The European Physical Journal D*, 146:545, 2008.

[102] J. Hubbard. Electron correlations in narrow energy bands. In *Proceedings of the royal society of london a: mathematical, physical and engineering sciences*, volume 276, pages 238–257. The Royal Society, 1963.

[103] A. J. Leggett. *Quantum liquids: Bose condensation and Cooper pairing in condensed-matter systems*. Oxford University Press, 2006.

[104] W. Krauth. Bethe ansatz for the one-dimensional boson Hubbard model. *Physical Review B*, 44(17):9772, 1991.

[105] A. R. Kolovsky and A. Buchleitner. Quantum chaos in the Bose-Hubbard model. *Europhysics Letters*, 68(5):632, 2004.

[106] E. Calzetta, B.-L. Hu, and A. M. Rey. Bose-Einstein-condensate superfluid–Mott-insulator transition in an optical lattice. *Physical Review A*, 73(2):023610, 2006.

[107] A. J. Leggett. Superfluidity. *Reviews of Modern Physics*, 71(2):S318, 1999.

[108] S. R. J. F. Clark. *Strongly correlated one-dimensional systems of cold atoms in optical lattices* . PhD thesis, University of Oxford, 2007.

[109] M. A. Cazalilla, R. Citro, T. Giamarchi, E. Orignac, and M. Rigol. One dimensional bosons: From condensed matter systems to ultracold gases. *Reviews of Modern Physics*, 83(4):1405–1466, 2011.

[110] S. Ejima, H. Fehske, and F. Gebhard. Dynamic properties of the one-dimensional Bose-Hubbard model. *Europhysics Letters*, 93(3):30002, 2011.

[111] T. D. Kühner, S. R. White, and H. Monien. One-dimensional Bose-Hubbard model with nearest-neighbor interaction. *Physical Review B*, 61(18):12474–12489, 2000.

[112] M. Pino, J. Prior, A. M. Somoza, D. Jaksch, and S. R. Clark. Reentrance and entanglement in the one-dimensional Bose-Hubbard model. *Physical Review A*, 86:023631, 2012.

[113] M. Pino, J. Prior, and S. R. Clark. Capturing the re-entrant behavior of one-dimensional Bose-Hubbard model. *Physica Status Solidi (B)*, 250(1):51–58, 2013.

[114] F. D. M. Haldane. Effective harmonic-fluid approach to low-energy properties of one-dimensional quantum fluids. *Physical Review Letters*, 47(25):1840, 1981.

[115] T. Giamarchi. *Quantum Physics in One Dimension*. Clarendon Press, Oxford, 2003.

[116] J. Ruostekoski, M. J. Collett, R. Graham, and D. F. Walls. Macroscopic superpositions of Bose-Einstein condensates. *Physical Review A*, 57(1):511, 1998.

[117] S. Rist and G. Morigi. Homodyne detection of matter-wave fields. *Physical Review A*, 85(5):053635, 2012.

[118] W. S. Bakr, J. I. Gillen, A. Peng, S. Folling, and M. Greiner. A quantum gas microscope for detecting single atoms in a Hubbard-regime optical lattice. *Nature*, 462:74–77, 2009.

[119] C. Weitenberg, M. Endres, J. F. Sherson, M. Cheneau, P. Schauss, T. Fukuhara, I. Bloch, and S. Kuhr. Single-spin addressing in an atomic Mott insulator. *Nature*, 471:319–324, 2011.

[120] J. Larson, B. Damski, G. Morigi, and M. Lewenstein. Mott-Insulator States of Ultracold Atoms in Optical Resonators. *Physical Review Letters*, 100:050401, 2008.

[121] W. Chen, K. Zhang, D. S. Goldbaum, M. Bhattacharya, and P. Meystre. Bistable Mott-insulator–to–superfluid phase transition in cavity optomechanics. *Physical Review A*, 80:011801, 2009.

[122] H. Habibian, A. Winter, S. Paganelli, H. Rieger, and G. Morigi. Bose-Glass Phases of Ultracold Atoms due to Cavity Backaction. *Physical Review Letters*, 110:075304, 2013.

[123] D. A. Ivanov and T. Yu Ivanova. Feedback-enhanced self-organization of atoms in an optical cavity. *JETP Letters*, 100(7):481–485, 2014.

[124] M. K. Pedersen, J. J. W. H. Sorensen, M. C. Tichy, and J. F. Sherson. Many-body state engineering using measurements and fixed unitary dynamics. *New Journal of Physics*, 16(11):113038, 2014.

[125] R. Walters, G. Cotugno, T. H. Johnson, S. R. Clark, and D. Jaksch. Ab initio derivation of Hubbard models for cold atoms in optical lattices. *Physical Review A*, 87:043613, 2013.

[126] D. A. Steck. Rubidium 87 D line data, 2001.

[127] C. Weitenberg, P. Schauß, T. Fukuhara, M. Cheneau, M. Endres, I. Bloch, and S. Kuhr. Coherent light scattering from a two-dimensional Mott insulator. *Physical Review Letters*, 106(21):215301, 2011.

[128] C. Weitenberg. *Single-atom resolved imaging and manipulation in an atomic Mott insulator*. PhD thesis, LMU, 2011.

[129] C. J. Foot. *Atomic Physics*. Oxford University Press, 2005.

[130] Ferdinand Brennecke, Rafael Mottl, Kristian Baumann, Renate Landig, Tobias Donner, and Tilman Esslinger. Real-time observation of fluctuations at the driven-dissipative Dicke phase transition. *Proceedings of the National Academy of Sciences*, 110(29):11763–11767, 2013.

[131] K. Eckert, O. Romero-Isart, M. Rodriguez, M. Lewenstein, E. S. Polzik, and A. Sanpera. Dicke quantum phase transition with a superfluid gas in an optical cavity. *Nature Physics*, 4:50, 2008.

[132] C. D'Errico, E. Lucioni, L. Tanzi, L. Gori, G. Roux, I. P. McCulloch, T. Giamarchi, M. Inguscio, and G. Modugno. Observation of a Disordered Bosonic Insulator from Weak to Strong Interactions. *Physical Review Letters*, 113:095301, 2014.

[133] S. Rist, C. Menotti, and G. Morigi. Light scattering by ultracold atoms in an optical lattice. *Physical Review A*, 81:013404, 2010.

[134] K. Łakomy, Z. Idziaszek, and M. Trippenbach. Thermal effects in light scattering from ultracold bosons in an optical lattice. *Physical Review A*, 80:043404, 2009.

[135] J. Ruostekoski, C. J. Foot, and A. B. Deb. Light Scattering for Thermometry of Fermionic Atoms in an Optical Lattice. *Physical Review Letters*, 103:170404, 2009.

[136] R. Roth and K. Burnett. Phase diagram of bosonic atoms in two-color superlattices. *Physical Review A*, 68:023604, 2003.

[137] http://ccpforge.cse.rl.ac.uk/gf/project/tntlibrary/.

[138] G. G. Batrouni, V. Rousseau, R. T. Scalettar, M. Rigol, A. Muramatsu, P. J. H. Denteneer, and M. Troyer. Mott domains of bosons confined on optical lattices. *Physical Review Letters*, 89:117203, 2002.

[139] G. Roux, T. Barthel, I. P. McCulloch, C. Kollath, U. Schollwöck, and T. Giamarchi. Quasiperiodic Bose-Hubbard model and localization in one-dimensional cold atomic gases. *Physical Review A*, 78(2):023628, 2008.

[140] P. Horak and S. M. Barnett. Creation of coherence in Bose-Einstein condensates by atom detection. *Journal of Physics B: Atomic, Molecular and Optical Physics*, 32(14):3421, 1999.

[141] D. Kaszlikowski, A. Sen(De), U. Sen, V. Vedral, and A. Winter. Quantum Correlation without Classical Correlations. *Physical Review Letters*, 101:070502, 2008.

[142] A. Vukics, C. Maschler, and H. Ritsch. Microscopic physics of quantum self-organization of optical lattices in cavities. *New Journal of Physics*, 9(8):255, 2007.

[143] I. B. Mekhov. Quantum non-demolition detection of polar molecule complexes: dimers, trimers, tetramers. *Laser Physics*, 23(1):015501, 2013.

[144] H. Pichler, A. J. Daley, and P. Zoller. Nonequilibrium dynamics of bosonic atoms in optical lattices: Decoherence of many-body states due to spontaneous emission. *Physical Review A*, 82(6):063605, 2010.

[145] S. Sarkar, S. Langer, J. Schachenmayer, and A. J. Daley. Light scattering and dissipative dynamics of many fermionic atoms in an optical lattice. *Physical Review A*, 90(2):023618, 2014.

[146] N. Syassen, D. M. Bauer, M. Lettner, T. Volz, D. Dietze, J. J. Garcia-Ripoll, J. I. Cirac, G. Rempe, and S. Dürr. Strong dissipation inhibits losses and induces correlations in cold molecular gases. *Science*, 320(5881):1329–1331, 2008.

[147] K. V. Kepesidis and M. J. Hartmann. Bose-Hubbard model with localized particle losses. *Physical Review A*, 85(6):063620, 2012.

[148] I. Vidanović, D. Cocks, and W. Hofstetter. Dissipation through localized loss in bosonic systems with long-range interactions. *Physical Review A*, 89(5):053614, 2014.

[149] J.-S. Bernier, D. Poletti, and C. Kollath. Dissipative quantum dynamics of fermions in optical lattices: A slave-spin approach. *Physical Review B*, 90(20):205125, 2014.

[150] A. J. Daley. Quantum trajectories and open many-body quantum systems. *Advances in Physics*, 63(2):77–149, 2014.

[151] C. Ates, B. Olmos, W. Li, and I. Lesanovsky. Dissipative binding of lattice bosons through distance-selective pair loss. *Physical Review Letters*, 109(23):233003, 2012.

[152] B. Everest, M. R. Hush, and I. Lesanovsky. Many-body out-of-equilibrium dynamics of hard-core lattice bosons with nonlocal loss. *Physical Review B*, 90(13):134306, 2014.

[153] C. Gardiner and P. Zoller. *Quantum noise: a handbook of Markovian and non-Markovian quantum stochastic methods with applications to quantum optics*, volume 56. Springer Science & Business Media, 2004.

[154] B. Juliá-Díaz, T. Zibold, M. K. Oberthaler, M. Melé-Messeguer, J. Martorell, and A. Polls. Dynamic generation of spin-squeezed states in bosonic Josephson junctions. *Physical Review A*, 86:023615, 2012.

[155] E. M. Kessler, G. Giedke, A. Imamoglu, S. F. Yelin, M. D. Lukin, and J. I. Cirac. Dissipative phase transition in a central spin system. *Physical Review A*, 86(1):012116, 2012.

[156] A. Auerbach. *Interacting electrons and quantum magnetism*. Springer Science & Business Media, 2012.

[157] K. Winkler, G. Thalhammer, F. Lang, R. Grimm, J. Hecker Denschlag, A. Daley, A. Kantian, H. P. Büchler, and P. Zoller. Repulsively bound atom pairs in an optical lattice. *Nature*, 441:853–856, 2006.

[158] S. Fölling, S. Trotzky, P. Cheinet, M. Feld, R. Saers, A. Widera, T. Müller, and I. Bloch. Direct observation of second-order atom tunnelling. *Nature*, 448:1029, 2007.

[159] U. Schollwöck. The density-matrix renormalization group. *Reviews of Modern Physics*, 77:259–315, 2005.

[160] T. Sowiński, O. Dutta, P. Hauke, L. Tagliacozzo, and M. Lewenstein. Dipolar Molecules in Optical Lattices. *Physical Review Letters*, 108:115301, 2012.

[161] O. Dutta, M. Gajda, P. Hauke, M. Lewenstein, D.-S. Luhmann, B. A. Malomed, T. Sowinski, and J. Zakrzewski. Non-standard Hubbard models in optical lattices: a review. *Reports on Progress in Physics*, 78(6):066001, 2015.

[162] G. Mazzucchi, S. F. Caballero-Benitez, D. A. Ivanov, and I. B. Mekhov. Quantum optical feedback control for creating strong correlations in many-body systems. *arXiv preprint arXiv:1606.06022 (TBP in Optica)*, 2016.

[163] Denis A Ivanov, Tatiana Yu Ivanova, and Igor B Mekhov. Incoherent quantum feedback control of collective light scattering by Bose-Einstein condensates. *arXiv preprint arXiv:1601.02230*, 2016.

[164] K. Stannigel, P. Hauke, D. Marcos, M. Hafezi, S. Diehl, M. Dalmonte, and P. Zoller. Constrained Dynamics via the Zeno Effect in Quantum Simulation: Implementing Non-Abelian Lattice Gauge Theories with Cold Atoms. *Physical Review Letters*, 112:120406, 2014.

[165] N. Erez, G. Gordon, M. Nest, and G. Kurizki. Repulsively bound atom pairs in an optical lattice. *Nature*, 452:724, 2008.

[166] S. Weinberg. What happens in a measurement? *Physical Review A*, 93(3):032124, 2016.